Development of Surface Plasmon Resonance based Instrument with a Novel Opto-mechanical Scanning Mechanism

THESIS

Submitted in partial fulfillment of
the requirements for the degree of

DOCTOR OF PHILOSOPHY

by

DEVANARAYANAN.V.P

Under the Supervision of

Prof. RAJ KUMAR GUPTA

BITS Pilani
Pilani | Dubai | Goa | Hyderabad

BIRLA INSTITUTE OF TECHNOLOGY AND SCIENCE, PILANI

2016

BIRLA INSTITUTE OF TECHNOLOGY AND SCIENCE PILANI - 333031 (RAJASTHAN) INDIA

CERTIFICATE

This is to certify that the research work presented in this thesis entitled "**Development of Surface Plasmon Resonance based instrument with a Novel Opto-mechanical Scanning Mechanism**" by **Devanarayanan.V.P**, ID No. **2011PHXF045P** at Department of Physics, BITS Pilani, Pilani campus for award of degree of Doctor of Philosophy (Ph.D), is carried out under my guidence and supervision and is fit to be considered for the award of the Ph.D. No part of the present thesis work has ever been submitted in part or in full to any other university or institution for the award of any other degree or diploma.

_____

Signature of the Supervisor

Dr. Raj Kumar Gupta

Associate Professor

Department of Physics

BITS Pilani, Pilani Campus

Date: _____

..... dedicated to my grand parents and parents.

Acknowledgement

I express my heartfelt thanks to Prof. Raj Kumar Gupta for his kind attention in guiding my thesis work to fruitful completion. I am grateful to him for providing me such a novel idea as my thesis objective. His supportive and friendly attitude towards new ideas realized the very aim of my thesis. I sincerely thank Prof. V. Manjuladevi for her support during my thesis work. I sincerely acknowledge the invaluable support of my DAC members Prof. Anshuman Dalvi and Prof. V. Manjuladevi for reviewing my thesis, providing valuable suggestions and constructive comments during the course of my research work. I, sincerely acknowledge to Prof. Souvik Bhattacharyya, Vice Chancellor, BITS Pilani for giving the opportunity for carrying out my thesis work in this institute. I am thankful to Prof. S.K. Verma, Dean, Academic Research Division, BITS Pilani, Prof. Hemant Jadhav, Associate Dean, Academic Research Division, BITS Pilani for their support during my research career in this institute. I am grateful to Prof. R.N. Saha for his support towards the fruitful completion of the DST project, which initially supported my research work. I am grateful to Prof. N.V.M. Rao, Dean, Central Purchasing Unit, BITS Pilani, and his team for their support in the purchases of the necessary components required for my research work. I am thankful to Prof. Anshuman Dalvi, Head of the Department, Physics, and Prof. Navin Singh, DRC convener, Physics Department, BITS Pilani for their valuable support during my thesis work. I am thankful to faculty members and research scholars of physics department for their support and encouragement that lead to the successful completion of my thesis. I am very thankful to the chemistry department and its research fellows for providing me necessary support in conducting chemistry related experiments.

I express my deep gratitude to Monika Poonia, and Keerti Choudhary for their collaborative support in my research work. I am thankful to Dr. C. Karthik, Mr. Jitendra Kumar for their invaluable support towards my thesis work. I acknowledge my sincere

thanks to all my friends in physics department as well as other departments for their invaluable support for providing me a pleasant life during my research tenure in this institute.

I am thankful to the people in workshop, BITS Pilani for rendering a strong support to me in fabrication of components needed for the successful completion of research work. I express my deep gratitude to the lab assistants in physics department for their support to my research work. I am thankful to Mr. Rajeev Garg of Optochem International, Dr. Dahiya of Optiregion and Mr. Jimmy Jose of Holmarc Opto-mechatronics for their constant support through providing required optical components on time for my research work. I express my deep gratitude to Dr. Jamil Akhtar and Dr. Sanjeev Kumar Gupta of CEERI Pilani for providing me the necessary collaborative support for the fruitful completion of my research work. I am thankful to Mr. Pradeep of CEERI Pilani for providing the required support for drilling the glass samples. I acknowledge my sincere thanks to Dr. Lakshminarayanan, RRI Banglore, for his support towards my research work.

I extend my sincere and utmost thanks to my family members for their constant support and encouragement towards my research career.

Abstract

The optical phenomenon, surface plasmon resonance (SPR) has become extremely popular owing to its high sensitivity, label-free and non-destructive measurement towards any molecular specific interaction. This is one of the widely used phenomena for biological, chemical and gas sensing devices. The surface plasmon polaritons (SPPs) are electromagnetic oscillations propagating at the inetrface between a dielectric and a conductor, evanescently confined in the perpendicular direction. At the resonance, the component of wavevector of incident light planar to the interface matches to that of surface plasmon wave resulting in the absorption of energy of the reflected beam. The wavevector matching is extremely sensitive to the change in dielectrics over the metal surface and such changes can be recorded in the label-free, non-descructive and at a very high sensitivity by recording the shift in the resonance parameter. This is the underlying principle for the development of SPR based sensor. The Kretschmann-Reather configuration consist of an optical wave-guide with a gold surface (or coupled to gold coated glass slide with same refractive index of the wave-guide), light source and a detector. The configuration can be operated in two modes: the wavelength and angular scanning modes. The wavelength scanning mode utilizes a polychromatic light source which is kept at a fixed angle of incidence at the waveguide and a spectrometer as detector. The fiber-optic SPR sensor operates in the wavelength scanning mode. The angular scanning mode consists of a monochromatic light source with a mechanism for varying the angle of incidence and simultaneously measuring reflected intensity using photodiode.

The angular scan based SPR sensor utilizes various mechanism to vary the angle of incidence of light and to record reflected intensity from the metallic surface via the waveguide. The angular interrogation mechanism should keep the interrogation spot on the metallic surface fixed during the angular scanning. The detector position remain fixed during such angular interrogation. This class of interrogation mechanism

overcomes the errors in SPR spectra originating from the inhomogeneity in thickness of metallic film as well as from the deflection of beam on the detector.

In this thesis, we describe the development of a SPR instrument using novel angular interrogation mechanism that keeps the interrogation spot fixed on the metallic surface as well as on the detector while recording the SPR spectra of an anlayte deposited on the metallic surface.

In order to achieve the fixed interrogation region on metallic surface, the prism-sensor assembly is translated vertically in a highly controlled manner governed by a feedback mechanism. In the feedback mechanism, the deflection of the reflected beam during the precise angular interrogation by the piezomotor controlled mirror is quantified by the quadrant photodiode, and the prism-sensor assembly is translated vertically so as to regain the original set point. This mechanism ensures the detector remains fixed during the record of SPR spectra of the analyte. The feedback mechanism is controlled through an in-house developed computer program in LabView software. The sensitivity of the instrument is estimated from the calibration curve obtained by recording the resonance angle (RA) for different concentrations of sucrose solution with known refractive indices. The lowest detectable concentration of sugar in aqueous medium is found out to be 1×10^{-13} M (100fM). The resolution of the instrument is found to be 1.92μ RIU. The sensitivity of the instrument thus obtained from the slope of the calibration graph is $52.6^o/RIU$. The flow cell for the study of kinetic parameters in liquid medium is fabricated in an interesting method for this SPR sensor. The design of the flow cell is simple, robust, cost effective and universal to prisms having various shape. The flow cell is tested with the record of adsorption and desorption curves of sugar from the gold surface.

This thesis, also considers the effect of metallic layer thickness on the SPR spectrum. The numerical simulation of reflected light from three layer model using Fresnel's equation is performed in Matlab. The SPR curves are simulated for metal-air and metal-water interfaces for three different metals (copper, silver, gold) with thickness of metal film ranges between 30 - 100 nm. The quality factor of each spectra is calculated from its respective depth and full width half minimum FWHM values. The quality factor for each thickness of the metallic film is plotted against its respective thickness. The

quality factor plots are generated for three metals in two interfaces e.g. air-metal and water-metal. The comparison study revealed that gold film with a thickness of 50 nm provides the consistent quality factor in both interfaces.

The SPR instrument thus developed is used to study the optical anisotropy in ultra-thin films. The ultra-thin films are deposited onto the gold film surface through three deposition methods (1) Spin coating (2) Langmuir-Blodgett method (LB) (3) Self assembly. The single walled carbon nanotubes (SWCNTs) and cadmium stearate (CdSA) are deposited through LB method. The self assembled monolayer of octadecanethiol (ODT) was deposited on gold surface. The stearic acid (SA) is deposited into a thin layer onto gold surface through spin coating method. The SPR spectra of these samples are recorded in orthogonal directions with respect to the plane of incidence. The SPR data revealed that SWCNT LB film shows the highest degree of optical anisotropy than other samples.

A thin layer of graphene on gold surface of the SPR instrument enhances the adsorption of biomolecules, which improves the sensitivity of SPR biosensor. This thesis reports a method to stabilize the graphene layer on gold surface. An intermediate self assembled monolayer of alkanethiol molecules between gold and the graphene stabilizes the graphene layer on gold surface. The study considers biphenyl dithiol (BPD), octadecanethiol (ODT), and mercapto undecanoic acid (MUA) for the deposition of SAM over gold surface. In order to deposit, graphene on SAM, these three SAM samples are dipped in alcohol solution of graphene for 24 hrs. The SPR spectra of SAM layer as well as the SAM-graphene layer on gold surface are recorded. The SPR spectra of the three SAM-graphene samples on gold surface reveal that SAM of BPD improves the adsorption of graphene layer than other SAM layers due to π-π interaction.

Contents

List of Figures

List of Tables

List of abbreviation

SP	Surface plasmon
SPR	Surface plasmon resonance
EM	Electromagnetic
SPP	Surface Plasmon Polariton
CCD	charge coupled device
RIU	Refractive index unit
LED	Light emitting diode
RA	Surface plasmon resonance angle
SD	spot deviation
MUA	Mercapto-undecanoic acid
ITO	Indium Tin Oxide
DAQ	Data Acquisition Hardware
RI	Refractive index
H_2SO_4	Sulphuric acid
H_2O_2	Hydrogen peroxide
SAM	Self assembled monolayer
QPD	Quadrant photodiode
LV	LabView
ISD	Initial spot deviation
PC	Personal computer
TI	Total Intensity
AO	Analog output
QF	Quality factor
FWHM	Full width Half maximum
D	Depth of the curve

LB	Langmuir-Blodgett
SWCNT	Single-walled carbon nanotube
ODT	Octadecanethiol
CdSA	Cadmium stearate
NH_4OH	Ammonium hydroxide
H_2O	Water
SA	Stearic acid
$CdCl_2$	Cadmium Chloride
DMF	Dimethylformamide
BPD	Biphenyl dithiol
HPLC	High Performance Liquid chromatography
AFM	Atomic force microscope
Si	Silicon
RMS	Root mean square
BAM	Brewster angle microscope
IDE	Interdigitated electrode
I-V	Current-voltage

List of symbols

E	Electric Field
$\overline{K}$	Wave-vector
λ	Wavelength
n	Refractive index
θ	Angle in degrees
r_p	Reflection coefficient
α	alpha
β	beta
ϕ	phi
R_p	Reflectance
ω	Angular frequency
e	Charge of electron
n_e	Electron density
m_e	Mass of electron
h	Plancks Constant
ϵ	Permittivity
Δ	Delta
I_i	Intensity
$\geqslant$	Greater than or equal
k	Complex coefficient of refractive index
Ω	Ohmic Resistance
h_i	Height at i_{th} pixel location
$\overline{h}$	Mean Height in thin film height profile
R_a	Average Roughness of thin film
R_q	Root Mean Square Roughness of thin film

Chapter 1

Introduction

A surface plasmon (SP) wave is generated due to charge density oscillation at metal-dielectric interface. The SP wave can be excited by a polarized light wave incident onto the metallic layer (e.g. gold film) via a coupling high refractive index medium (e.g. glass prism) [1, 2]. At surface plasmon resonance (SPR), the component of wavevector of incident light planar to the interface matches to that of surface plasmon wave resulting in the absorption of energy of the reflected beam [3]. SPs are first observed in 1902, when a metallic grating was illuminated with polychromatic light and a narrow dark bands in the spectrum of diffracted light was observed [5, 6]. In 1958, Thurbadar observed a large drop in reflectivity when illuminating thin metal film deposited on a substrate [7]. In 1968, Otto explained Turbadar's results and demonstrated that the drop in the reflectivity in the attenuated total reflection method is due to the excitation of surface plasmons [8]. In the same year Kretschmann and Reather reported excitation of surface plasmons in another configuration employing the attenuated total reflection method. In the late 1970s, surface plasmons were first employed for the characterization of thin films [4]. Leidberg demonstrated first SPR biosensor in 1983 [5].

SPR phenomenon is observed due to the wave-matching condition between the wavevector of SP (K_{SP}) and the respective wave vector of incident light (K_l).

$$\vec{K}_{SP} = \vec{K}_l \tag{1.1}$$

The wavevector of the SP wave is dependent on the dielectric constant of the metal and the medium over the metal. The wave matching condition is easily perturbed by the minute changes in dielectric environment surrounding the metal surface. This

characteristic of SPR phenomenon enables it as a sensitive label free sensing method for the biomolecular interaction analysis.

Wavevector (K_l) of a electromagnetic (EM) wave has amplitude as well as direction. The amplitude of the wave-vector is inversely proportional to its wavelength (λ) and the direction is given in terms of cosine of angle of incidence (θ).

$$\frac{2\pi \cos\theta_{SP}\hat{\theta}}{\lambda_{SP}} = \frac{2\pi \cos\theta_{l}\hat{\theta}}{\lambda_{l}} \tag{1.2}$$

The wave-vector matching condition relation (Equation (1.2)) shows that the condition can be achieved by varying the incident angle (θ) of the electromagnetic beam with the constant wavelength or vice-versa. This condition leads to the transfer of energy from EM wave to the surface plasmons. The EM wave intensity extinguishes (minimizes) in this phenomenon. The condition for SPR provides two different modes in the development of sensors (1) wavelength based SPR sensor (2) angle based SPR sensor.

1.1 Surface Plasmon dispersion equation

Let us consider an interface between two media of refractive indices $n_1 < n_2$ as shown in Figure 1.1.

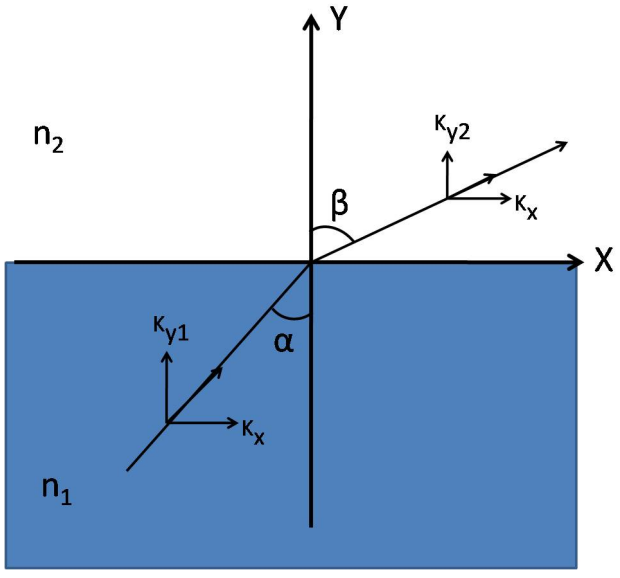

Figure 1.1: Refraction of light at an angle α, at an interface of two materials with refractive indices n_1 and n_2.

The complex reflection coefficient r_p for p-polarized incident light electric field is described with the following Fresnel equation for reflection

$$r_p = \frac{E_i}{E_r} = |r_p|e^{i\phi} = \frac{tan(\alpha - \beta)}{tan(\alpha + \beta)}e^{i\phi} \tag{1.3}$$

where E_i and E_r are the incident and reflected electric fields, respectively, and the angles α and β are of respective incident and reflected beams with the normal. The α and β are again related by Snell's law (Equation (1.4)).

$$n_1 sin\alpha = n_2 sin\beta \tag{1.4}$$

and ϕ is the phase change of reflected light from the incident beam.

Reflectance (R_p) is defined as

$$R_p = |r_p|^2 \tag{1.5}$$

There are two special cases exist: $\alpha + \beta = \pi/2$. Then the denominator of (Equation (1.3)) becomes very large and R_p becomes zero. This situation describes Brewster angle where there is no reflection for p-polarized light. The other special case is α - $\beta = \pi/2$ leading to the infinite value for the R_p. This can be achieved when $E_r \Rightarrow 0$. This situation corresponds to resonance. This relation between α and β provides the dispersion relation. In this condition $\cos\alpha$ = -sin β and $\tan\alpha = k_{1x}/k_{1y} = -n_2/n_1$. For the components of wave vector $\vec{k} = (k_x,k_y)$, we can write

$$k_x^2 = k_1^2 - k_{y1}^2 = k_1^2 - k_x^2\frac{\epsilon_1}{\epsilon_2} \tag{1.6}$$

$$k_x = \frac{\omega}{c}\sqrt{\frac{\epsilon_1\epsilon_2}{\epsilon_1 + \epsilon_2}} \tag{1.7}$$

$$k_{yi} = \frac{\omega}{c}\sqrt{\frac{\epsilon_i^2}{\epsilon_1 + \epsilon_2}} \tag{1.8}$$

where ϵ_1 and ϵ_2 are the dielectric constants of materials 1 and 2, respectively. Equations (1.7) and (1.8) are the sought SPR dispersion equations for an interface between two media. When medium 2 is a metal, it has enough free electrons leading to negative dielectric constant at an angular frequency $\omega < \omega_p$

$$\epsilon_2(\omega) = 1 - \frac{\omega_p^2}{\omega^2} \tag{1.9}$$

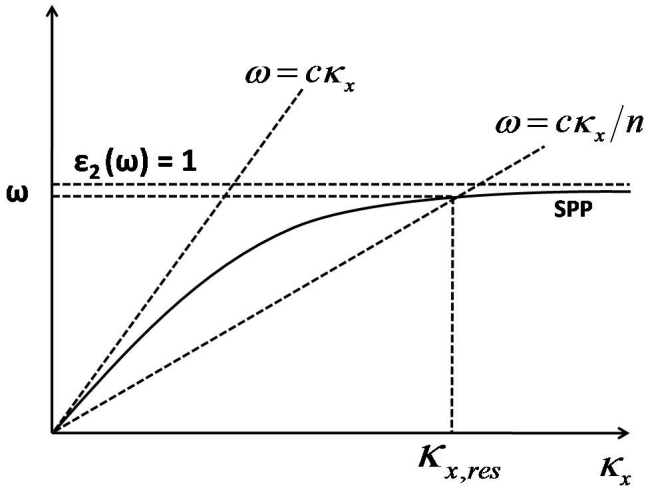

Figure 1.2: Dispersion relation of surface plasmon with free-space light ($\omega = ck_x$) and the light in glass ($\omega = ck_x/n$).

$$\omega_p = \sqrt{4\pi n_e e^2/m_e} \tag{1.10}$$

where ω_p is called the plasma frequency, n_e is the free electron density and e and m_e are the electron charge and mass, respectively. The relation (Equation (1.8)) shows that electromagnetic field having frequency $\omega < \omega_p$ cannot propagate in the metal film. The metal film having $\epsilon_2 > \epsilon_1$, the k_{yi} is imaginary and k_x is real. This shows a electromagnetic wave exist which propagates strictly along the interface. The wavevector (K_{sp}) of the surface plasmon having $\hbar\omega$ energy is always larger than the wavevector of light in free space. The momentum of surface plasmon is large due to the strong coupling between light and surface charges. The electromagnetic field has to drag the surface charges along the metal surface. This shows that the light propagating in free space cannot excite surface plasmons. Thus the wavevector of light has to be increased over its free space value. Figure 1.2 shows that the addition of an interface is a solution to increase the wavevector value of the exciting light above its free space value [1].

Evanescent wave Evanescent waves are excited as the plane wave incident at an angle $\alpha > \theta_c$ on a flat interface between two media of refractive indices n_1 and n_2 as shown in Figure 1.1. θ_c is the critical angle of the interface. Under this condition the light will undergo a total internal reflection. This evanescent wave has a standing wave characteristic with its electric field amplitude exponentially decays along the y-direction. The evanescent field has a mathematical form as indicated in Equation (1.11). The

evanescent waves can have an enhanced intensity than the incident beam due to surface polarization. The metal thin layer on glass surface interface improves the enhancement in intensity. This strong enhancement in intensity is due to the excitation of surface plasmon polaritons (SPP).

$$E = E_o e^{-k_{y_2} y} exp(j\omega t - jk_x x) \tag{1.11}$$

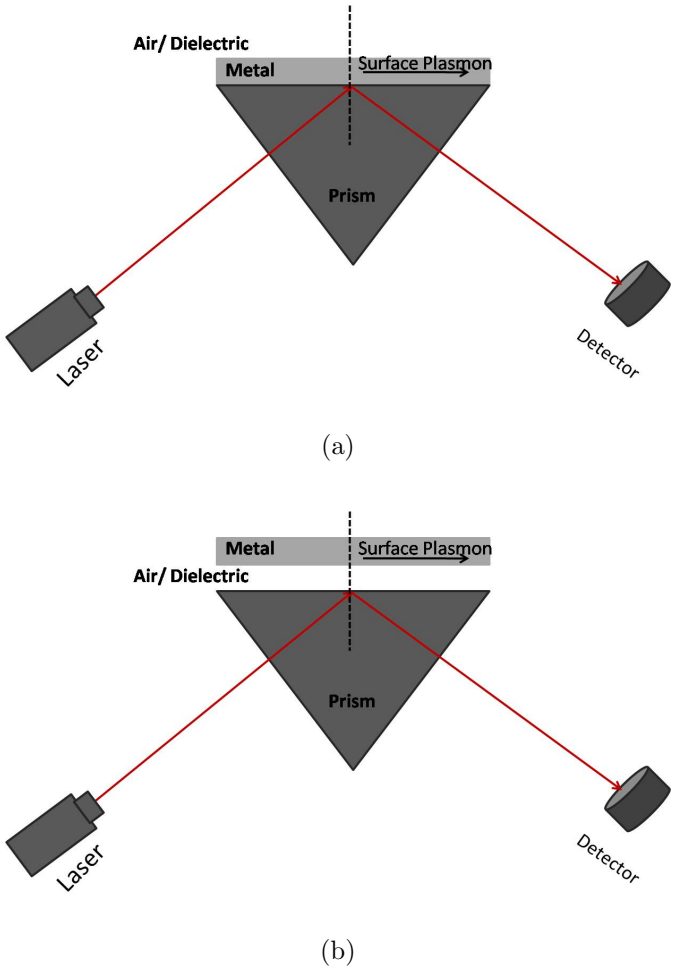

Figure 1.3: (a) Kretschmann-Reather geometry (b) Otto geometry for SPR excitation using prism as waveguide.

The excitation of surface plasmon with the evanescent wave is possible in two configurations: (1) Kretshmann- Reather geometry and (2) Otto geometry. In Kretschmann-Reather geometry (Figure 1.3a), a high refractive index (RI) waveguide (n_w) is interfaced with a metal-dielectric waveguide having thin metal film with permittivity ϵ_m and thickness (t), and a semi-infinite dielectric with a refractive index n_d ($n_d < n_w$). The high

RI waveguide is generally glass prism. Here, the light propagating through the prism is made incident on the metal film. Above the critical angle of the waveguide, the light undergoes total internal reflection. In this condition, a part of the EM energy propagates as evanescent wave. Evanescent wave couples with the surface plasmons on the metal surface when the metal film is sufficiently thin ($t < 100$ nm). The wave-vector of surface plasmons along the thin metal film is influenced by the presence of dielectric on other side of metal film. The change in the dielectric constant on the metal surface leads to the change in wave-vector of surface plasmon wave. This condition alters the wave matching condition and thereby shifts the resonance condition.

The Otto geometry is shown in Figure 1.3b, where the high RI waveguide is interfaced with dielectric-metal waveguide consisting of a thin dielectric film with refractive index n_d ($n_d < n_w$) and thickness (t) and semi infinite metal with permittivity, ϵ_m. Here, the thickness of dielectric layer chosen to be appropriate for the coupling of evanescent wave to the surface plasmon.

The Kretschmann-Reather configuration has flexibility in altering the nature of dielectric layer on the gold surface. In Otto geometry, the dielectric layer deposition is in between wave-guide and the metallic film. The dielectric thickness above a particular value leads to the extinction of evanescent wave intensity without coupling to the metallic surface. This dielectric thickness parameter modulation creates practical difficulties in the detection of analytes. Thus, Otto configuration is least adopted for the commercial sensor development. Kretschmann-Reather proposed configuration is commonly adopted for SPR instrument development.

1.2 Wavelength interrogation based SPR instrument

Wavelength interrogation based SPR instrument records the drop in intensity in the wavelength spectrum of the total internally reflected beam from the sensor assembly (waveguide with metal coated surface) when it is illuminated by collimated polychromatic light beam. The incident optical wave and the surface plasmon wave in the metal couples at a particular wavelength with respect to the coupling condition as discussed earlier. At SPR, the intensity of a particular wavelength extinguishes from the spectrum. The change in the dielectric medium over the metal surface causes change in

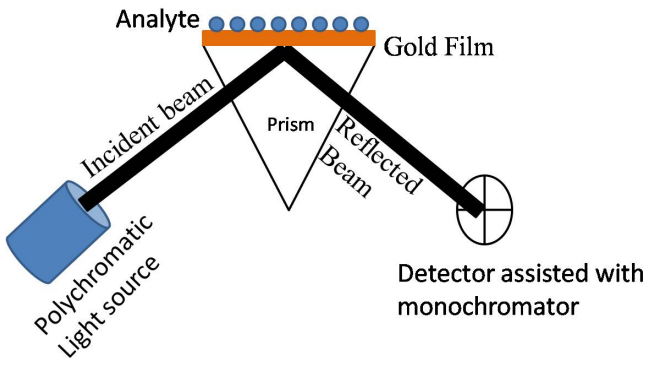

Figure 1.4: The Schematic representation of the prism based wavelength scanning SPR sensor.

the SPR condition and thereby a shift in the resonant wavelength is observed in the spectrum. Therefore, the variations in the refractive index of the sensing medium can be detected by measuring the change in resonant wavelength [9]. The sensitivity of such a system is defined as the ratio of shift in resonance wavelength on analyte adsorption to RI variation of medium containing the analyte [10]. The schematic representation of such a sensor is as shown in Figure 1.4.

In the wavelength interrogation, method white LED is used as the light source and a monochromator is used to record wavelength spectrum. The sensitivity of the instrument is $\sim 5.83 \times 10^{-4}$ RI units [11]. In an interesting SPR setup in the wavelength interrogation method, the source is used as a number of LEDs of five different wavelengths. The angle of incidence was altered by rotating mirror and was fixed at the resonant angle for the central wavelength in the spectrum. The charge coupled device (CCD) camera was used as the detector to record the intensity profile for each wavelength. The interference filters with a full-width half maximum of 10 nm was used to decrease the noise in central wavelength. The setup provides a resolution of 3×10^{-6} RIU. Such a system may become popular because of compactness, economic feasibility and on high sensitivity to analytes similar to a monochromator assisted SPR spectral sensor [12].

1.2.1 SPR instrument with optical fiber as wave-guide

The miniaturization of the wavelength mode SPR sensor is further possible with the introduction of optical fiber as waveguide. In the optical fiber based SPR sensor, the

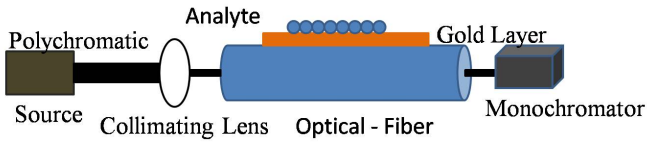

Figure 1.5: The Schematic representation of the fiber-optic SPR sensor.

fiber acts as a coupling medium. The fiber optic based SPR sensor utilizes a standard single mode optical fiber with gold deposition on the cladding stripped region. The guided mode of the light beam excites the SP in the gold layer. SPR sensors using single mode fibers utilize wavelength interrogation mode yielding broad SPR dips caused by the variation on SPR condition along the sensing region leading to low sensitivity to refractive index variation on the metallic surface [13, 14]. The sensitivity is improved using the splicing of single mode fiber to multimode fiber. The spliced region of single mode fiber has gold deposition of 50 nm. The splicing junction acts like prism in Kretschman-Reather configuration. This technology makes the fundamental mode to propagate inside the fiber leads to better sensitivity (6196 nm/RIU) in refractive index measurement [15]. The schematic of a fiber-optic SPR sensor is shown in Figure 1.5.

The multiwavelength SPR techniques described with prism or optical fiber as the sensing element has great portability but lacks resolution and sensitivity in analyte detection. SPR instruments based on these techniques are presently available in the market. The fiber-optic spectrophotometer for the wavelength selection improves the portability of the instrument but results in low resolution and sensitivity to analyte detection. High resolution with cost effective design is possible in an angular based SPR instrument.

1.3 Angular interrogation based SPR sensor

This is the most popular mode of SPR sensor because it provides high sensitivity towards analytes adsorption at very low concentration. In angular interrogation method, the angle of incidence of a tightly focused monochromatic light onto the sensing area via the coupling prism is changed and reflected intensity is collected, simultaneously. The dip in intensity at a particular angle indicates the resonance. The angle of incidence at which SPR occurs is known as resonance angle (RA). Any adsorption on the sensing

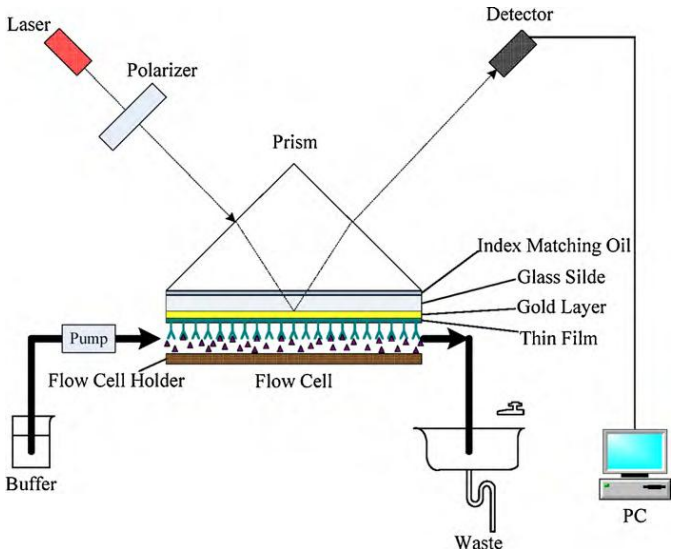

Figure 1.6: The Schematic representation of the angular scan based goniometer assisted SPR sensor [16].

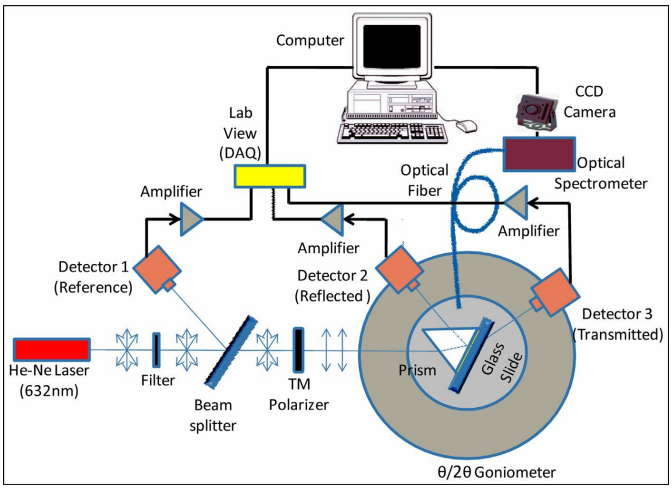

Figure 1.7: The schematic of a SPR instrument with rotating prism-sensor assembly [17].

element causes a shift in the resonance angle. The angular interrogation can be achieved either by rotating prism-assembly or by rotating source and detector, simultaneously. Such a mechanical driven scanning system makes the instrument bulky, costly and complex in operation. In general, the basic SPR instrumentation involves the mounting of optical components on the arms of a goniometer. In this configuration, the angle of incidence and reflection are changed equally, and the reflected intensity is measured, simultaneously [16, 17]. The configuration is shown in Figure 1.6

The another angular interrogation based SPR instrument (Figure 1.7) consists of a goniometer with a mechanism of rotation of prism sensor assembly as shown in Figure 1.6 [17]. The incident angle of the beam with the normal of the prism is varied by rotating a prism. The reflected and transmitted lights are collected using two detectors. The angular resolution obtained in this configuration is 0.01^o–0.001^o. The detector realigment with respect to change in angle of incidence during the rotation of the prism stage causes inconvenience in the operation of SPR instrument. The fixed detector position is desirable to perform the sensitive and convenient scanning in SPR instruments. The fixed detector position irrespective of change in incident angle is achieved by coupling the illuminated prism with another prism [18, 19].

The two-prism configuration has a prism coupled as a wedge at the face of the illuminated prism with an angular separation of Δ through which the reflected light passes after total internal reflection. The configuration results in the reflected beam least vulnerable to lateral motion at the detector. The prism alignment in the configuration is shown in Figure 1.8.

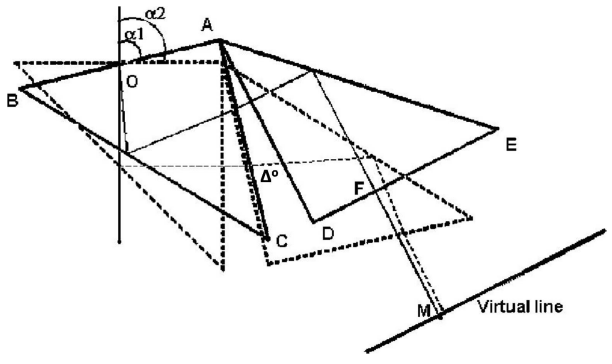

Figure 1.8: The two-prism configuration with $angle = \Delta^o$ between two prisms and ray traces within the prisms. [20]

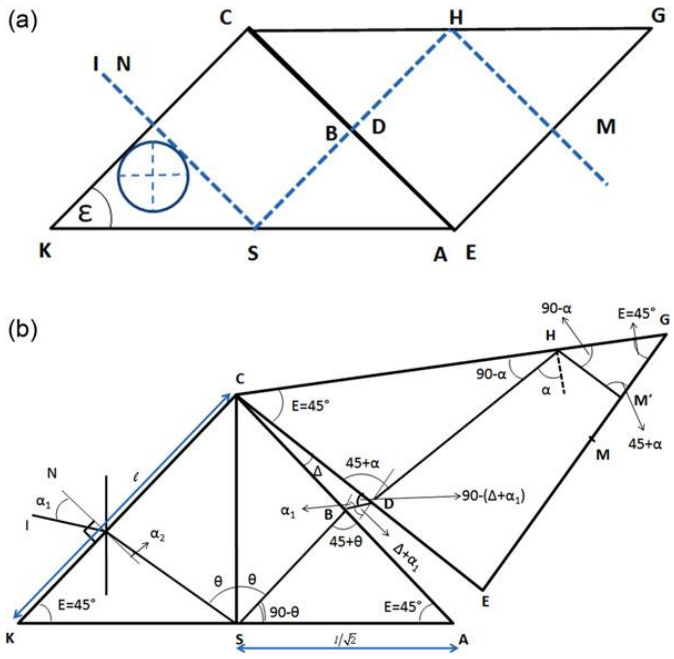

Figure 1.9: The configuration of the two prism SPR system with constant spot interrogation [**?**].

In this configuration, the reflected light beam coincides at the detector at right angles irrespective of the incident angle. This configuration permits side wise deflection of the beam at the detector. The angular scan range decides the extent of side wise deflection. Every range of angular scan, has a respective wedge separation Δ at which the deflection distance minimises like 10^o for the angular scan range of 80^o to 110^o causing a deflection of 1.767 nm and 4^o for the range of 85^o to 115^o respectively [20]. This method provides least lateral motion to the reflected spot for angular scanning SPR instrument but it never fixates the interrogation spot on the gold surface of the prism. This is achieved by the positioning of prism with respect to the axis of rotation (O) of the prism table as shown in Figure 1.9.

The fixed beam spot at the sensing element is enabled through the rotation the second prismto 90^o such that the beam exiting from the first prism passes to the second as a parallel plate.The lateral motion of the reflected spot at the second prism face depends on the separation between the two prism. The lateral motion of the spot over the second prism surface reduces to 0.9 mm for 30^o angular scan range [21]. This methods fixes the photodetector position in rotatory mode of angular modulation in SPR instrument.

The lateral motion of the reflected spot at the second prism face depends on the separation between the two prism. The lateral motion of the spot over the second prism surface reduces to 0.9 mm for 30^o angular scan range [**?**]. This methods fixes the photodetector position in rotatory mode of angular modulation in SPR instrument.

The SPR instruments that employ's the recently mentioned angular scanning methods are not compact due to the requirement of large number of optic components. The large number of optic components increases the alignment difficulties and also affects the stability of the system during transport from one place to another. The optics configuration with least number of optical elements and a proper simple scanning mechanism overcome these problems related to the instruments. The following description gives a brief introduction about an optical configuration and a relatively simple scanning mechanism which utilizes least number of optical components and have a sensitivity comparable to commercially available SPR instruments.

We adopted a new opto-mechanical scanning mechanism to obtain the SPR spectra in the high sensitive angular interrogation mode without employing a goniometer. Here, the laser as well as the detector is kept stationary. As the angle of incidence changes due to rotation of the scanning mirror, the reference spot position on the gold surface shifts and as a consequence the spot of reflected beam on the quadrant photodiode (QPD) shifts. In order to retain the spot position fixed onto the gold surface, the prism-sensor assembly is translated vertically till original reference spot position is regained. Under this condition, the total internally reflected intensity and the angle of incidence are recorded. The proposed scheme employs only a few number of optical components with and therefore the overall optical complexity, size and mass of the instrument reduces, and thereby increases the portability of the instrument.

SPR Spectrum (I Vs θ) : SPR spectrum is the variation of reflected intensity as a function of incident angle of the p-polarized light. The angle at which the maximum loss of the reflected intensity occurs is called as the SP resonance angle or (RA) angle. The SPR spectrum for gold (metal) in contact with air (dielectric) is shown in Figure 1.10. The resonance angle of gold-air interface deflects (shift) with the deposition of a single layer of mercaptoundecanoic acid (MUA) on gold surface as shown in Figure 1.11.

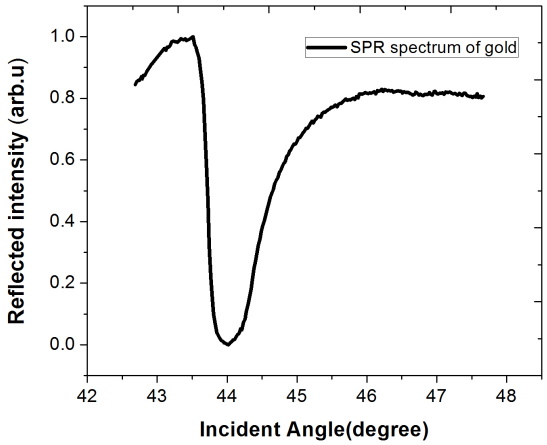

Figure 1.10: The SPR spectrum from gold-air interface. The SPR angle is found to be 44^o.

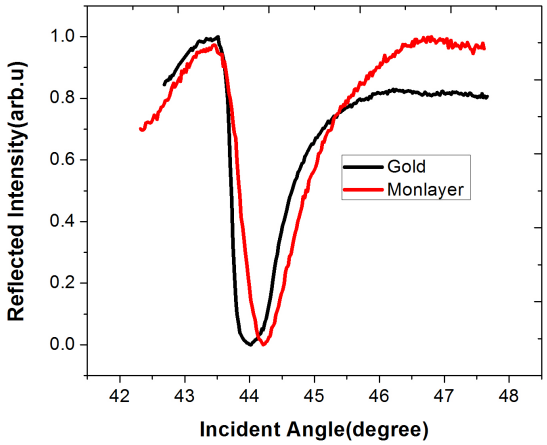

Figure 1.11: The SPR spectra of gold-organic monolayer interface. The SPR angle shift is found to be 0.11^o.

Calibration curve : SPR instruments are characterized in terms of its sensitivity (S) toward any analyte detection. The sensitivity of the instrument is its capability to resolve the very close refractive indices of two dielectric materials. SPR instruments sensitivity is given in terms of refractive index units (RIU). It is calculated from the RA shift values (ΔR) for solutions of various concentration of same analyte in the same solvent with known values of refractive index (RI). The refractive indices of the solutions are plotted against the respective RA angle. This is also known as calibration curve. The slope of the calibration curve () provides the respective sensitivity of the instrument.

$$S = \frac{d(\Delta R)}{d(RI)} \tag{1.12}$$

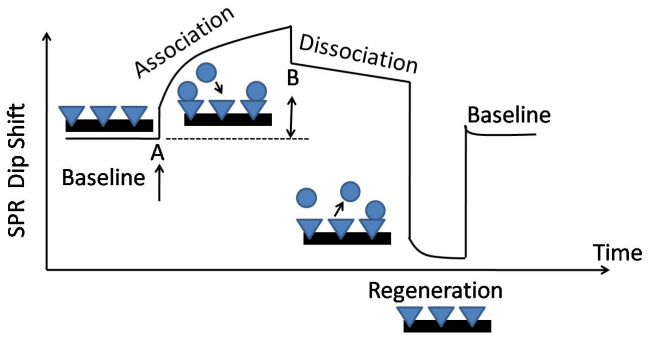

Figure 1.12: The SPR sensorgram showing the steps of kinetic cycle analysis. The point "A" and "B" shows the bulk refractive index shift on injections of analyte solution as well as on buffer solution over the functinalized surface.

Kinetic curve : SPR is an excellent method to record refractive index changes due to the adsorption of analyte on to the metal surface. Figure 1.12 shows the shift in SPR angle (ΔR) on change of dielectric material over the metal surface. The shift in minimum intensity position from the reference position with respect to time yields the instantaneous change in refractive index at the metal-dielectric interface. The instantaneous shift in SPR angle (Δ R) for a small angular shift range of $1 - 3^o$ is measured by recording the change in intensity (δI) in that particular time [22]. Such an instantaneous record of SPR angle during any molecule specific interaction yields sensorgram. The kinetic parameters of molecular interactions can be determined from the recorded sensorgram. A typical sensorgram is shown in Figure 1.12.

The SPR sensors are used for various sensing applications due to its versatility and high sensitivity to analytes. The method is label free in nature. Thus, it is widely used in biosensing and biomedical application. It has application in the detection of harmful chemicals and noxious gases. Some of the applications are briefly described in the following section :-

Gas sensing : The nitrogen dioxide (NO_2) is one of the harmful gas for living being. Short term exposure itself may lead to inflammation in respiratory organs. This is one of the common air pollutants and has to be monitored regularly. Sensor based on SPR is used for the detection of NO_2 in air. There is a report wherein spin coated phthalocyanine over the gold surface was used as the functional layer for the detection of NO_2 gas. The lowest detectable concentration of NO_2 was found to be 1 ppm [23]. The SPR sensor possessing one active layer for the detection of a particular gas molecule fails to detect due to the presence of a variety of gas molecules. This is lack of selectivity of the sensor and one of the toughest challenges in the world. The tin oxide layer on gold surface improves not only the sensitivity but also the selectivity of gas sensor. The lowest detection limit of 100 ppm for nitrogen oxide-nitrogen dioxide mixture was achieved [24]. The SPR sensor is developed with polyethylene glycol ($n = 600$) and is employed for sensing hydrocarbons, aldehydes and alcohols. The calibration curves for each of these species showed different sensitivity and therefore indicated the possibility of selective detection of such gas molecules [25]. In an interesting work by Bingham et al [26], the sensing of inert gas molecules e.g. He, Ar and N_2 was studied using the localized SPR phenomenon in silver and gold nanoparticles. A change in refractive index $\sim 2.45 \times 10^{-4}$ refractive index unit (RIU) was measured reliably and reproducibly. The sensitivity was observed as $\sim$ 200 nm/RIU. This indicates that the localized SPR technique is highly sensitive and reliable even for the inert analytes during the detection process. The SPR sensors which are based on angular or wavelength scanning modes employ prism as a wave-guide. Therefore, such instruments are neither portable nor modular to perform geometrically confined localized as well as remote experiments. The SPR sensor based on optical-fiber technology can be portable and field deployable. The fiber-optic SPR sensors are used for the detection of gases in remote areas. The reported ammonia sensor utilizing the fiber-optic SPR technique possesses polyaniline film on indium tin oxide (ITO) as the sensing layer. The sensor performs in wavelength interrogation mode.

The lowest detection limit for ammonia with such a sensor is 10 ppm [27]. The doping of nickel oxide with ITO for the deposition of sensing layer on the fiber improves the sensitivity of fiber-optic sensor for the hydrogen sulphide gas [28].

Chemical sensing : Nonylphenol is an organic material that is generally used in oil, laundry and detergent industries. It is non-biodegradable and can pollute the aquatic resources. Human can consume nonylphenol through fish and other edible water resources. The pollutants can lead to imbalance in hormonal secretion and may lead to cancer. It can present in river water ~ 4 ng/L. SPR technology is used for the detection of nonylphenol in shell fish [29]. The functional layer on the gold layer was created by immobilizing 9-(p-Hydroxyphenyl) nonanoic acid on dextran matrix using amine coupling chemistry. The lowest detectable concentration of nonylphenol was 0.2 ng/L. In the fish samples, nonylphenol was detected as low as 10ng/g. SPR sensor can be utilized for the detection of glucose level in diabetic patients. The detection of glucose was performed in wavelength mode with prism as the wave-guide. The detection limit of the sensor is 8.67×10^{-6} RIU which is equivalent to 6.23 mg/dL of glucose in water [30]. Quality of the milk available in market may have contaminants that are harmful to human body. Such contaminants can be easily detected using the SPR sensors. The reported method detects staphylococcal enterotoxin B contaminant in milk using the SPR technique. The sensor works in wavelength mode with a prism as the optical waveguide. The detection sensitivity is found out to be 5ng/ml without the functionalization of sensing element. The functionalization provides a lowest detection limit of 0.5ng/ml [31]. In order to improve the milk yield, the cows are treated with recombinant bovine somatotropin (rBST). However, the studies showed that the milk from the treated cows can possesses insulin-like growth factor (IGF-1) with rBST. IGF-1 can lead to cancer and is a potential threat to human health. Guidi et al [32] have developed a solid phase enzyme-linked immunoassay (ELISA) and characterized the hyperimmune polyclonal-anti- IFG-1 antibodies with respect to its specific binding to IGF-1. Such antibodies were used as functional material and a lowest detectable level of IGF-1 in milk was detected as 1 ng/L. The detection is automated and real time. Heavy metals in potable water pose serious threat on human health. Potable water gets contaminated with heavy metal due to industrial discharge and other form of pollutions. The detection of heavy metal in water can be achieved using SPR technology. The squarylium dye (SQ) changes refractive

index of a copolymer on interaction with copper ion (Cu^{2+}). A thin film of consisting of copolymer, polyvinyl chloride-polyvinyl acetate-polyvinyl alcohol, SQ and others was deposited onto the gold surface. Such functional layer was employed for the detection of different alkali metals, alkaline earth metals and transition metal ions. The SPR sensor showed highest selectivity for the Cu^{2+} ions. The lowest detectable concentration of the ion was reported to be 1 pM [33]. In another interesting work, the functional layer for the detection of heavy metal was created using metallothinein protein [34]. Such sensor was employed for the detection of Cd, Zn and Ni in buffer at concentration down to 100 ng/mL. The online (invitro) detection of chemicals in fluids is possible with the help of optic fiber SPR probe. The fiber-optic probe for the detection of urea is such an example for online chemical sensor. The sensor works in wavelength mode wherein the sensing element is functionalized with specific enzyme, urease onto silver layer. The sensitivity of the sensor is improved by the addition of silica layer between silver and the enzyme. This silica layer will protect silver from oxidation and improves the enzyme reactivity. The sensor is able to perform well for the urea concentration range of $0-160$ mM [35].

Biosensor : SPR is very popular for biosensing application because it provides not only label-free measurement but also very sensitive to the targeted analytes. Some of the interesting biosensing application using SPR technology is discussed below. The sensitivity of the SPR biosensor with bare metal surface is less due to the inertness of noble (gold) metals towards any other chemical species. In order to establish the molecular specific interaction, the metal surface should be treated chemically to yield specific functionalization. The self assembled monolayer (SAM) of organothiols is stable in nature over the noble metal (gold) surface. The SAM of such organothiol can act as a platform for immobilization of any ligands. This is the essence of any biosensor with appropriate functionalization of the gold surface. The SPR sensor for the detection of cardiac muscle death in less than 10 minutes was achieved. Myoglobin and cardiac troponin I are known to be the markers for cardiac muscle injury. The antibodies of the specific antigens were developed and were immobilized to the carboxymethylated dextran layer on a gold surface. The troponin level lies in the range of $1-3$ ng/mL in the human blood after the myocardial damage. Using the SPR sensor, the lower detection limit of myoglobin and troponin was found to be 2.9 and 1.4 ng/mL [36]. Prostate specific

antigen (PSA) is a marker for prostate cancer. The healthy level of PSA in serum <4 ng/mL. Monoclonal antibodies against PSA was immobilized onto the sensing surface of SPR instrument and it was used for the detection of PSA. The lowest detectable limit was found to be 0.15 ng/mL [37]. The graphene layer is one of the candidate which can enhance the sensitivity of the SPR sensor [38]. The graphene sheets having carboxylic acid group can bind with the biomolecules through amine linking chemistry. This stable adsorption of biomolecules over sensing layer enhances the sensitivity of SPR biosensors [39]. The utility of SPR biosensing application can be enhanced using the optic fiber sensor. A novel smartphone based optic fiber SPR sensor was developed. Here, the flash light present in the phone act as the light source and the camera of the phone acts as the detector. The sensor utilizes the relative intensity change as the signature of binding between analyte and ligand. This sensor has a detection limit of 47 nM for the IgG protein [40].

Others : The SPR sensors are used for the detection of change in dielectric properties of molecular fluids. A study was conducted for the detection of cation and anion in solution using SPR sensors. The authors have used the electric field assisted method for the detection of cations and anions. They recorded change in intensity of reflected light as the measure of adsorption of cations or anions absorbed on the metallic surface [41]. The side polished fiber based refractive index wavelength sensor provides the detection of refractive index (RI) of liquids having RIU 1.32 to 1.40 with sensitivity up to 4365.5 nm/RIU and a figure of merit (FOM) of 51.61 RIU^{-1} [42]. Prism based SPR sensor is used to measure the optical anisotropy in the thin films of molecules. The method utilizes the anisotropic molecular layers obtained through various thin film deposition techniques like spin coating and Langmuir-Blodgett (LB) technique [43]. The refractive index measurements in two orthogonal directions yield remarkably different values. Wang et al have shown the SPR phenomenon can be employed for voltage driven tunable optical filter. In their interesting work, the RI of the gold/liquid crystal interfaces was altered by the application of electric field. For a given applied voltage, due to resonance condition, a band of wavelength was found to be absorbed in the reflected beam leading to the appearance of complimentary color in the reflected light. Such technique can be equally applied for the development of tunable infrared filter [44].

The SPR phenomenon is widely used in the modern sensing technology. The selectivity of analytes is still a big challenge in the field. Major scientific attentions are now devoted towards the development of specific SPR sensor which can yield reliable and reproducible data. Some of the latest development in the field are sensing through SPR imaging, SPR fluorescence, and electrochemical SPR.

This thesis work is based on the following objectives

- Development of surface plasmon resonance instrument with following essential features : Portable, sensitive, low cost.
- Development of a novel opto-mechanical design which can eliminate the bulky and complex goniometer.
- Development of the unique feedback mechanism for a fixed spot angular interrogation.
- Development of a low cost flow cell.
- Development of software for control and data acquisition.
- Testing and calibration of the instrument using ultrathin films.

Bibliography

[1] Principles of Nano-Optics,Lukas Novotony and Bert Hecht, Cambridge(2006).

[2] Handbook of Surface Plasmon Resonance, Richard B M Schasfoort and Anna J Tudos, RSC publishing.

[3] R.W.Wood,Philos.Mag.,1902,4,396.

[4] E.Kretschmann and H.Raether,Z.Naturforsch,.1968,230,2135.

[5] Turbadar T, Proc Phys Soc, 1959,73,40.

[6] Otto A, Zeits Phys, 1968, 216, 398.

[7] Pockrand I, Swalen JD, Gordon JG, Philpot MR, Surf Sci., 1978, 74, 237.

[8] Handbook of Surface Plasmon Resonance, Richard B M Schasfoort and Anna J Tudos, RSC (2008).

[9] J. Homola, Sens. Act. B, 1997, 41, 207.

[10] A. Shalabney, C. Khare, B. Rauschenbach, and I. Abdulhalim, Sens. Act. B, 2011, 159, 201.

[11] Knut Johansen, Hans Arwin, Ingemar Lundstro, Bo Liedberg, Rev. Scie. Instr., 2000, 71, 3530.

[12] A. Sereda, J. Moreau, M. Canva, E. Maillart, Biosensors and Bioelectronics, 2014, 54, 175.

[13] Radan Slavik, Jiri Homola, Jiri Ctyroky, Sens. Act. B, 1999,54, 74.

[14] Sachin K. Srivastava, Roli Verma, Banshi D. Gupta, Sens. Act. B, 153, 194.

[15] Zhihai Liu, Yong Wei, Yu Zhang Bo Sun, Enming Zhao, Yaxun Zhang, Jun Yang, Libo Yuan, Sens. Actuators B, 2015, 221, 1330.

[16] Y. Liu, S. Xu, B. Tang, Y. Wang, J. Zhou, X. Zheng, B. Zhao, and W. Xu, Rev. Sci. Instr., 2010, 81, 036105.

[17] Huamin Liang, Heini Miranto, Sens.Act.B, 2010, 149, 212.

[18] Kunal Tiwari, Suresh C. Sharma, Sens.Act. A, 2014, 216, 128.

[19] Yu Liu, Shuping Xu, Bin Tang, Ye Wang, Ji Zhou, Xianliang Zheng, Bing Zhao, and Weiqing Xu, Rev. Scie. Instr., 2010, 81, 036105.

[20] Bhaskar Chandra Mohanty , S. Kasiviswanathan, Rev. Scie. Instr., 2005, 76, 033103.

[21] K. Sathiyamoorthy, B. Ramya, Sens.Act. A., 2013, 191, 73.

[22] N.J. Tao, S. Boussaad, Rev. Scie. Instr., 1999, 70, 4656.

[23] John D. Wright, Arielle Cado, Stanley J. Peacock, Vincent Rivalle, Ann M. Smith, Sens. Actuators B., 1995, 29, 108.

[24] Dongfang Yanga, Hui-Hsin Lub, Bo Chena, Chii-Wann Linb, Sens. Act. B., 2010, 145, 832.

[25] M. Miwa, and T. Arakawa, Thin Solid Films, 1996, 466, 281.

[26] J. M. Bingham, J. N. Anker, L. E. Kreno, and R. P. V. Duyne, J. Am. Chem. Soc., 2010, 132, 17358.

[27] Satyendra K. Mishra, Deepa Kumari, Banshi D. Gupta, Sens. Act B., 2012, 171, 976.

[28] Satyendra K. Mishra, Samta Rani, Banshi D.Gupta, Sens.Actuators B., 2014, 195, 215.

[29] J. V. Samsonova, N. A. Uskova, A. N. Andresyuk, M. Franek, and C. T. Elliott. Chemosphere, 2004, 57, 975.

[30] W. W. L a m, L.H. Chu, C.L. Wong, Y.T. Zhang, Sens. Act. B., 2005, 105, 138.

[31] Jiri Homola, Jakub Dostalek, Shengfu Chen, Avraham Rasooly, Shaoyi Jian, Sinclair S. Yee, International Journal of Food Microbiology, 2002, 75, 61.

[32] A. Guidi, L. L. Robbio, D. Gianfaldoni, R. Revoltella, and G. D. Bono, Biosens. Bioelect., 2001, 16, 971.

[33] K. Ock, G. Jang, Y. Roh, S. Kim, J. Kim, and K. Koh, Microchem. J., 2001, 70, 301.

[34] L. P. Wu, Y. F. Li, C. Z. Huang, and Q Zhang, Anal. Chem., 2006, 78, 5570.

[35] Priya Bhatia, Banshi D.Gupta, Sens.Act. B., 2012, 161, 434.

[36] J. –F. Masson, L. Obando, S. Beaudoin, and K. Booksh, Talanta., 2004, 62, 865.

[37] G. A. J. Besselink, R. P. H. Kooyman, P. J. H. J. van Os, G. H. M. Engbers, and R. B. M. Schasfoort, Anal. Biochem., 2004, 333, 165.

[38] R. Verma, B. D. Gupta, and R. Jha, Sens. Act. B., 2011, 160, 623.

[39] Nan-Fu Chiu, Teng-Yi Huang, Sens. Act. B, 2014, 197, 35.

[40] Yun Liu 1, Qiang Liu, Shimeng Chen, Fang Cheng, Hanqi Wang, Wei Peng, scientific reports. 2015, 1.

[41] H. Ko, J. Kameoka, and C. B. Su, Sens. Act. B, 2009, 143, 381.

[42] J. Zhao, S. Cao, C. Liao, Y. Wang, G. Wang, X. Xu, C. Fu, G. Xu, J. Lian, and Y. Wang, Sens. Act B., 2016, 230, 206.

[43] V. P. Devanarayanan , V. Manjuladevi , M. Poonia , R. K. Gupta , S. K. Gupta , and J. Akhtar, J. Mol. Struct., 2016, 281,1103.

[44] Y. Wang, Appl. Phys. Lett., 1995, 67, 2759.

Chapter 2

Instrumentation

In this chapter, we discuss about the instrumentation of the developed SPR instrument. The developed instrument functions in angular interrogation mode based on Kretschmann configuration. The prism-sensor assembly comprises of a semi-cylindrical prism coupled to glass substrate of same refractive index through refractive index matching oil. The glass substrate is deposited with a very thin layer of noble metal (e.g. gold) on one side. The thin layer of gold is deposited using the traditional e-beam, sputtering or thermal evaporation techniques. In the developed instrument, the laser and the detector are kept stationary. The angle of incidence of the beam at the prism-sensor assembly changes by rotating a mirror. The change in angle of incidence onto the gold surface by the rotating mirror causes a lateral shift of beam position on the gold surface. Such shift in the beam position can shift the reference point under investigation and therefore it is undesirable. The shift in beam position at the gold surface is detected by observing change in intensity distribution at a quadrant photodiode detector. The prism-sensor assembly is translated in vertical direction so that the position of beam on the gold surface is retained fixed. This mechanism of scanning ensures the constant interrogation position on the sensing area. This makes the instrument reliable and provides error free data. The novel scanning mechanism makes the instrument simple, compact and portable with high degree of accuracy in refractive index measurements as compared to other available SPR instruments. The design of the instrument is shown in Figure 2.1. Laser beam is reflected by a piezomotor controlled rotating mirror. The beam reflected from a mirror is made incident at an angle higher than the critical angle of the prism-sensor assembly. The total internally reflected beam from the prism-air interface falls at a detector. The photo-detector is wired to a data acquisition hardware (DAQ). DAQ

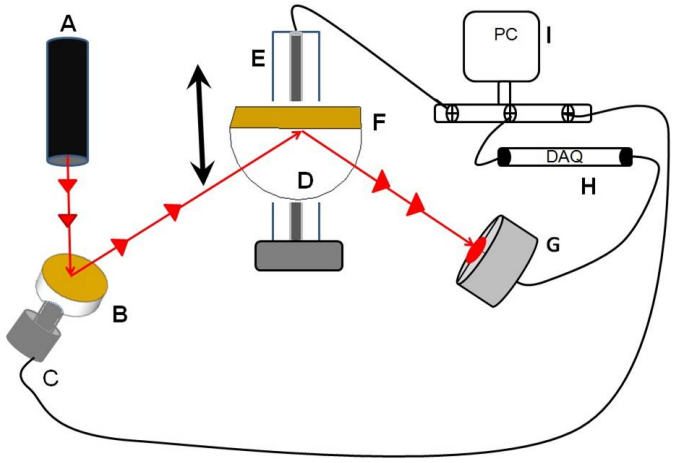

Figure 2.1: Schematic diagram of the SPR instrument. The major components are as follows - A: Laser, B: Mirror, C: Piezomotor, D: Prism, E: Translation stage, F: Gold coated substrate, G: Photodetector, H: Data acquisition hardware, I: Computer.

converts the analog voltage from the photodiode to a digital format and feeds to the computer. The details of the components involved in the developed instrument are as follows:

2.1 Major components

2.1.1 Laser (A)

A laser diode (LPM series, Newport, USA) with an operating voltage of 5 V dc having power stability of better than 5% used as the light source in the instrument. Laser diode assembly includes a convex lens to provide focused plane polarized beam of wavelength 635 nm. The beam width is regulated with the rotation of this lens using manufacturer provided spanner wrench. The laser assembly is encapsulated in black anodized cylindrical case (mount). The laser beam is adjusted to p-polarization by the rotation of laser assembly within the mount. The power stability of the laser is checked by recording intensity with the time using a power meter (ILX, Light wave). The average value of power for the given time is 2.153 mV and the standard deviation of power for the same duration was calculated to be $\pm 4.03\mu$ V. Therefore the standard deviation is merely $\pm 0.2\%$ of the average power. The trend in the graph also indicate that the intensity fluctuation improves with increasing time. The large fluctuation in intensity can cause

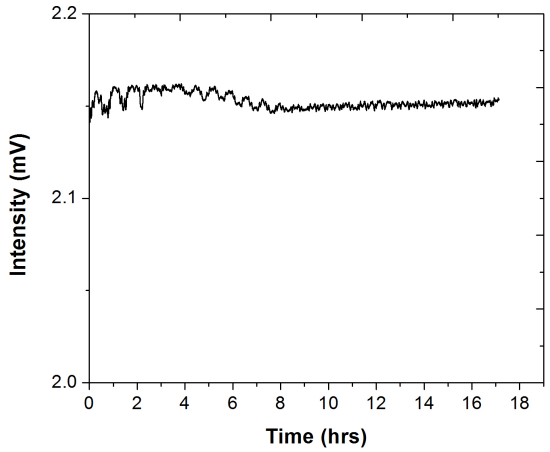

Figure 2.2: The power stability curve of the laser obtained by recording intensity with time using a power meter (ILX Light Wave).

difficulties in determination of resonance angle of a given system. The large fluctuation in intensity value suppresses the SPR characteristic curve leading to sensitivity to change in refractive index due to adsorption of analytes. The simultaneous subtraction of reference beam intensity from the recorded SPR intensity suppresses such laser induced intensity fluctuations and thus can improve the sensitivity of sensor [1]. This method requires the introduction of optical components for the division of laser beam into two beams of different polarization (s and p) of equal intensity. This introduction of optical components always affect the compactness of the system. The stable laser based SPR instrument does not need reference intensity subtraction. This makes SPR instruments very compact.

2.1.2 Mirror (B)

A cylindrical glass piece of 2.5 cm in diameter and 1.5 cm in thickness, deposited with 200 - 500 nm of sputtered silver layer is used as the mirror. The mirror is procured from Optiregion, Delhi. The mirror has a reflectivity of 98% in the wavelength range of 400-700 nm.

2.1.3 Piezomotor (C)

The mirror (F) is coupled to a piezomotor (A) and the angle of incidence is changed very precisely by driving the motor. The schematic is shown in Figure 2.5. The motor (LR 80, Piezomotor Co-Operation, Sweden) works under piezoelectric phenomenon. The direct drive ensures the motion without backlash. The piezomotor with a microposition controller (PMD 90) provides the precisely controlled rotation of the mirror with a resolution of $2.1m^o$. The compact size with high-torque output of 55 Nm is a unique characteristic of the motor. The motor is driven by the serial port based communication. The motor is encapsulated in an aluminium open cylinder having a dimension of 5 cm in diameter and 2 mm in thickness with the provisions to hold the motor fixed.

2.1.4 Prism (D)

The SPR instrument consists of a semi-cylindrical glass prism (Optiregion, Delhi) of material BK7 having refractive index of 1.51. The rectangular surface of the prism has a dimension of 2.5 cm $\times$ 2 cm (l $\times$ b). The diameter of the semi-cylinder is 1.7 cm.

2.1.5 Substrate (F)

The direct deposition of gold on the prism surface for the generation of SPP causes inconvenience in surface regeneration process. Therefore, the gold layer can be deposited onto the glass substrate exhibiting the same refractive index value (i.e. 1.51). The glass substrate can be coupled to the prism by using a refractive index matching oil (Cargille, USA). This assembly makes the SPR instrument practically convenient. The substrates are procured from Optochem International, Delhi. The procured substrates are of 0.5 mm thickness and of dimension 2.5 cm $\times$ 2 cm (ℓ $\times$ b). Substrates are initially treated with acetone followed by piranha solution (Conc. H_2SO_4, H_2O_2, ratio of 1 : 3). The gold adhesion to the cleaned bare substrate surface is poor. The poor adhesion of gold layer to the bare substrate surface leads to the removal of gold layer during the rejuvenation treatments to the gold surface. The gold surface is rejuvenated after the sensing process of analytes through mild oxidation of gold layer. A prior deposition of adhesion layer of titanium or chromium of thickness 3 - 5 nm improves the adhesion of gold on substrate surface and protects the gold film during the rejuvenation treatments. However, the thicker adhesion layer dissipates the evanescent waves largely and hence SPP does not

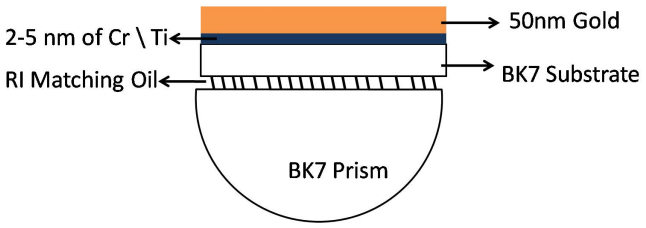

Figure 2.3: The prism-sensor assembly.

get excited on the gold surface. The prism-sensor assembly with different layers is as shown in Figure 2.3.

The gold layer should be functionalized to attract specific analyte. Therefore, the surface of gold will be tailored by the deposition of self assembled monolayers (SAMs). Such SAMs can facilitate the immobilization of appropriate ligand.

2.1.6 Photodetector (G)

In the proposed SPR instrument, not only the reflected intensity is measured but also the deflection in the reflected beam should be monitored. This can be achieved by employing a segmented photodiode. In our setup, we have used a quadrant photodiode (QPD) for the dual purpose as mentioned above. The detector is active in the visible and near infra-red region of electromagnetic spectrum. The detector has four segments having individual positive terminals and a common ground. The center diameter of the photodiode is 2.5 cm with an active area of 1 cm in diameter. The detector is encapsulated in an open plastic cylindrical enclosure which acts as a mount having threaded screw provisions of 3 mm for its attachment to optical post. The mount acts as a supporting structure for the terminal wires and protect them from any breakage. The terminals of the detector are connected to the data acquisition hardware (DAQ) for analog to digital data conversion. Segmented nature of the detector helps in monitoring the reflected beam deflection due to change in angle of incidence. The intensity distribution at the segments of the photodetector varies with the change in incident angle at the prism-sensor assembly. Total intensity is the sum of the individual quadrant intensities.

A Bi-cell can also be used for the measurement of reflected intensity of the laser beam. However, Bi-cell fails to detect the deflection of beam out of plane of polarization. The

degree of lateral motion of the beam shows the in-plane optical alignment of constituent optical elements. The null deflection value in QPD shows the in-plane alignment of optics in the instrument. Bi-cell can be used for the record of intensity after the alignment of optics.

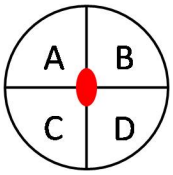

(a) $SD = 0 \Rightarrow$ The initial position of the spot (solid ellipse) at the detector before the rotation of mirror.

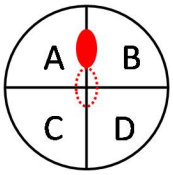

(b) $SD = +ve \Rightarrow$ The deflected spot (solid ellipse) from the initial position (dotted) after the rotation of mirror to $-\theta$ deg.

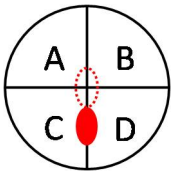

(c) $SD = -ve \Rightarrow$ The deflected spot (solid ellipse) from the initial position (dotted) after the rotation of mirror to $+\theta$ deg.

Figure 2.4: The schematic showing the spot position of the reflected beam on QPD. A, B, C, and D are the 4 segments of the QPD

Figure 2.4a shows the initial position of the reflected beam spot at the photo-detector. Here, the spot is at the center of the segmented detector with segments A, B, C and D. If the value of intensities in the segments A, B, C and D are I_A, I_B, I_C and I_D respectively, then the spot deviation (SD) in vertical direction is defined as Equation (2.1).

$$SD = (I_A + I_B) - (I_C + I_D) \tag{2.1}$$

and the total intensity (I_T) is calculated by adding the intensities from all segments as given in Equation (2.2).

$$I_T = I_A + I_B + I_C + I_D \tag{2.2}$$

When the angle of incidence (θ_i) of the beam changes to lower angle (Figure 2.4b), the spot moves from the center of the segments to the top half leading to the positive SD value. The spot deflects to the lower half of the detector as the incident angle changes to higher value. This can lead to negative value of SD. Similarly, if the beam deflects sideways (horizontally) the intensity distribution changes in the quadrants. Such deflection in the reflected beam can be quantified using the Equation (2.3).

$$SD_1 = (I_A + I_C) - (I_B + I_D) \tag{2.3}$$

Data Acquisition (DAQ) hardware) (H) : Data acquisition hardware (DAQ) converts the analog signals to digital signals. We have used DAQ card from National Instrument Corporation, USA (NI USB-6009). The DAQ has eight analog input channels, two analog output (AO) channels, 12 digital input/output (DIO) channels, and a 32-bit counter with a full-Speed USB interface. This has 4 differential channels and 8 single ended channels with an analog input resolution of 14 bits per second. The accuracy of detection varies with the voltage range. The detection accuracy is 7.73 mV for the maximum voltage range of -10 V to +10 V and 1.53 mV for the minimum voltage range of -1 V to +1 V. The size of the DAQ is 8.51 cm × 8.18 cm × 2.1 cm. The photodetector terminals are connected to the analog inputs of the DAQ. The DAQ converts the analog signals from the individual quadrants of the photo detector to their respective digital signals and feeds to the computer. The computer program is developed in LabView platform to record the intensity and to detect the spot deviation.

2.1.7 Scanning mirror assembly

The schematic of scanning mirror assembly is shown in Figure 2.5. Hollow aluminium cylindrical mount (E) with a dimension of 2.6 cm in outer diameter and 2 mm thickness is used to hold the mirror. A mirror (F) is coupled with a piezomotor (A) and the angle of incidence is changed very precisely by driving the motor. Hollow copper cylinder (C) of dimensions 3 mm in diameter and of equal thickness with a screw is used to connect the shaft of the piezomotor and the mirror assembly.

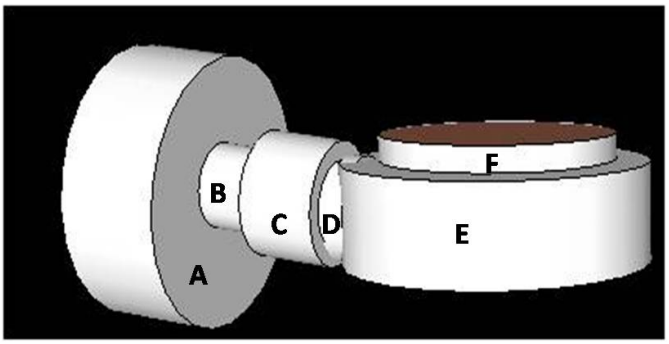

Figure 2.5: The piezomotor mirror assembly. A: Piezomotor, B: Piezomotor shaft, C: Coupler, D: Shaft of mirror assembly, E: Mirror holder, F: Mirror.

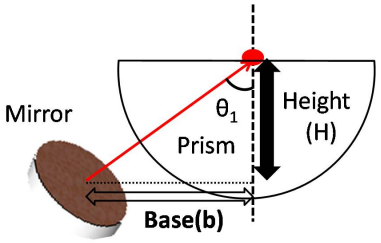

(a) $\tan\theta_1 = \frac{b}{H}$.

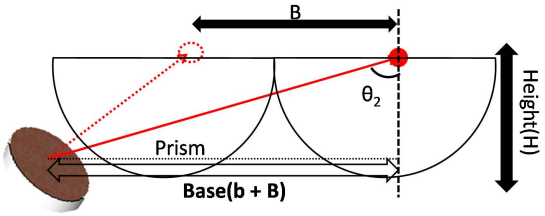

(b) $\tan\theta_2 = \frac{b+B}{H}$.

Figure 2.6: The angular deflection from θ_1 to θ_2 on horizontal translation of the prism (e.g. 45^o to 55^o, 65^o to 80^o).

2.1.8 Translation stage (E)

In our design, the prism-sensor assembly has to be translated vertically so as to retain a fixed interrogation spot on the sensing element (gold surface). The prism-sensor assembly also requires horizontal translation so as to change the range of angular scan. The translation of the prism sensor assembly is achieved by mounting it on bi-directional translation stage (Holmarc Optomechatronics, Kochi, India). The translation stage has a resolution of 0.15 micron per step. The motor has a torque of 10 Kg-cm. The stage was made of black anodized aluminium alloy with threaded holes for 6 mm and 4 mm diameter screws. The controller of the translation stage communicates with a computer through RS 232 port.

Figure 2.6 shows a schematic for changing the range of angular scan by translating the prism-sensor assembly horizontally. The maximum vertical translation of the prism-

sensor assembly was limited by the vertical range of the translation stage. In the present case it was 2.54 cm. Therefore for a given optical setup, the initial angle of incidence will be $\theta_1 = \tan^{-1}\frac{b}{H}$, where b and H are as indicated in the Figure 2.6. If the prism-sensor assembly is translated to the maximum limit of 2.54 cm, then the final angle of incidence will be $\theta_1' = \tan^{-1}\frac{b}{H-2.54}$. Thus an angular range of θ_1 to θ_1' is obtained for SPR scanning. In order to select another angular range of θ_2 to θ_2', the prism-sensor assembly is translated horizontally by an amount of B as shown in Figure 2.6b.

2.2 Optics Alignment

The p-polarized laser beam that has an electric field parallel to the plane of incidence act as the source of light for the SPR instrument. The mirror assembly shown in Figure 2.5 is clamped underneath onto the same post that has the laser assembly. This kind of optical assembly of components ease out the mutual alignment adjustments convenient. The proper alignment of the laser with the mirror makes the reflected beam track a straight line during the rotation of mirror. At zero degree angle of incidence, the reflected beam joins with the incident beam of the laser. The p-polarized in-plane laser beam can excite the surface plasmon at the gold surface. The prism-sensor-assembly is clamped to the vertical translation stage. The laser beam reflected from the mirror surface falls at the prism at an angle greater than the critical angle of the prism (i.e. 32^o for BK7 prism) results in the total internal reflection of the laser beam. The mutual alignment of prism and mirror in the same optical plane is critical for the proper functioning of the feedback mechanism. Such a proper mutual alignment leads to in-line alignment of reflected beam from the prism with the transmitted beam of the mirror. The total internal reflection results in the exponentially decaying evanescent waves at the prism surface. These evanescent waves excites the SPP on the gold layer deposited onto BK7 glass substrate. Such gold deposited substrate is coupled to the prism using refractive index matching fluid. The excitation of SPP is detected as the fall in total intensity at the detector (QPD). The detector is clamped to the horizontal translation stage which insulate the detector from mis-alignment during shift in angular range related to change in ambient conditions. The horizontal translation of the prism-sensor-assembly shifts the angular range as explained in section 1.6. The photodetector is wired to DAQ as shown schematically in Figure 2.7. DAQ is USB interfaced to the computer. The detector

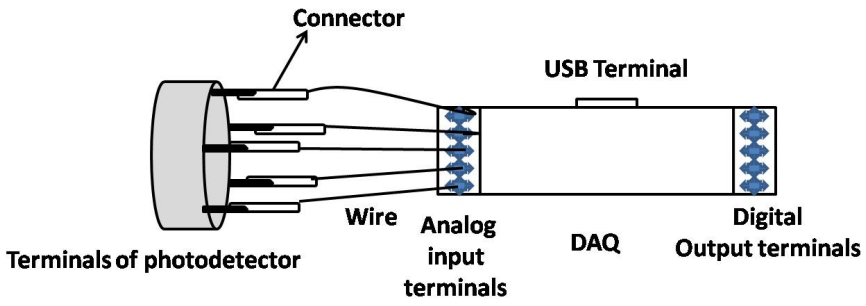

Figure 2.7: The connection between the photo-detector and DAQ.

is properly oriented to record maximum total intensity. Such well in-plane mutual alignment of optical elements supports the proper functioning of feedback mechanism as well as the record of total intensity.

The leads of photo-detector are inserted into the wire adapters. Wire adapters has a plastic jacket that encloses a copper cylinder having two open ends through which separate wires can be joined temporarily or permanently. Wires from the DAQ analog terminals are inserted into the adapters at the photo-detector leads. DAQ feeds the corresponding digital signals to the computer through the inserted USB cable at the USB port.

Feedback Mechanism : In the above descriptions, we have discussed about individual characteristics of optical elements and how they are set in the final instrument. The basic method applied in SPR instrument is the angular interrogation wherein the angle of incidence at the prism-sensor assembly is changed and the reflected intensity is recorded. The angle at which the intensity falls to minimum is the SPR phenomenon for the given interface.

In the traditional angular interrogation method, the beam spot on the gold surface deflects laterally due to change in angle of incidence using the laser - mirror assembly as discussed above. The change in angle of reflection deflects the position of the reflected spot at the detector. Therefore, the scanning mechanism suffers from three problems, one: the reflected beam deflects out of the active area of the detector; two: the range of angular scan is very limited (only a few degree) and three: the refernce point on

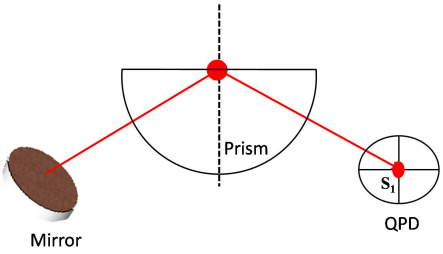

(a) Initial position S_1 of interrogation spot.

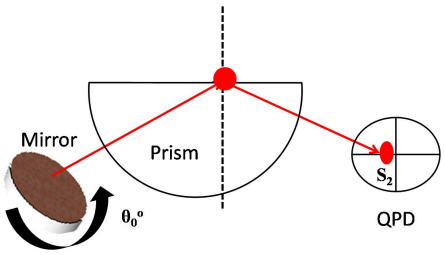

(b) Spot position S_2 after the mirror rotated to θ_o.

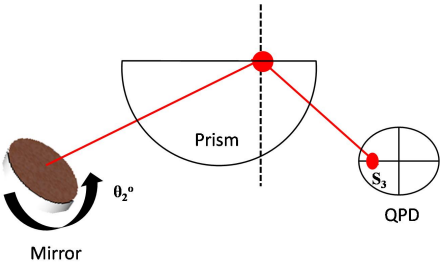

(c) Spot position S_3 at lower angle.

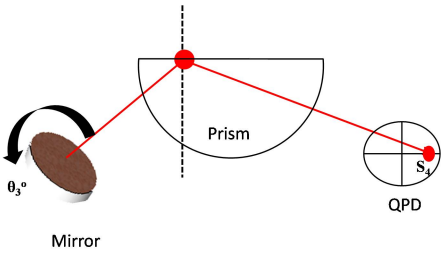

(d) Spot position S_4 at higher angle.

Figure 2.8: Laser beam scanning of prism-sensor assembly without feedback mechanism.

the sensing element changes due to change in angle of incidence. Figure 2.8 shows the schematic of the movement of beam spot due to change in angle of incidence.

Figure 2.8a shows the initial position of the interrogation beam spot at the detector as well as the prism surface. Figure 2.8b and Figure 2.8c shows the deflection of spot at the detector as the mirror rotates to lower angle. Figure 2.8d shows the deflection of spot at the detector as the mirror rotates to higher angle.

The angular interrogation of the beam causes in a wide range deflection to the position of beam on the detector as well as on the prism-metal interface. This deflection in beam position shown in Figure 2.8 affects the sensitivity of SPR instrument. The present configuration engages feedback mechanism to regulate the deflection of beam on the detector as well as on the prism-metal interface. The feedback mechanism ensures the components of the instrument mobile with respect to one another. Here, in this instrument the translations of the prism and the piezomotor are interconnected. We have observed the range of deflection of interrogation beam spot at the detector during

the angular interrogation. The mechanism to regulate the interrogation beam spot deflection improves the angular interrogation sensitivity.

The present instrument engages the feedback mechanism method to regulate the interrogation beam spot deflection on the prism surface during the angular interrogation of prism-sensor assembly. Feedback mechanism is detailed as the mechanism of movement of an element with respect to the information from another element. The present mechanism translates the prism with respect to the rotation of the mirror in order to keep the interrogation spot constant. Angular interrogation is possible by the rotation of the mirror. The angular change at the prism surface leads to the lateral shift of the reflected spot at the prism surface as well as at the detector surface. The lateral shift of the reflected spot at the photodetector varies the distribution in intensity at the segments of the detector resulting the change in the spot deviation value. The angular interrogation terminates as the spot deviation value changes from the initial value obtained. The vertical translation of the prism regains back the spot deviation value. The translation of the prism terminates as the spot deviation value regains. The mechanism ensures that there will be no appreciable change in the total intensity value, but slight changes is possible due to the instability of laser, due to resolution of DAQ as well as to the intensity variations at different angular inclination of beam at the detector at different angles. The manual performance of this mechanism leads to errors in SPR measurement. We have used the developed computer program in Labview 2012 platform for the perfect functioning of the mechanism.

Figure 2.9a shows the initial position of the spot on the prism-gold interface as well as on the detector (S_1). When the mirror rotates to an angle of θ_0, the beam deflects to the another point (S_2) on the detector. A translation of prism to a height of "H" will position back the spot to "S_1". This enables the interrogation of a fixed point on the prism-gold interface. This mechanism overcomes the errors in SPR data related to the deflection of beam on the sensing surface.

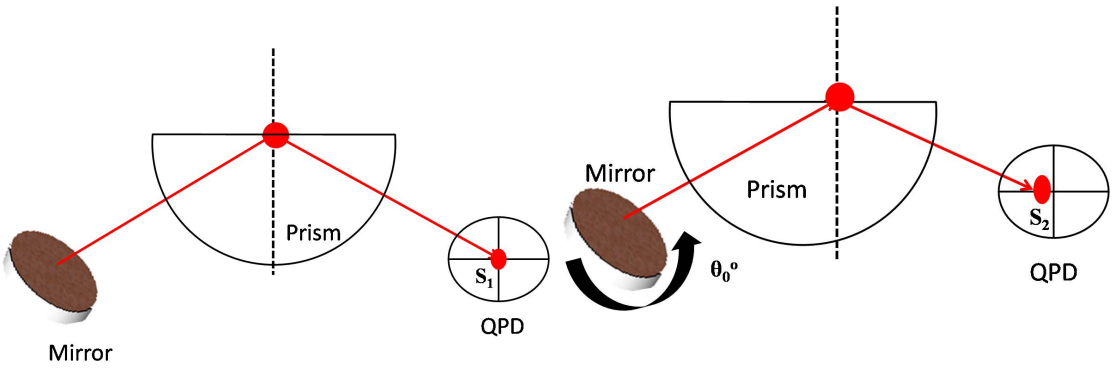

(a) Initial position S_1 of interrogation spot.

(b) Spot position S_2 after the mirror rotated to θ_o.

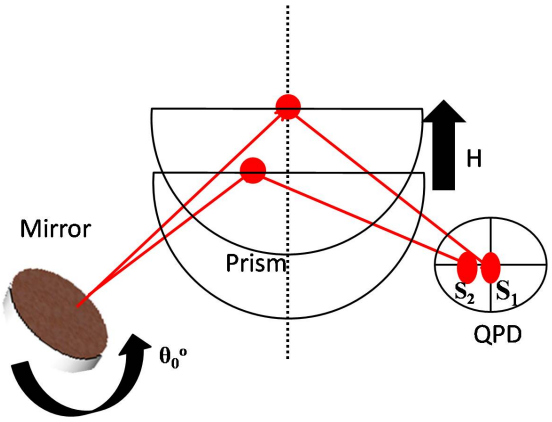

(c) Translation of the prism regains back the spot to initial position (i.e. S_2 to S_1.)

Figure 2.9: The schematic representation of feedback mechanism.

The properly aligned SPR instrument is enclosed in a wooden box for providing dark ambience for the optical setup. The intrusion of external light leads to errors in SPR measurement. The drivers for the respective components are packed in a separate box in compact fashion. The real image of the lab oriented instrument is shown in Figure 2.10

2.3 Software Development

Labview Platform : The control of the SPR instrument, data collection and visualization is done using Labview (National Instruments). Labview (LV) platform has graphical programming syntax which offers simple program development environment

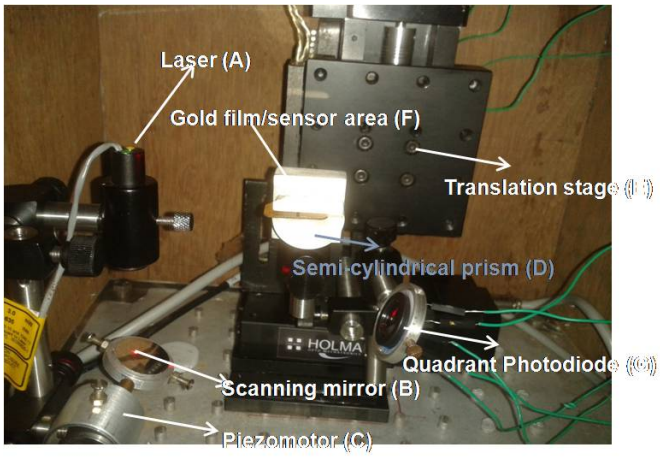

(a)

(b)

Figure 2.10: (a) The real image of optical alignment in the instrument (b) The compact packaging of encoders for the various components used in the instrument.

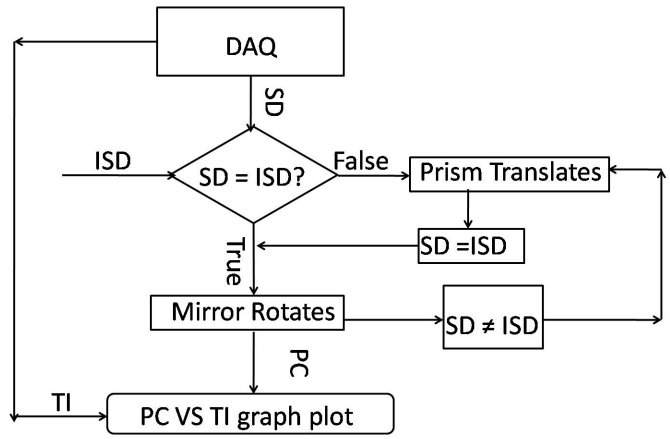

Figure 2.11: The flow chart of the developed program where TI : Total intensity, PC : Piezocount, SD : Spot deviation value, ISD : Initial spot deviation value.

for scientists and engineers. The program coding is carried out in a block diagram window of the platform. Block diagram window has the required function and tool palette for the program code development. The developed code of the program has functional structures which are interconnected through wire tool can resemble an electronic circuit board. The front panel window of the platform supports the execution of the program with the desired input values. The resulted output values or plots from the execution of the code are visible in this window. The developed code is executable with the computers having installed LV. The program execution is possible without the support of installed LV platform by converting the code into an executable file. This enables the program to run in any system as normal software.

The Figure 2.11 shows the flow chart of the developed program. The program starts with the record of initial spot deviation (ISD) value. The translation stage as well as the piezomotor are activated by the initialization of the respective I/O ports into the program. The execution of the program reads the spot deviation value (SD) and compares with the ISD value. The true conditions of the comparison supports the rotation of mirror for varying angle of incidence with simultaneous plotting of total intensity values against the piezomotor counts. The false condition of the comparison supports the termination of rotation of mirror and plotting of graph. The false condition simultaneously supports the translation of the prism until and unless the SD values recovers to ISD value.

2.3.1 Developed Program

Initialization: The translation stage and piezomotor are initialized using their drivers provided by the manufactures. Serial port communication controls the translation stage and piezomotor. The serial port communication has three command input functions that involves in the development of program to control the instruments through RS-232 port. The input functions are the following (1) Serial port initialization (2) Serial write and (3) Serial read. The time delay function provides the necessary delay in between the execution of serial write and read functions. Serial port initialization function has a characteristic input value called *Baud rate* that specifies the communication to the instrument. The values of baud rate are different for different instruments. The *Baud rate* of translation stage and piezomotor are 19200 and 57600 respectively. The data acquisition hardware gains input through DAQ assistant function of LV. This DAQ assistant is initialized with the selection of various characteristics (1) number of terminals to be read (2) physical quantity to be measured and (3) the mode of measurement in a specified range of physical quantity value. In our program, seven input terminals are selected to read the physical quantity of voltage with differentiation as the mode of measurement in the voltage range of -10 volts to +10 volts.

After the initialization of the instruments, individual serial communication structures for the particular instruments were added into the program. Feedback mechanism is enabled by utilizing the *case loop* structure characteristics. *Case loop* structure has conditional terminal which can be wired to any condition related functions. The true or false conditions satisfying at the condition terminal of the loop decides the execution of either *true* or *false case* commands. The serial communication structure related to each instrument was enclosed in *case loop*. The conditional terminal of the *case loop* is wired to the output of the spot deviation comparison function.

The spot deviation comparison function in the program compares the condition ($\leq$) between the real time spot deviation value and the value of initial spot deviation. In the "true case", the real time spot deviation value becomes lesser than or equal to the initial spot deviation value, initiates the stepwise rotation of piezomotor specified in the serial communication structure related to piezomotor. "True case" also supports the execution of graph function for plotting the total intensity against the piezocount. The

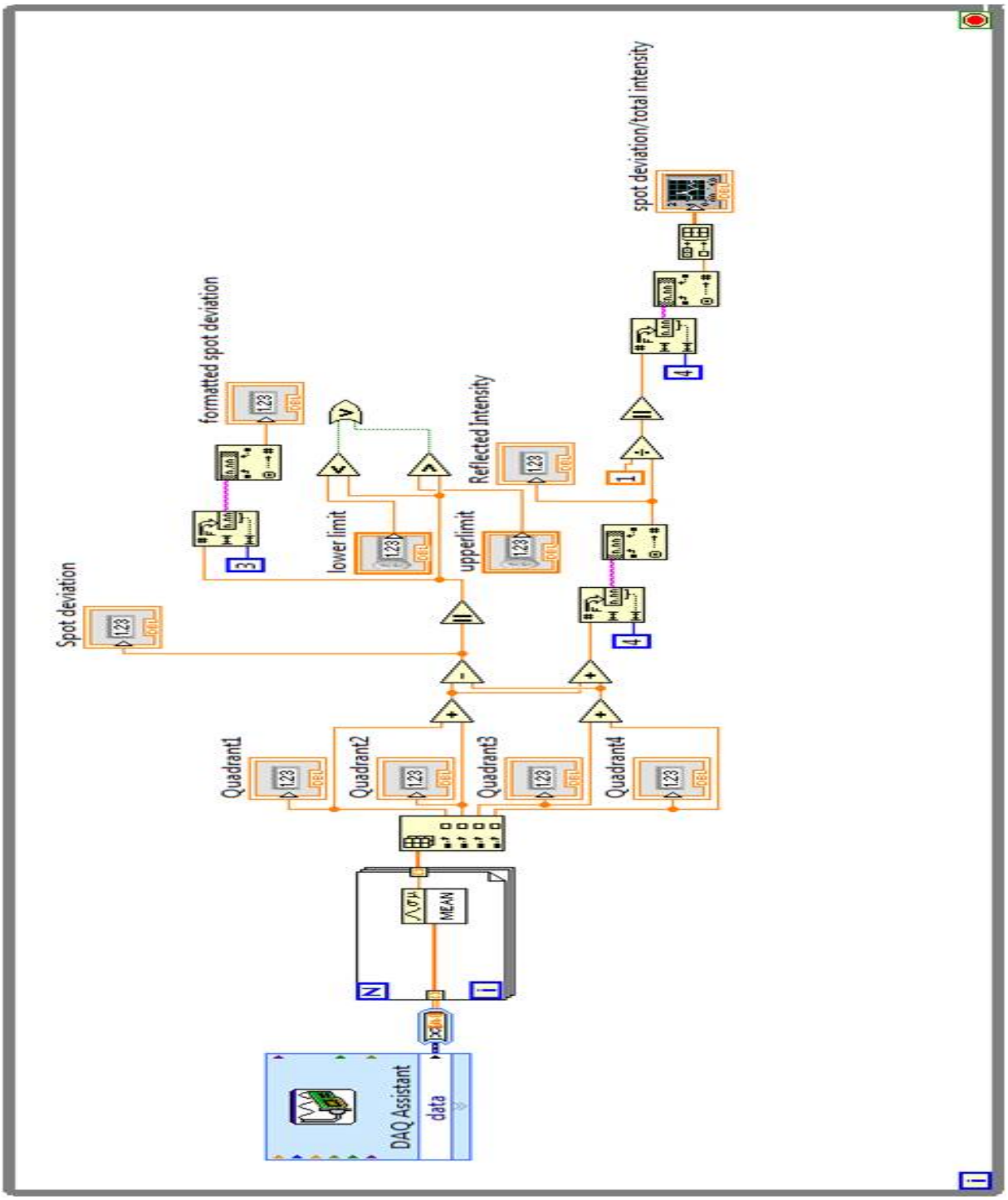

Figure 2.12: The snapshot of the block diagram of the DAQ function for data acquisition and visualization.

comparison function shows false with the deflection of the beam position at QPD. The *case loop* structures executes the false condition. The false conditions in the *case loop* structures includes the termination command for piezomotor to terminate the rotation of mirror. The graph function terminates as "false case" of its *case loop* has no functional structures. The false condition of the *case loop* that has the serial communication structure for the translation stage executes the translation of the prism with respect to input values specified for the stepsize and direction of translation. Serial communication for the initiation and termination of movement of translation stage is encoded in a different manner.

Translation stage communication : The vertical translation stepsize required for the translation stage is provided as three hexa-decimal numbers. The decimal number to hexadecimal number conversion function available in the arithmetic palette is utilized to specify the stepsize of the translation stage. The next command is fed as a decimal number, that specifies the direction of translation. The decimal number 125 signifies the reverse direction and 175 for forward direction of translation. The hexa-decimal numbers for the opposite direction motion as well as the decimal number for the direction specification has to be fed as zeros to complete the input commands for the translation. The translation stage initiates the translation only after the receipt of response of decimal number 28 for the direction specific command for the translation in opposite direction. The response 28 from the translation stage followed by the simultaneous feeding of operation commands continues the translation without halt. This mechanism is enabled by the insertion of serial communication for translation into the $for\ loop$ and addition of $shift\ registers$ wired with the comparison function for 28 at the boundaries of $for\ loop$. The decimal character 104 terminates the translation of prism with the retention of spot deviation value.

The character for termination is followed by the termination commands successfully complete the translation. he program for the initiation and termination of translation executed in this manner regulates the feedback mechanism. The screen shot of the program that regulates the translation stage is shown in the Figure 2.13.

This complete program is enclosed in a *while loop* for continuous execution of program. The terminal button of *while loop* structure is wired to *stop* function. This *stop*

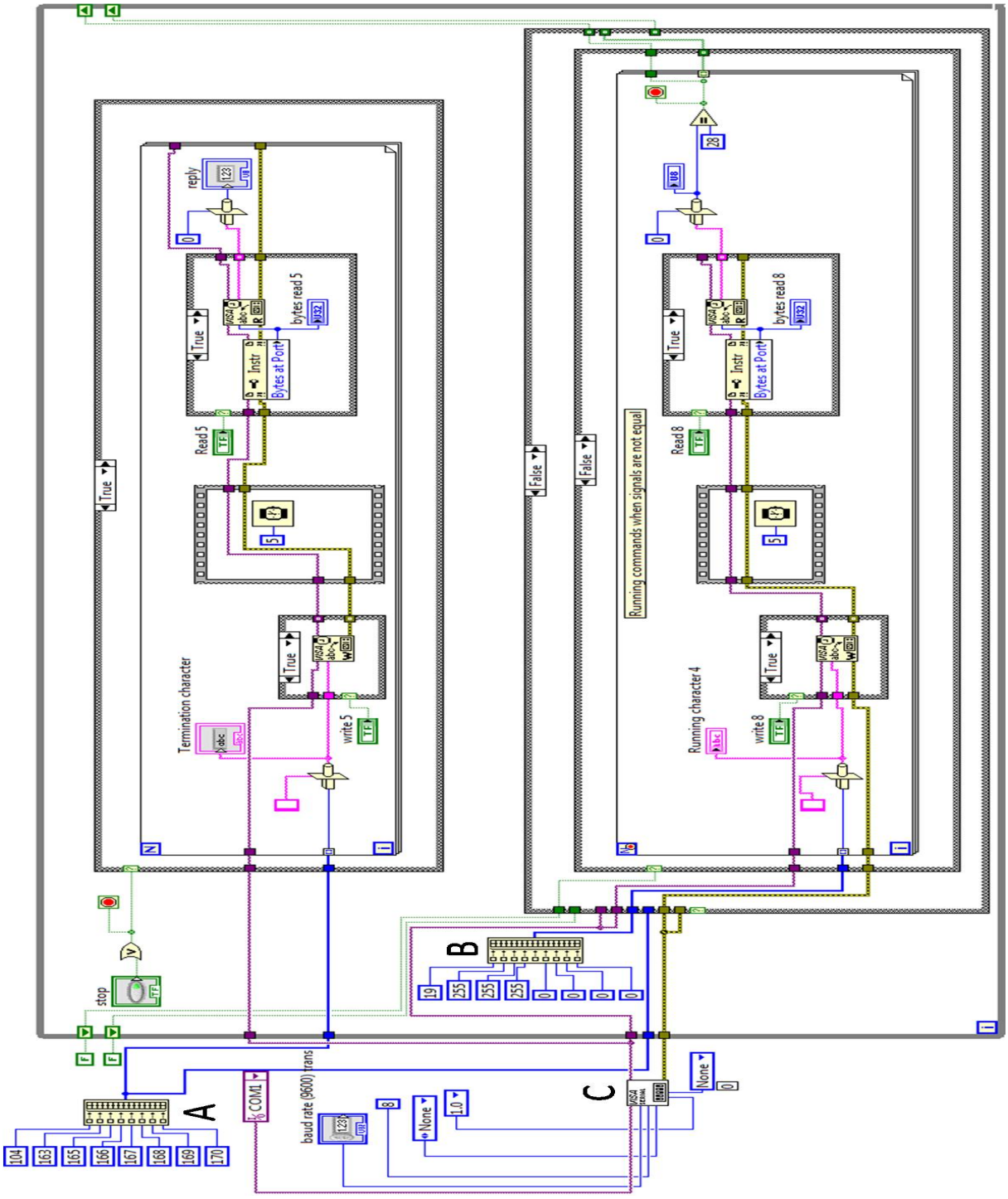

Figure 2.13: The snapshot of the block diagram showing the flow of data for the functioning of translation stage. A: Termination commands, B: Commands to run the program, C: Initialization of command port.

function is wired to termination command line enclosed in the case structure. Termination commands are fed and executed to successfully terminate the *while loop*. The termination of program without the execution of termination commands leads to the error signal in encoder of translation stage. This condition causes the discontinued reception of commands into serial port related to translation stage. The encoder to be restarted to initiate the translation stage.

Piezomotor Communication : Piezomotor communication has two distinct commands for initiation and termination of the rotation of motor. The initiation command specifies the number of steps to be translated. The sign (+/-) with the number specifies the direction (forward/reverse) of translation. The *stop* command terminates the piezomotor motion. The *true* output of comparison function satisfies the *true* case of *case loop* that encloses the piezomotor serial communication for the initiation of rotation of mirror. The $false$ output of the *comparison* function satisfies the $false$ condition of *case loop*. The "false case" has the command line for the termination of rotation of mirror.

Plotting of Graph : The graph function receives the piezocount input from piezomotor serial read function and the respective total intensity value from the DAQ function. The graph function is enclosed in a "true case" to regulate the plotting of graph. The graph function is added to the *true case* of *case loop*. This enables the termination of graph as soon as the comparison function output flips to false. The "true case" of

The resultant graph has piezocounts in X-axis and reflected intensity in Y-axis. Piezocounts are converted to angle of incidence by some calibration. The snapshot of the program for the plotting of graph is given in Figure 2.14. The ecomparison function drives the piezomotor in the respective step size while graph function accepts the piezocount value as the input. The "false case" being empty of graph function leads to termination of the graph. $Shift\ register$ feedback with build array function stores the input values recorded during execution and avoids the removal of recorded graph during the "false case" execution.

Front Panel : The front panel have editable command input for the respective instrument. The rotation step size of the piezomotor and the preferred ISD value are edited at

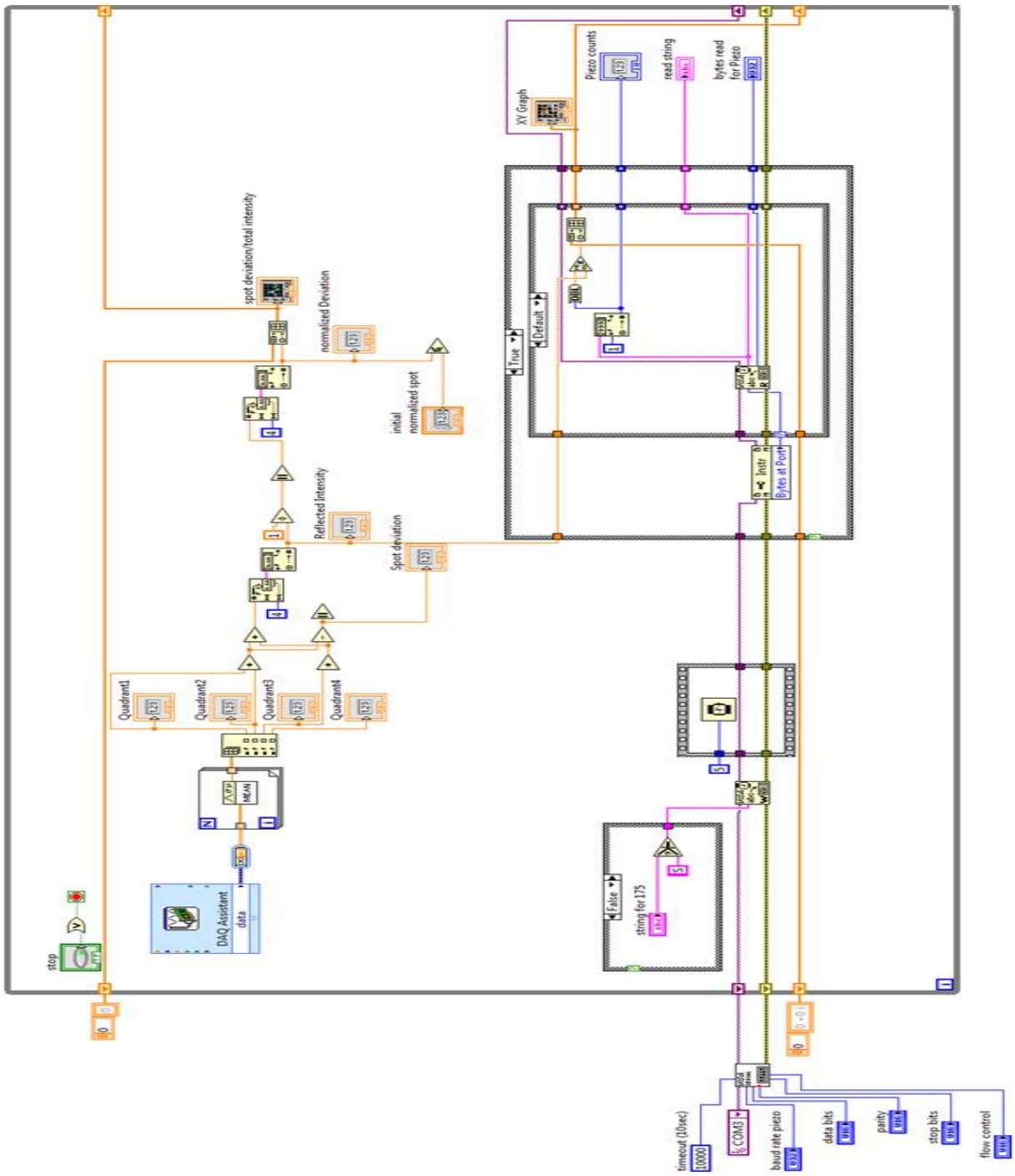

Figure 2.14: The snapshot of the block diagram for the acquisition of input values from DAQ and piezomotor for plotting the graph, piezocount Vs total intensity.

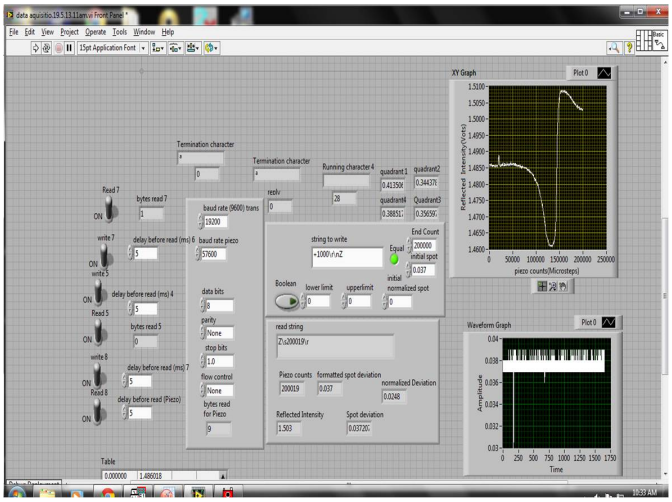

Figure 2.15: The snapshot of the front panel for the control of the instrument and the record of SPR spectrum.

the respective input. The output command line from the respective instrument shows the number of steps travelled by it during execution of program. The resultant plot from the execution of program shows the nature of SPR spectrum. After the record of the spectrum, the values are exported to MS-excel for calculation and analysis. The resulted front panel for gold in air environment is shown in the Figure 2.15.

The shape of spectrum is attributed to the alignment of optical components, nature of gold deposition and nature of analyte. The 50 nm thick gold layer with 3 nm adhesion layer of chromium/titanium deposition provides a sharp dip as shown in Figure 2.15. The variation in deposition parameters can alter the spectrum characteristics. The SPR spectrum of the gold film is recorded from various positions on the gold surface and averaged. The averaged spectrum is taken as the reference spectrum for the analysis of shift in SPR value due to deposition of analytes.

In order to check the stability of the feedback mechanism for a wider angular range, the SPR spectrum of gold-water interface is recorded. The resonance angle was found out to be 68^o. We observed that the feedback mechanism may fail due to the mismatch in optical alignment. The proper optical alignment results in the record of proper SPR spectra of gold in both the interfaces.

The record of proper SPR spectrum of gold-air as well as the gold-water interface shows the proper alignment of the instrument. This configuration is used to record the SPR characteristics of different analytes and are described in the respective chapters.

2.4 Calibration of the instrument

In this section, we discuss about the calibration of the developed instrument. The developed instrument is calibrated with a standard sample to show that the instrument is able to provide similar results as by other instruments functioning under the same phenomenon. The calibration also includes the measurement of sensitivity, angular resolution, and lowest detection limit of the instrument. In the case of SPR sensors, the sensitivity is measured in terms of refractive index units (RIU). RIU is defined as the change in refractive index per unit change in wavelength or angle of incidence.

2.4.1 Calibration for angular measurement

The angle of incidence at the prism is varied using the piezomotor controlled rotating mirror as explained in section 2.1. The system is calibrated to yield piezocount as the angle of incidence. The laser and the piezomotor attached mirror are kept in straight line as well as in equal height such that the laser beam reflects back to the laser after reflection from the mirror surface. This position of the mirror is considered to be zero degree angle of reflection to the normal of the mirror. The mirror is rotated until the reflected beam joins the line that passes through the center of the mirror at either the top or bottom of the mirror. This condition occurs when the angle of reflection is 45^o with mirror normal. We have found out that 2100000 steps of piezocount required to cover 0^o- 45^0. Thus, a degree is covered with 47000 piezocount.

Sensitivity of the instrument

The lowest detectable concentration (LDC) and sensitivity of the developed instrument are estimated using the sucrose solution. The instrument is used to detect the sucrose in aqueous medium (ultrapure ion-free water) for different molar concentrations. The SPR angle for the non-functionalized gold surface in aqueous medium is found out to be 68^o. The variation in SPR angle Vs molar concentration of sugar solution is shown in Figure 2.16a.

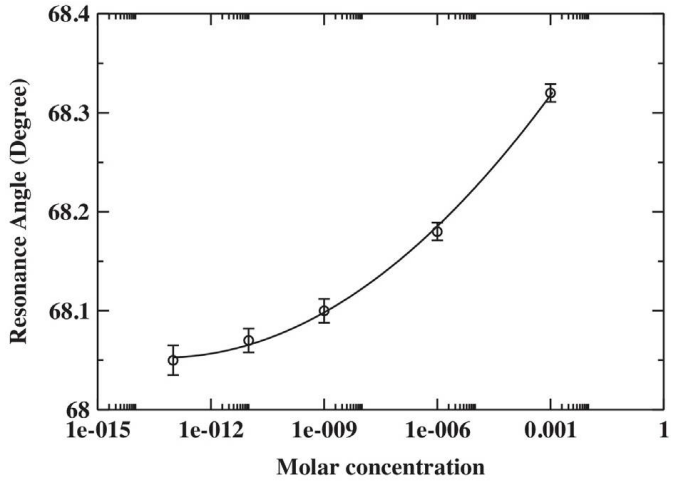

(a)

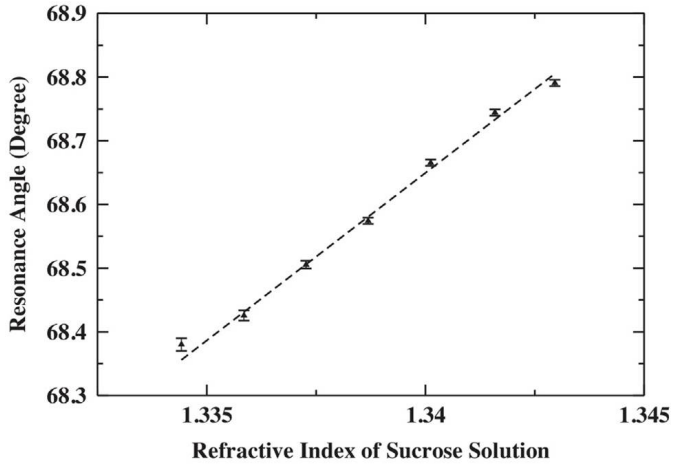

(b)

Figure 2.16: (a) The change in SPR angle with the change in sucrose solution concentration (b) The calibration curve showing the variation in resonance angle as the function of refractive index of the sucrose solutions. Symbols are experimentally obtained data points. Dashed line is best fit linear curve.

The lowest detectable concentration of sugar in aqueous medium is found out to be $1 \times 10^{-13} M$ (100fM). The resolution of the instrument is found out to be 1.92μ RIU[22]. The sensitivity of the instrument is estimated from the calibration curve obtained by recording the RA for different concentrations of sucrose solution with known refractive indices[3]. The calibration curve is shown in Figure 2.16b. The variation in data is best fitted with a linear curve and the slope is estimated. The sensitivity of the instrument thus obtained from the slope as $52.6^o/RIU$.

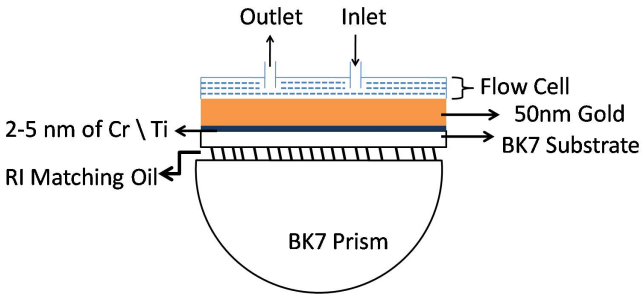

Figure 2.17: The schematic of flow cell with sensing element.

2.5 Flow Cell

The SPR setup can be used for the qualitative and quantitative studies of molecular interaction at interfaces and thus can be employed for sensing analytes by a chemically tailored surface. For sensing in aqueous medium, a flow cell has to be attached to the sensing element for the delivery of analytes. Specifically, the bio-chemical interaction studies involve the analysis of analyte and ligand interaction at the sensing element surface. The analyte molecule in the liquid environment interacts with the immobilized ligand on sensing element. This interaction between the analyte and ligand leads to the change in refractive index of the dielectric layer on the thin metal surface. This method helps to investigate the kinetics of interaction between them through the refractive index change analysis associated with it. A general schematic structure of prism-sensor assembly holding the flow cell for injecting fluid is shown in Figure 2.17

The SPR instruments available in the market utilizes various flow cell designs. We had adopted a flow cell design recently reported in literature [4]. The details on the

fabrication of flow cell is discussed in the next section.

2.5.1 Fabrication of flow cell

The fabrication of flow cell preparation is simple, robust and can be carried out without the need of complicate mechanisms. The method is distributed into simple steps as follows

(1) **Drilling of glass substrate**

The microscopic glass slide of thickness 1 mm is cut into a square substrates of size 2 cm × 2 cm. In order inject fluids, two holes of diameter 2 mm and spacing of 2 cm are drilled on such glass substrate with the glass drilling machine.

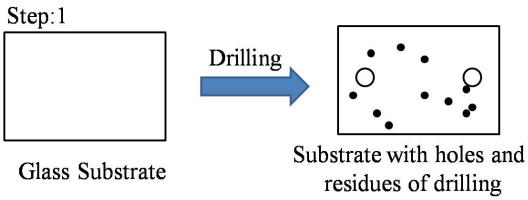

Figure 2.18: The microscopic glass slide (left) before drilling, (right) after drilling of holes. The drilled substrate is adsorbed with oil (coolant during drilling) residues (dark spots.)

(2) **Cleaning the drilled glass substrate**

The drilling method causes the accumulation of contaminant on substrate surface. The substrate surface is cleaned with the normal soap solution thereafter treated with Piranha solution (Conc.H_2SO_4 : H_2O_2, 3:1). This makes the substrate very clean.

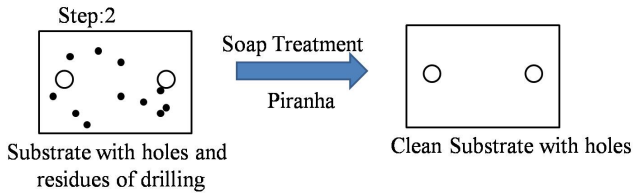

Figure 2.19: Soap as well as Piranha treated glass substrate with holes.

(3) **Flow channel preparation**

A double sided tape is cut to the length appropriate to the substrate. The central strip of the tape which includes the holes is removed carefully such that a rectangular free

space forms between the holes. The open side of the double sided tape is covered with its plastic cover to avoid the losses of gum on that side.

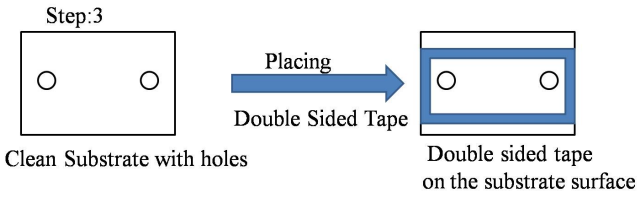

Figure 2.20: The glass substrate with a channel in double sided tape.

(4) **Liquid outlet and inlet preparation**

The pippet tips (100 μl) are used for the creation of proper inlet and outlet of the flow chamber. The tips that are cut to appropriate dimension (cut diameter is larger than the hole diameter) are glued at the holes. This creates the proper leak free inlet and outlet channels for the flow chamber.

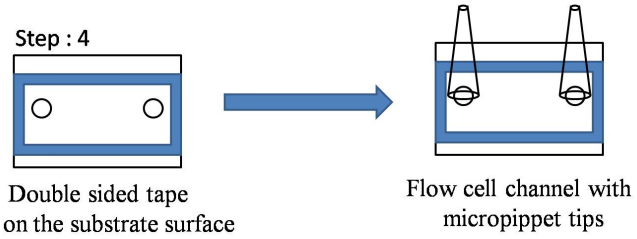

Figure 2.21: The micropippet tips on the drilled substrate with the flow channel.

(5) **Creating the flow cell on gold coated substrate**

The cover on the open side of the double sided tape is removed and flow chamber is placed and fixed on the gold surface of the SPR instrument. This creates perfect and leak free flow cell for injecting fluids into the SPR instrument. The fluid can be injected using peristaltic pump.

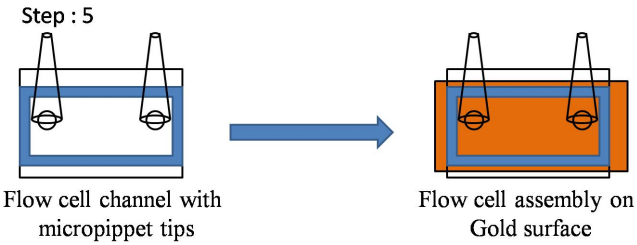

Figure 2.22: The final flow cell for the kinetic analysis.

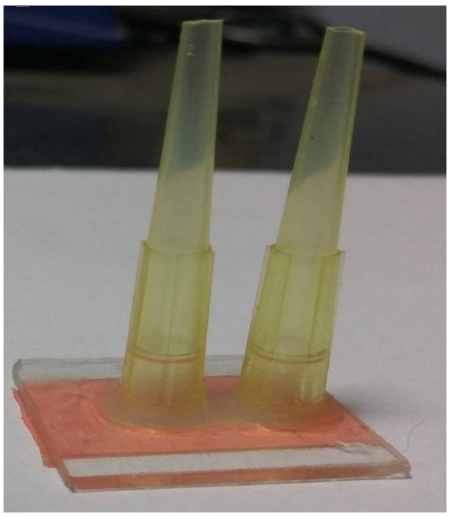

Figure 2.23: The real image of the flow channel with micropippet tips.

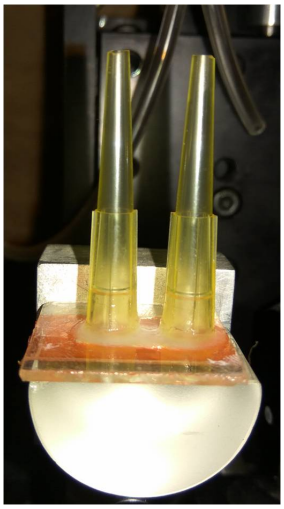

Figure 2.24: The real image of the flow cell attached to the sensing assembly of the SPR instrument.

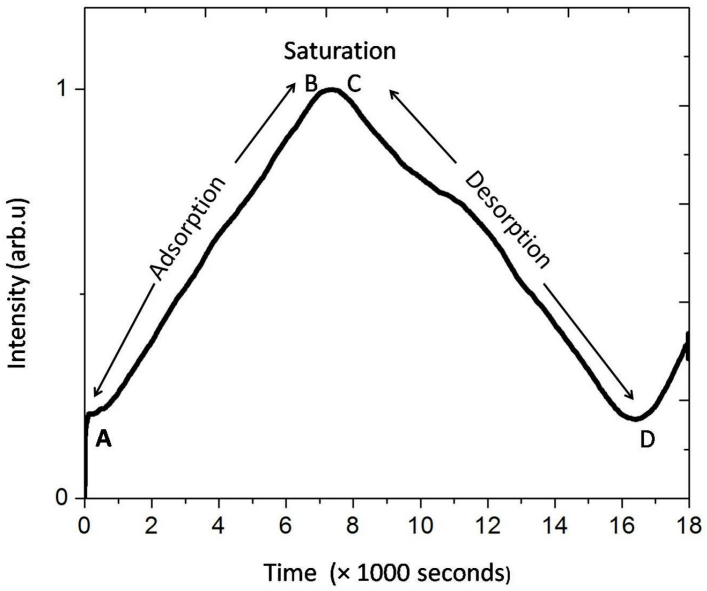

Figure 2.25: The adsorption-desorption curve for sugar molecules on gold surface.

2.5.2 Result

The developed flow cell is coupled to the SPR sensing assembly through the refractive index matching oil. The flow cell is used for injecting sugar solution and the kinetics of adsorption-desorption is studied using the SPR system. The peristaltic pump is used for the injection of liquid at a given flow rate. Sugar solution of concentration 1mM is used as the stock sample. The adsorption and desorption curve is as shown in the Figure 2.25

The interaction of sugar molecules with the gold surface is non-specific and therefore sucrose molecules can adsorb-desorb at random sites on the gold surface during circulation of sugar solution. The adsorption curve (A - B) shown in Figure 3.24 monotonically increases with time. The period for saturation of adsorption of sugar molecules on gold surface is extended due to the phenomenon of adsorption-desorption of sugar molecules at random sites on gold surface during circulation of sugar solution. The gold surface saturates with the sugar molecules after 6000 seconds (B - C). The C - D part of the curve shows the dissociation of sugar molecules during the circulation of ion-free water. The increasing trend after the point “D” is due to the renewed injection of sucrose

solution for the next cycle.

The technical specifications of the developed SPR instrument is given in Table 2.1. The mass of the instrument at the current stage is $\sim$ 5 Kg. However, it can be optimized to have very low mass. A mass optimization is shown in Table 2.2. With this optimization, the mass will be $\sim$3 kg. The manufacturing cost of the instrument is analysed by considering the cost incurred for individual components. The cost of each component is shown in Table 2.3. The total cost for the instrument will be $\sim$Rs. 5 lakh. The cost, weight, and technical specification of the developed instrument is compared with some of the commercially available SPR instruments. The comparison table is given in Table 2.4.

The table is in the next page

Table 2.1: **Technical specification of the developed SPR instrument.**

Sl.No.	Technique	Surface Plasmon Resonance sensor
1	Measuring principle	Constant spot measurements (excludes goniometer). Such technique minimizes the error in measurement which occurrs due to change in the reference point on the sensor area.
2	Configuration	Krestchmann-Reather configuration, angular interrogation.
3	Light source	Diode Laser with 635 nm wavelength, 3 mW, $< 5\%$ stability.
4	Optical channel	One
5	SPR angle range	8^o (with the same optics and same sensor slides and in the same scan, no need for prism exchange!, no manual manipulation needed)). Since this is an open system, this angle range can be adjusted according to the requirement. It can be adjusted from 20 to 80^o.
6	Prism coating	Optical gel index matching (no need for messy oil operation between measurements).
7	Sensor slide	Gold deposited slide; $\ell \times$ W = 5 mm $\times$ 5 mm $\times$ to 40 mm *times* 30 mm. Thickness = 0.2 mm to 1 mm.
7	Angular resolution	Flexible. For an optical setup, it can be adjusted from 20 millidegree to 0.02 millidegree by choosing the step size of the piezomotor from 1000 to 1, respectively. For the step size 100, the best resolution obtained is 10.42^o per RIU (obtained using sugar solution) or 20 pM per degree. 1.92 μ RIU to 1920 μ RIU.
9	Flow cell with peristaltic pump	A flow cell connected with a dual channel peristaltic pump. The flow rate can be adjusted from 1.3 μ l/sec to 19 μ l/sec.
10	Weight	$\sim$ 5 kg (un-optimized).
11	Computer and other hardware requirement	The minimum PC requirements are: MS Windows® XP / VISTA / 7 both 32 and 64 versions are supported serial port-1, USB port-3. 12-bit NI-DAQ.
	Total Cost	$\sim$ **Rs. 11.27 lakhs**

Table 2.2: **Weight analysis of the optimized instrument.**

Sl.No.	Component	Weight
1	Laser unit	100 gm
2	Mirror assembly (piezomotor included)	350 gm
3	Translation stage	1 kg
4	Prism assembly	250 gm
5	Detector	250 gm
6	Enclosure for the instrument	500 gm.
7	Encoder assembly	1 Kg
	Total weight	**3 Kg**

Table 2.3: **Cost analysis of the optimized instrument**.

Sl.No.	Component	Cost (Rs.)
1	Laser (635 nm)	100000
2	Piezomotor	150000
3	QPD	35000
4	Translation stage (z)	90,000
5	Optical components	15000
6	NI DAQ (14 bit)	60000
7	Housing/packaging	20000
8	Flowcell	10,000
	Total	**4.80 lakh**

Table 2.4: **Comparison table for developed instrument with other commercially available SPR instrument.**

Sl. No.	Instrument	Manufacturer	Method	Angular resolution	Refractive index range	Angular range	Weight
1	Our SPR	BITS-DST	Constant spot mechanism	Variable : 0.000002^o to 0.2^o	1–1.6	20–80^o	<5 Kg
2	$BioNavis^{TM}$	BioNavis	Goniometer, rotating laser	0.001^o	1-1.4	38-78^o	30 Kg
3	SR7500DC SPR System	Horiba	Multiple angles with fixed light input		1.32-1.52	58-85^o	
4	BIACOR 3000 system	Biocore	Wedge shaped beam, diode array detector	0.0001^0	1.33-1.4		50 Kg
5	IBIS MX96	IBIS Technologies BV	Angle scanning	0.01^0	1.33-1.43	10^o	65 Kg
6	$Indicator^{TM}$	Sensia	Polarized divergent laser beam, concentric rotation of prism and multiphotodiodes	0.001^o	1.33-1.5	45^o	28 Kg

Bibliography

[1] Le Liu, Zhaoxu Hu, Suihua Ma, Ying Zhang, Yonghong He, Jihua Guo, Optics and Lasers in Engineering 48 (2010), 1182–1185.

[2] J. Hamola, Chem. Rev. 108 (2008) 462

[3] Q. Zou, L.L. Kegel, K.S. Booksh, Anal. Chem. 87 (2015) 2488

[4] Alexander Johnson-Buck, Xin Su, Maria D Giraldez, Meiping Zhao, Muneesh Tewari, Nils G Walter, Nature Biotechnology 33 (2015), 730.

Chapter 3

Numerical simulation of SPR spectrum and estimation of optimized thickness of metallic layer essential for the SPR instrument development

3.1 Introduction

The SPR curve, reflected intensity versus angle of incidence can be simulated using Fresnel's equation [1]. In the simulation, the reflection of light was considered from three different layers e.g. prism-gold-dielectric. The SPR spectrum is found to be very sensitive to the refractive index and the thickness of the layers involved. Therefore, in the present scenario, the modelling has to be done by considering the reflection of light from all the involved layers with their known thickness. The surface plasmon polariton (SPP) based sensor sensitivity depends on the nature and thickness of the metallic layer deposited on the sensing element. In this chapter, we demonstrate through computer simulation about the significant effect of minor changes in thickness of the metallic layer on the quality factor of the sensor. The SPR sensors have either air or water as the ambient medium. The sensor for biological and bio-medical samples have aqueous whereas the gas sensor has air as ambient medium. We have studied the quality factor of SPR sensor in air and water media for different noble metals as a function of the

film thickness. The SPR instrument designing and development needs such studies for the proper generation of SPP in metallic layers and its coupling with the dielectrics deposited on it for the analysis. The SPR spectra are simulated theoretically using Fresnel's equation for modelling the reflection from three layers viz. prism-noble metal-medium.

3.2 Theory

The SPR spectra are simulated by modelling reflection of light from a three layer system viz. prism, gold and air. In the 3-layer system, the Fresnel's equation is obtained by considering the reflection from two interfaces viz. prism-gold, gold-air [5]. The final Fresnel's equation of reflectance R_p for the p-polarized light is given by Equation (3.1)

$$R_p = \mid r_p^2 \mid \tag{3.1}$$

where r_p is the reflection coefficient for p-polarized wave.

$$r_p = \frac{(M_{11} + M_{12}q_4)q_1 - (M_{21} + M_{22}q_4)}{(M_{11} + M_{12}q_4)q_1 + (M_{21} + M_{22}q_4)} \tag{3.2}$$

$$M_{ij} = (\prod_{k=2}^{3} M_k)_{ij} \tag{3.3}$$

For the k^{th} layer,

$$M_k = \begin{bmatrix} cos\beta_k & -isin\beta_k/q_k \\ -iq_k sin\beta_k & cos\beta_k \end{bmatrix} \tag{3.4}$$

Here,

$$q_k = (\mu_k/\widetilde{\varepsilon}_k)^{1/2} cos\theta_k \cong \frac{(\widetilde{\varepsilon}_k - n_1^2 sin^2\theta_1)^{1/2}}{\widetilde{\varepsilon}_k} \tag{3.5}$$

$$\beta_k = d_k \frac{2\pi}{\lambda} (\widetilde{\varepsilon}_k - n_1^2 sin^2\theta_1)^{1/2} \tag{3.6}$$

where, $\mu_k \cong 1$, θ_1 and θ_k are the angle of incidence at the interface of media 1 - 2 and (k-1)-k, n_1 is the real part of refractive index of the medium 1, $\widetilde{\varepsilon}_k$ and d_k are the complex dielectric constant and thickness of k^{th} layer, respectively.

The metallic layer utilized in the SPR sensor is characterized by its quality factor (QF) value. Quality factor is defined as the ratio of characteristic values of depth and the full width half minimum (FWHM) of the SPR spectra of the respective metallic layer. Figure 3.1 shows a typical SPR spectrum. The "w" gives the value for FWHM of

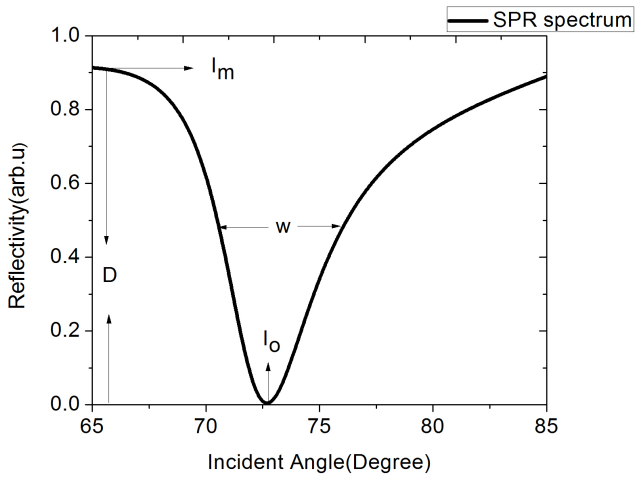

Figure 3.1: The calculation of the FWHM (w) and depth (D) from the SPR spectrum

the curve. It is the spectral region at which the intensity rises to half of the minimum intensity. The FWHM of a SPR curve of a particular metal depends on the ratio of its real (ϵ_r) and imaginery (ϵ_i) parts of dielectric constant, $\mid \epsilon_r/\epsilon_i \mid$ [6]. The "D" value gives the depth of the respective curve. It is the difference between maximum intensity (I_m) and the minimum intensity (I_0) as indicated in Figure 3.1. The quality factor of the given SPR curve is in the form of Equation (3.7).

$$QF = \frac{D}{w} \tag{3.7}$$

At resonance, the intensity reaches to minimum value (I_o). The SPR sensor has better resolution with larger "D" value. The smaller "D" value provides small range of reflected intensity which cannot resolve adsorbing events happening at low concentration at the surface. The angular position of the minimum intensity is difficult to distinguish with a low "D" value. This is shown in Figure 3.2 for 100 nm gold layer. The SPR sensor resolution depends on the detection of shift in resonance angle (RA) due to the analyte adsorption on the sensing area. The "D" value reduction introduces calculation errors in fixing the RA.

The sharp SPR spectrum with low value to "w" provides the highest angular resolution. The high "w" value for the spectrum of gold layer makes it difficult to distinguish

not only the RA but also shift in RA due to analyte adsorption on the sensing area. During the detection of analytes, the "w" value of the spectrum of gold with analyte becomes higher than the "w" value of bare gold spectrum. This phenomenon leads to the flattening behaviour of minimum intensity region in analyte spectrum. This condition makes the identification between RA and other angular points difficult. Thus SPR curves of gold with flat minimum intensity region provides poor angular resolution during the sensing process.

3.3 Result and discussion

The theoretical SPR curves are obtained using the numerical data from the simulation of Equation (3.6) using Matlab software. The simulation parameter are shown in Table 3.1.

Table 3.1: Refractive index parameter considered for the noble metals films at a wavelength $\lambda = 635$ nm.

Metallic layer	Refractive index (n_1)	complex dielectric constant (ϵ_k)
Gold	0.173	3.422
Silver	0.157	3.821
Copper	0.302	3.457

The quality of sensors based on SPR technology primarily depends on the generation of SPP and the sensitivity of the resonance condition with respect to the change in dielectric on the metallic surface. The SPR is very sensitive to the thickness of the metallic layer and its electromagnetic properties. In order to develop a high quality sensor, the thickness of the metallic layer should be optimized to yield highest quality towards sensing application. The ambient for sensing are either gas or water. We obtained theoretically optimized thickness of the metallic film for air and water environments. The SPR sensors are used for the studying the kinetics of reaction in pharmacy and biochemistry fields. Such studies are generally conducted in liquid (water) environments. The understanding on the thickness based quality of SPR instrument helps to optimize the thickness of the sensing layer in biosensors. The SPR curves of the gold-air interface

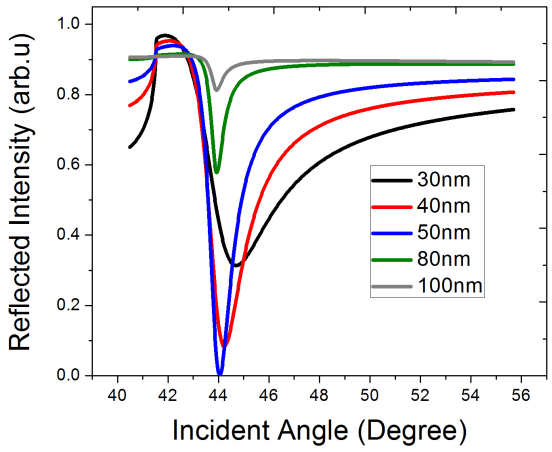

Figure 3.2: The SPR curves obtained for different thickness of gold layer for gold - air interface.

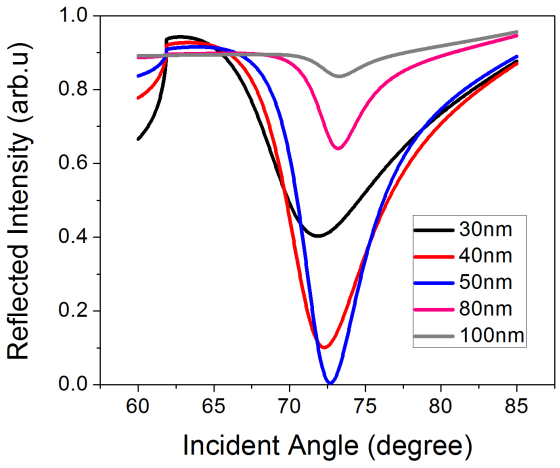

Figure 3.3: The SPR curves obtained for different thickness of gold layer for gold - water interface.

with different thickness of gold layer are shown in Figure 3.2. The gold layer depositionthickness varies from 30 nm to 100 nm in the step of 5 nm. The sharp SPR peak is observed for the thickness of 50 nm of gold layer deposition. Figure 3.3 shows the simulated SPR spectra for gold-water interface with different thickness's of gold layer for an angular range of 25^o.

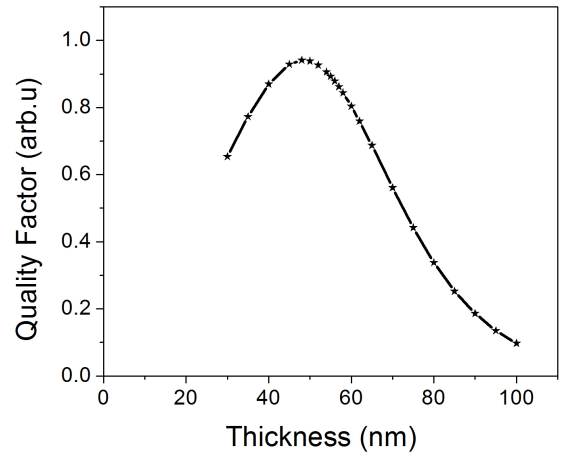

(a)

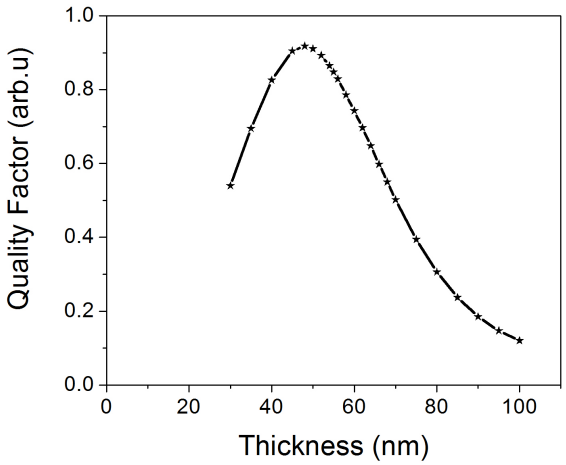

(b)

Figure 3.4: Variation of QF of SPR instrument with respect to thickness of gold layer for (a) air interface (b) water interface

The thickness of the gold layer is varied in the range $30 - 100$ nm in the step of 5 nm. The SPR spectra of gold-water interface are broader than the respective SPR spectra of gold-air interface. The SPR angle of gold layer is shifted from 44^o to 68^o as the interface changes from air to water.

The quality factor (QF) variation of samples with deposition thickness range of $30 - 100$ nm of gold for gold-air interface is shown in Figure 3.4a. The QF for the 30 nm gold layer is found to be 0.654, and shows an increasing trend with the increase in thickness of deposition. The maximum quality factor of 0.938 is obtained for the gold layer of

thickness of 50 nm. The further increase in deposition thickness causes a decreasing trend in the value of quality factor. As the deposition thickness reaches 100 nm, the quality factor reaches to a low value of 0.1. The quality factor variation with thickness of gold layer for gold-water interface is shown in Figure 3.4b. The trend is similar to that of gold-air interface.

The quality factor (QF) variation of samples with deposition thickness range of $30 - 100$ nm of gold for gold-air interface is shown in Figure 3.4a. The QF for the 30 nm gold layer is found to be 0.654, and shows an increasing trend with the increase in thickness of deposition. The maximum quality factor of 0.938 is obtained for the gold layer of thickness of 50 nm. The further increase in deposition thickness causes a decreasing trend in the value of quality factor. As the deposition thickness reaches 100 nm, the quality factor reaches to a low value of 0.1. The quality factor variation with thickness of gold layer for gold-water interface is shown in Figure 3.4b. The trend is similar to that of gold-air interface.

Figure 3.5a shows the QF behaviour of silver-air interface with respect to various thickness silver layer. The thickness of the silver layer deposition is varied from $30 - 100$ nm in the step of 5 nm. The QF of the SPR instrument for silver-air interface with 30 nm silver layer deposition is 0.25, and the value increases as the thickness of silver layer increases. The quality factor reaches highest value of 1.6 for the deposition of silver layer of thickness 58. The highest value of quality factor for gold-air interface was 0.938 for 50 nm gold layer. The high QF of silver-air interface is attributed to the high dielectric ratio ($\mid \epsilon_r/\epsilon_i \mid$) value for silver i.e. 38 whereas the respective value for gold is 7.33 [6]. This characteristic of silver makes it more sensitive to refractive index change than gold layer during the detection of analytes. Further, increase in thickness of silver layer decreases the QF, and attains a low value of 0.15 for the 100 nm thick deposition.

The QF of silver layer falls as the interface changes from air to water as shown in Figure 3.5b. The maximum QF of 0.31 obtains for the deposition of 54 nm of silver layer for the silver-water interface. The maximum value of QF was 0.938 for gold-water interface at 50 nm gold layer. This indicates that gold layer of 50 nm can equally applicable for high quality gas and bio-sensors. The quality of gas sensor based on 58 nm thick silver layer is 1.7 times better than gold layer based sensor. However, the

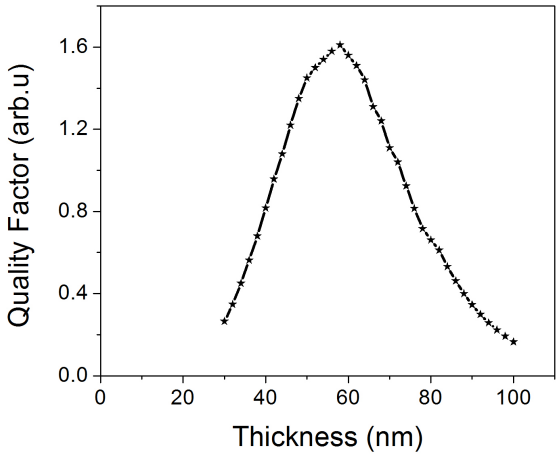

(a)

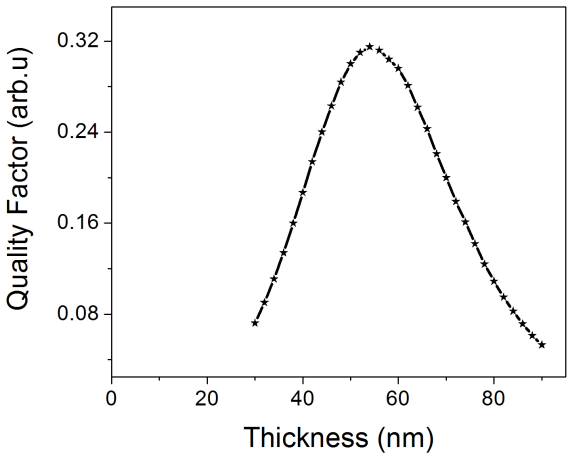

(b)

Figure 3.5: Variation of QF of SPR instrument with respect to thickness of silver layer for (a) air interface (b) water interface

quality degrades drastically in the water ambient.

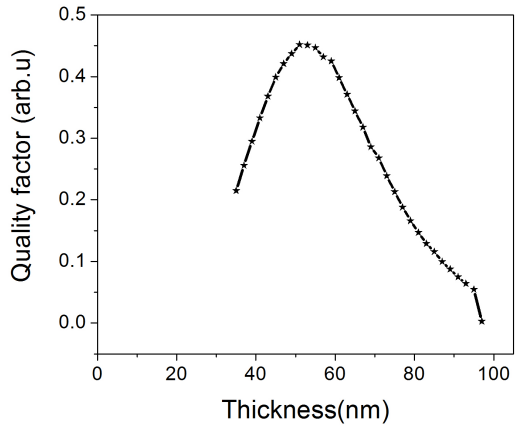

(a)

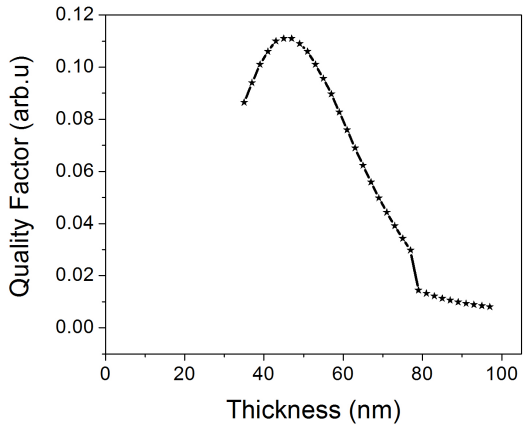

(b)

Figure 3.6: Variation of QF of SPR instrument with respect to thickness of copper layer for (a) air interface (b) water interface

Even with high QF value of silver, it is not commonly used as a sensing layer in SPR sensors because of poor stability of silver towards oxidation. The silver layer can be protected by a fluro-polymer coating [7]. The inertness of gold to corrosion is an advantage over silver for the selection of it as a candidate for the sensing layer in SPR sensors.

The QF of copper layer based SPR sensor for various thickness at air interface is shown in Figure 3.6a. The QF of copper layer of thickness 30 nm is 0.211, and it shows an increasing trend as the thickness increases. It shows maximum value of 0.45 at the

thickness of 51 nm. The value of QF decreases with further increase in thickness and attains a low value of 0.003 for the deposition thickness of 100 nm. For water interface (Figure 3.6b), the maximum QF is 0.11 at a thickness of 45 nm and the minimum value of 0.008 attains at a thickness of 100 nm.

3.4 Conclusion

The theoretical study reveals the behaviour of noble metals at various interfaces in the SPR based analysis. The SPR instrument sensitivity is based on QF of the involved metallic layer. The QF of various noble metals at different interfaces derived from the undertaken theoretical modelling is given in Table 3.2. The gold layer of thickness 50 nm can be employed for the best sensing performance in air as well as water medium.

Table 3.2: The QF data for noble metals obtained from theoretically modelled SPR curves at different interfaces.

Metallic layer	Value of QF (optimum thickness) in gas medium	Value of QF (optimum thickness) in water medium
Gold	0.938 (48 nm)	0.918 (48 nm)
Silver	1.611 (58 nm)	0.311 (54 nm)
Copper	0.451 (53 nm)	0.111 (45 nm)

Bibliography

[1] E.Kretschmann, Z.Physik. 1971, 241, 313.

[2] Kazuyoshi Kurihara, Kaori Nakamura, Koji Suzuki,Sens. Actuators B.2002, 86, 49.

[3] Yu Huang, Jiming He, Zhaoming Chen, Dongyun Tang, Lijuan Liu, Shixuan He, Optik.2013, 124, 4445.

[4] Wen Bin Lin, Monique Lacroix, Jean Marc Chovelon, Nicole Jaffrezic-Renault, Henri Gagnaire, Sens. Actuators B.2001, 75, 203.

[5] R.M.A. Azam, N.M Bashara, Ellipsometry and Polarized light, NH publishing Co., Amsterdam, 1977.

[6] Masaru Mitsushio, Kenichiro Miyashita, Morihide Higo, Sensors and Actuators A.2006, 125, 296.

[7] A. Abdelghani, J.M. Chovelona, N. Jaffrezic-Renaulta, C. Veilla, H. Gagnaire, Analytica Chimica Acta.1997, 337, 225.

Chapter 4

Measurement of optical anisotropy in ultrathin films using SPR Instrument

4.1 Introduction

The surface plasmon resonance angle (RA) is extremely sensitive to any change in dielectric layer adsorbed onto the gold surface. The RA shifts with respect to the reference for any change in the dielectric layer adsorbed over the gold surface. The dielectric (hence optical) properties of the adsorbed material can be estimated by modelling the reflection from different interfaces involved during the process by employing the Fresnel's equation as discussed in chapter 3 [1]. Wang [2] has demonstrated the condition for altering the SPR by altering the dielectrics of a liquid crystal material on the metal surface due to the application of electric field. The molecular tilt in well oriented ultrathin films deposited through Langmuir-Blodgett (LB) technique introduces optical anisotropy in the film due to tilt of the molecules with respect to the surface normal. Ellipsometry is widely used for investigating the anisotropy of such films [3, 4]. Brewster angle microscopy (BAM) is also used to visualize optical anisotropy qualitatively in the Langmuir monolayer of amphiphilic molecules. The tilt in molecules in the ultrathin films causes the intensity modulation in BAM images. The molecular tilt variation in such ultrathin films is shown as the stripes and spirals in BAM images [5].

In this chapter, we report the measurement of optical parameters (refractive index) in the orthogonal directions of the ultrathin films of well organized bundles of single-walled carbon nanotubes (SWCNTs), octadecanethiol (ODT) and cadmium stearate (CdSA) using the developed SPR instrument. These three system exhibit different degree of anisotropy in their ultrathin film. The ultrathin films of SWCNTs and CdSA are fabricated through Langmuir-Blodgett (LB) technique whereas that of ODT through self assembly on the gold surface. Self assembled monolayers (SAM) can be employed to tailor the interfacial properties of metal. SAMs are organic assemblies formed by the adsorption of organic molecules from solution onto the surface of solids. The adsorbates may organize spontaneously (and sometimes epitaxially) into crystalline (or semi-crystalline) structures. The molecules which form SAM posses chemical functionality which has specific affinity towards the substrate surface. In case of substrate of noble metals, the molecules having thiol (-SH) group linked chemically with the metal surface to forms the SAM [20]. The LB technique has been utilised for a number of years for the preparation of ultrathin films of precisely controlled thickness and molecular architecture. It has usually involved the vertical movement of a substrate through the Langmuir monolayer at the air-water interface using a geometry in which the plane of the substrate surface is orthogonal to the plane of the water surface [7]. Such ultrathin films offer a well organized and orientationally ordered single layer of the molecules [19, 11], which may exhibit anisotropy due to the orientation of the molecules in a preferential direction on the substrate. The anisotropy in the films depends on the shape anisotropy of the molecules and their tilt orientation on the substrate with respect to the surface normal [8]. The SPR spectra of the fabricated ultrathin films are recorded in the orthogonal directions of the film i.e. parallel (0^o) and perpendicular (90^o) with respect to the plane of incidence.

We aligned the long axis of SWCNTs in the ultrathin film along the direction of dipping of the substrate during the LB film fabrication process [12]. The SPR spectra of such LB film of SWCNTs show very interesting result. The film of SWCNTs behaves metal-like and insulating dielectric layer when the long axis of SWCNTs is aligned parallel and perpendicular to the plane of incidence, respectively. The ultrathin films of structurally similar molecules viz. ODT and stearic acid on the gold surface differ with respect to the orientational tilt of the molecules in the single layer. ODT in SAM

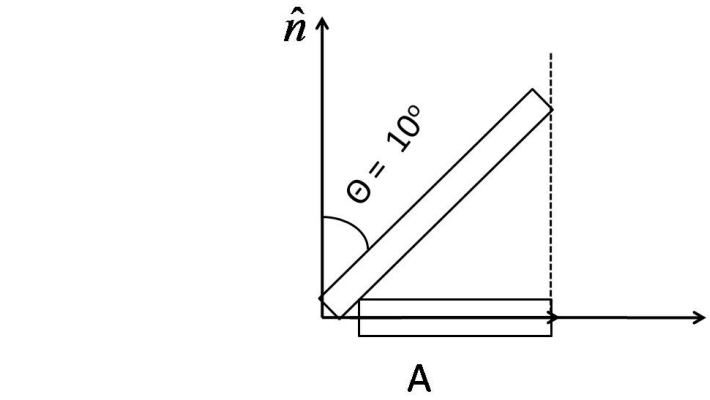

(a) CdSA

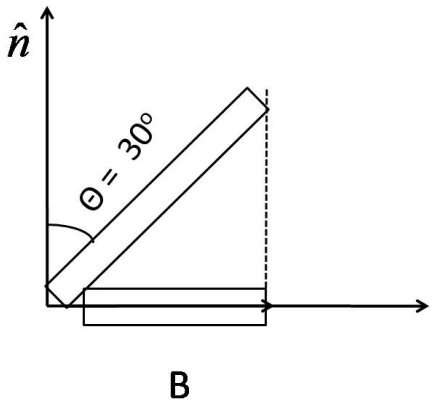

(b) ODT

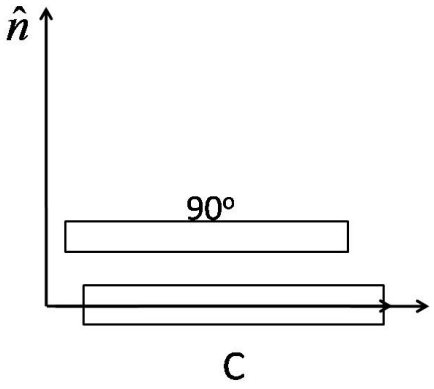

(c) SWCNT

Figure 4.1: Schematic showing the tilt of the molecules with respect to the substrate normal ($\widehat{n}$) and their projection on the substrate. The qualitative amount of projections are indicated as A, B and C

and CdSA in LB are known to tilt $\backsim 30^o$ and $\backsim 10^o$ with respect to the surface normal, respectively [13, 14]. Therefore, there is a different degree of anisotropy in SAM of ODT as compared to that of LB film of CdSA. This is shown schematically in the Figure 4.1. We found the optical anisotropy as a change in the real part of refractive index (Δn_r) of SAM of ODT and LB film of CdSA to be 0.24 and 0.10, respectively.

4.2 Materials and Methods

The SPR setup in Kretschmann configuration was developed in the laboratory (Figure 2.1). The instrumentation and other details are discussed in chapter 2. The ultrathin films of CdSA and SWCNT were fabricated by LB technique using a teflon LB trough

(Apex Instruments). The stearic acid (SA) was obtained from Sigma-Aldrich. A chloroform solution of the SA having a concentration of 3.5 mM was spread onto an aqueous subphase of 1×10^{-5} M of cadmium chloride ($CdCl_2$) in ultrapure ion-free water (MilliQ, DQ5). The gold substrate was treated with the HF solution (NH_4OH: H_2O_2 : H_2O = 1 : 1 : 5). The HF treatment removes the contaminants from the gold surface. The cleaned gold substrate is mounted in the LB system. A single layer of LB film of CdSA is deposited on the gold substrate at a target surface pressure of 30 mN/m. The tilt of the aliphatic chains of the molecules in the LB films was reported to be around 10^o with respect the surface normal [14]. Isotropic thin film of SA was deposited onto the gold substrate by spin coating technique. A 5 $\mu\ell$ of the chloroform solution of SA was spread onto HF cleaned gold substrate rotated at a speed of 7000 rotations per minute. In order to obtain isotropy and homogeneity in the film, it was annealed at a temperature of about 80^o C for 15 min. A uniformly dispersed solution of 9×10^{-3} mg/ml of SWCNTs (Carbon Solutions, P2-SWNT) was obtained by dissolving the nanotubes in dimethylformamide (DMF) solvent and ultrasonicating the dispersion for about 1 h. The Langmuir film of SWCNTs is found to be stable with a collapse surface pressure of 11 mN/m. The LB films of SWCNTs are deposited onto solid substrates at 2 mN/m and the surface morphology were studied using atomic force microscope (Solver-Pro, NTMDT). We found that the long axis of SWCNTs oriented along the direction of deposition of the film [12].

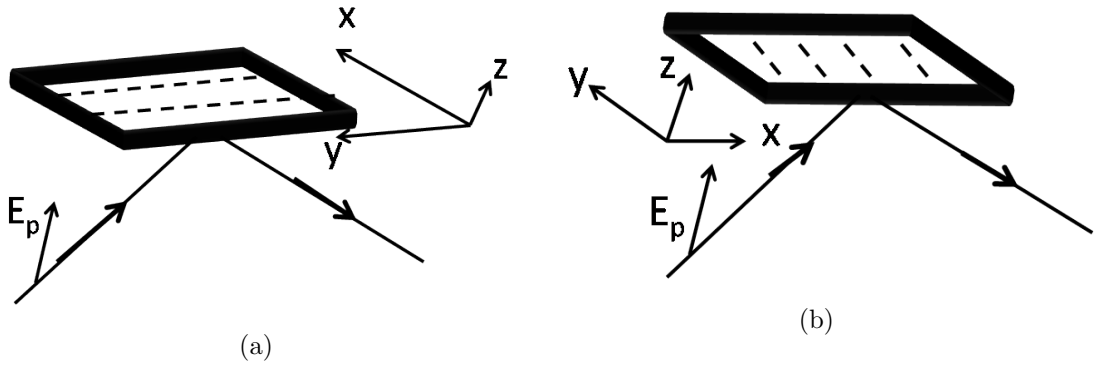

Figure 4.2: The SPR spectra are collected in the orthogonal directions as indicated in (a) and (b) The direction of electric field is in (a) y-z plane and (b) z-x plane. The substrate dipping direction during LB film fabrication is along y-axis.

Such morphology can yield exceptionally high anisotropy in the electrical and optical properties when measured in orthogonal directions. The SAM of ODT was prepared by immersing the HF treated gold substrates into the 1 mM solution of ODT in absolute ethanol for about 12 h. The ODT deposited gold substrates were rinsed thoroughly by absolute ethanol followed by HPLC grade chloroform before mounting on the scanning stage of the SPR instrument. The SPR spectra were collected by changing the angle of incidence at a step of 21.2 $milli^o$ and recording the reflected intensity, simultaneously. The SPR spectra are collected in the orthogonal directions as shown in Figure 4.2.

In order to check the reproducibility of the data, the SPR spectra were collected from different locations of the films, and from the films deposited onto substrates in different batches. The RA for the gold film (gold-air interface) was found to be 44^o. The average shift in RA ($\Delta\theta$) for the ultrathin films of different materials were estimated with reference to that of RA for the gold film (i.e. 44^o). The standard deviation of the RA was found to be in the range of $0.01^o - 0.02^o$.

4.3 Result and Discussion

The SWCNTs are highly anisotropic material exhibiting extraordinary electrical, optical and mechanical properties. We aligned the bundles of SWCNTs onto the substrates by LB technique. During the LB film fabrication process, in a very simple mechanism the SWCNTs can be aligned either parallel or perpendicular to the dipping direction by aligning the substrate-normal perpendicular or parallel to the film compression direction [15], respectively. The surface topography of the LB film of SWCNTs obtained using the atomic force microscope is shown in the inset of Figure 4.3. The bundles of SWCNTs are found to orient with its longer axis parallel to the dipping direction of the substrate during the LB film fabrication process. The LB films of SWCNTs were deposited onto patterned interdigitated electrodes (IDE) and the current-voltage (I-V) measurement was carried out. The I-V curves for the parallel and perpendicular orientation of SWCNTs in the LB films with respect to the applied voltage V are shown in Figure 4.3. The I-V curves obtained for parallel orientation of the SWCNTs shows the normal ohmic behavior, and the estimated film resistance is found to be merely 7.8 Ω. Therefore, such orientation of the SWCNTs with respect to the applied electric field (E) indicates metallic nature of the film. However, the I-V curve for the film with SWC-

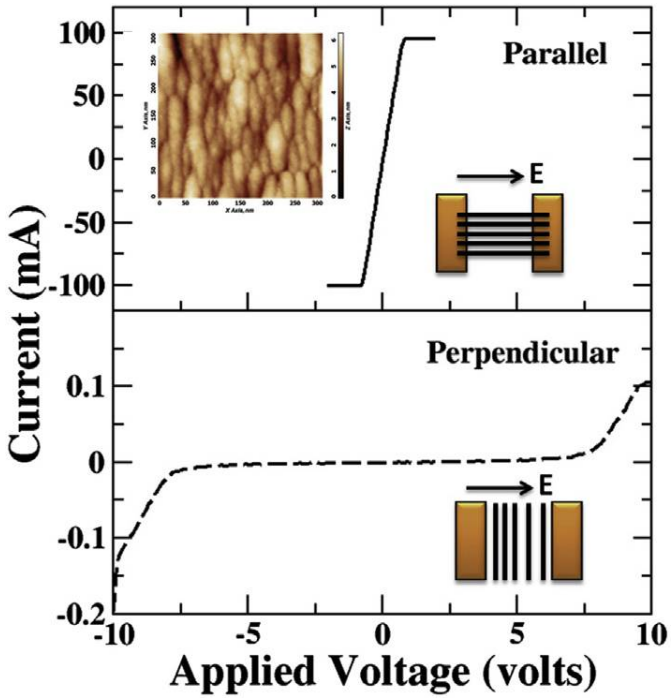

Figure 4.3: Current-Voltage (IV) curves of the LB films when SWCNTs are aligned parallel and perpendicular to the electric field (E). The inset in the top figure shows the AFM image of the LB film of SWCNTs. The bundles are aligned in the direction of dipping the substrate during LB film fabrication. The right-bottom of each figure shows schematic for the alignment of SWCNTs on interdigitated electrodes.

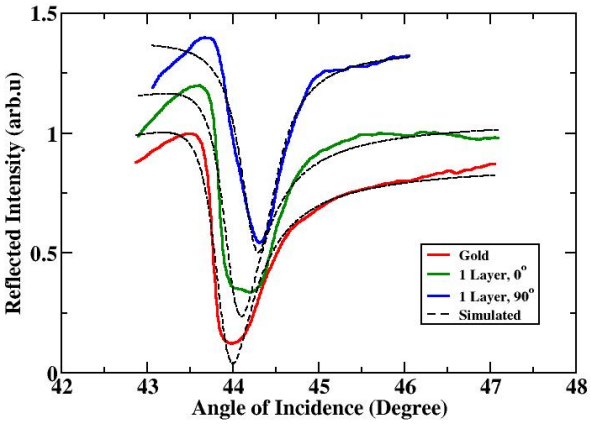

Figure 4.4: Surface plasmon resonance spectra of gold and one layer of LB film of SWCNTs where the long axis of SWCNTs are aligned parallel (0^o) and perpendicular (90^o) to the plane of incidence. The curves are shifted vertically for visual clarity.

NTs align orthogonal to the applied electric field shows non-metallic behaviour. Hence, such orientation of the SWCNTs with respect to the electric field can be considered as insulating dielectric film.

A single layer of SWCNTs is deposited onto gold substrate at a target surface pressure of 2 mN/m [16]. The SPR spectra of the LB films were obtained for two different orientations of the long axis of SWCNTs with respect to the plane of incidence viz. parallel (0^o) and perpendicular (90^o)(Figure 4.4). The spectra are simulated using the Equation (3.1) and the optical parameters like real part of RI (n_r) and imaginary part of RI (n_{im}) are estimated. The values are tabulated in Table 4.1.

Table 4.1: Estimated values of refractive index (RI) of LB film of SWCNTs through simulation. n_r and n_{im} are the real and imaginary part of RI. The average shift in RA is $\Delta\theta$. The refractive index for the gold was chosen to be 0.172 (n_r) and 3.421 (n_{im})

LB film of SWCNTs	$\Delta\theta$	n_r	n_{im}
Parallel (0^o)	0.07^o	0.2	3.3
Perpendicular (90^o)	0.28^o	1.04	0.0045

The average shift in RA with respect to the gold film ($\Delta\theta$) for SWCNTs aligned parallel to the plane of incidence (i.e. 0^o) is found to be merely 0.07^o whereas the $\Delta\theta$ is found to be 0.28^o for the film where SWCNTs aligned perpendicular (i.e. 90^o) with respect to the plane of incidence. Since, the $\Delta\theta$ is not significant, the LB film with zero degree alignment of SWCNTs can be treated as a metallic film deposited over the 50 nm gold film. The SPR spectrum for such film is simulated using Equation (3.6) and the values of n_r and n_{im} are estimated to be 0.2 and 3.3, respectively. Since the $\Delta\theta$ for such film is very low, the values of n_r and n_{im} are comparable to that of gold. The $\Delta\theta$ for the film with 90^o orientation of SWCNTs with respect to the plane of incidence is found to be 0.28^o. Such orientation of SWCNTs in the LB film yields a dielectric insulating layer. Therefore, the SPR spectrum shows a large shift in RA as compared to that of film with parallel alignment of SWCNTs.

We have also studied the SPR spectra of the ultrathin films composed of structurally similar rod shaped organic molecules viz. ODT and SA. Such film forming molecules possess lower length-to-width ratio and hence exhibit much less anisotropy in properties as compared to that of SWCNTs. The amount of anisotropy in the ultrathin films of the rod shaped molecules depends on the amount of molecular tilt with respect to the surface normal [17, 2]. The molecular tilts of ODT molecules in SAM on gold is reported to be around 30^o [20] and CdSA in the LB films deposited at 30 mN/m is around 10^o [14]. Therefore, we studied the SPR behavior of self assembled monolayer of ODT and LB films of CdSA on gold substrates. The SAM of ODT may offer more anisotropy as compared to that of LB films of CdSA. The recorded SPR spectra of the SAM of ODT on the gold substrate in the orthogonal directions are shown in Figure 4.5. The $\Delta\theta$ of the SAM of ODT measured in the orthogonal directions are 0.2^o and 0.3^o. The spectra are simulated using Equation (3.6) and n_r and n_{im} are estimated. The refractive index is tabulated in Table 4.2. The Δn_r is found to be 0.24. The SPR spectra of the spin-coated thin film of SA on gold substrate are shown in Figure 4.6b. In the spin-coated thin films, the molecules orient isotropically onto the surface. The average shift in the RA for the two orthogonal directions are found to be constant ($= 0.2^o$). This clearly indicates that the difference in shift in SPR angle during the orthogonal scanning is essentially due to difference in refractive index in the film which normally arises due to film anisotropy.

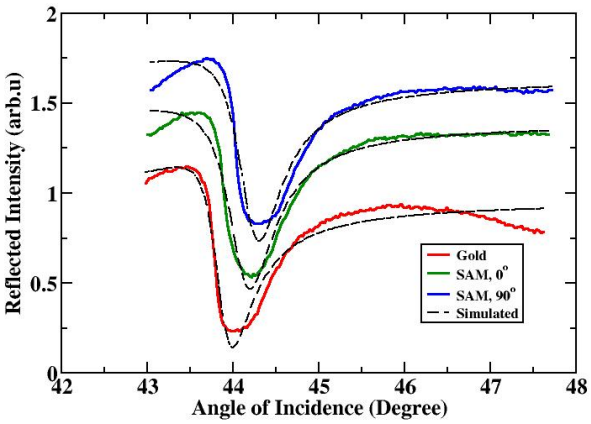

Figure 4.5: Surface plasmon resonance spectra of gold and self assembled monolayer (SAM) of octadecanethiol for the orthogonal directions: parallel (0^o) and perpendicular (90^o) to the plane of incidence. The curves are shifted vertically for visual clarity.

Table 4.2: Estimated values of refractive index (RI) of SAM of ODT through simulation. n_r and n_{im} are the real and imaginary part of RI. The average shift in RA is $\Delta\theta$. The refractive index for the gold was chosen to be 0.172 (n_r) and 3.421 (n_{im})

SAM of ODT	$\Delta\theta$	n_r	n_{im}
Parallel (0^o)	0.2^o	1.24	0.01
Perpendicular (90^o)	0.31^o	1.48	0.01

The LB films of CdSA deposited at a target surface pressure of 30 mN/m yield an ordered film with molecular orientation $\sim 10^o$ with respect to the surface normal [14]. The SPR spectra of one layer of LB film of CdSA is shown in Figure 4.6a. The $\Delta\theta$ corresponding to the orientations 0^o and 90^o are 0.195^o and 0.10^o, respectively. The spectra are simulated and the refractive indices of the dielectric films are estimated. The simulated values of refractive indices for the different films are tabulated in Table 4.3. The Δn_r is found to be 0.10

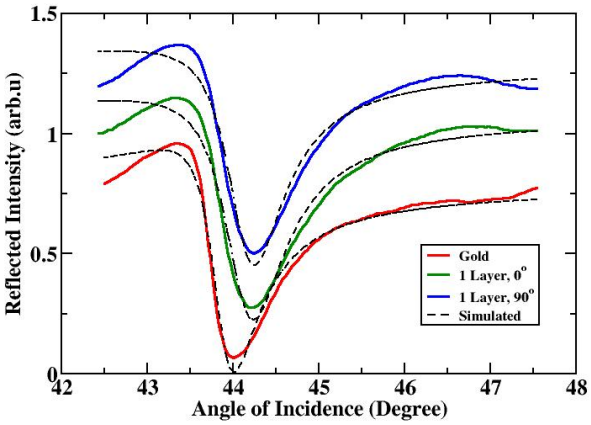

(a)

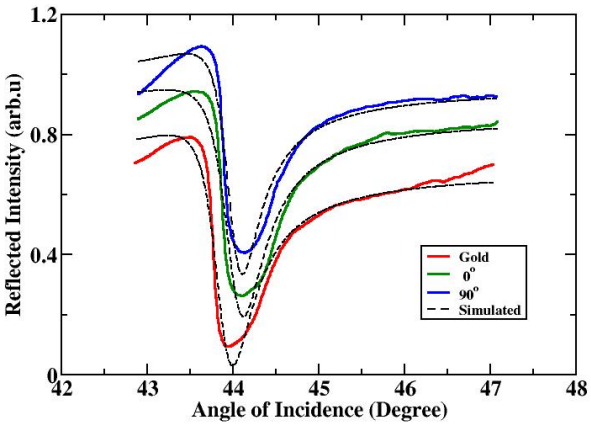

(b)

Figure 4.6: Surface plasmon resonance spectra of gold and (a) One layer of LB film of CdSA where the dipping direction is oriented parallel (0^o) and perpendicular (90^o)) to the plane of incidence (b) spin coated film of stearic acid (isotropically oriented molecules) for the orthogonal directions. The curves are shifted vertically for visual clarity.

Table 4.3: Estimated values of refractive index (RI) of LB film of CdSA through simulation. n_r and n_{im} are the real and imaginary part of RI. The average shift in RA is $\Delta\theta$. The refractive index for the gold was chosen to be 0.172 (n_r) and 3.421 (n_{im})

LB film of CdSA	$\Delta\theta$	n_r	n_{im}
Parallel (0^o)	0.195^o	1.21	0.01
Perpendicular (90^o)	0.1^o	1.11	0.01

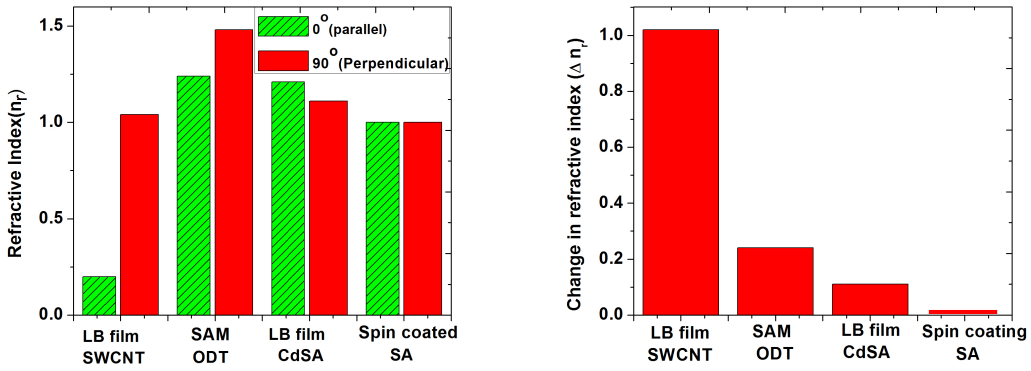

(a) (b)

Figure 4.7: The bar diagram showing (a) the real part of refractive index (n_r) for the ultrathin films of different materials measured in the orthogonal directions. The two bars for each of the film represent the n_r in the orthogonal directions (b) The bar diagram showing the amount of optical anisotropy (Δn_r) of ultrathin films measured using SPR instrument.

The estimated n_r for the ultrathin films of different organized materials in the orthogonal directions are shown as bar diagram in Figure 4.7a. The optical anisotropy (Δn_r) of ultrathin film fabricated by various techniques is shown in Figure 4.7b. The highly ansotropic LB film of SWCNTs shows largest (Δn_r) values whereas the isotropic spin-coated film of SA shows $\Delta n_r = 0$

4.4 Conclusion

SPR is a very powerful technique to identify molecular specific interaction. The technique is label free and very sensitive to detect even few of molecular specific interaction at the given metal-dielectric interface. The change in the optical (or dielectric) properties due to the anisotropy in thin films can be detected using SPR. In this work, we

have demonstrated the capability SPR for the measurement of optical anisotropy of the ultrathin films grown using the conventional LB and self assembly. The LB film of SWCNTs shows interesting results. The LB film of SWCNTs shows both the metallic and dielectric behavior when scanned in 0^o and 90^o alignment of SWCNTs with respect to the plane of polarization, respectively. The SAM of ODT with 30^o tilted molecules shows anisotropy in the real part of refractive index of about 0.24 whereas the LB films of CdSA with 10^o tilted molecules shows anisotropy in the real part of refractive index of about 0.10. Future work includes study of SPR of ultrathin films of different shape anisotropic liquid crystal molecules under the influence of of external perturbation e.g. electric, magnetic field and temperature.

Bibliography

[1] R.M.A Azamm, N.M. Bashara, Ellipsometry and Polarized light, N H Publishing, Co, Amsterdam, 1977.

[2] Y.Wang, Voltage-induced color-selective absorption with surface plasmons, appl.phys. Lett.1995, 67, 2759.

[3] S. Henon and J. Meunier, J. Chem. Phys. 98, 1993, 9148.

[4] I.A. Badmaeva, L.A. Nenasheva, V.G. Polovinkin*, S.M. Repinsky, L.L. Sveshnikova, Thin Solid Films. 2004, 455 – 456, 557.

[5] R. K. Gupta, K. A. Suresh, S. Kumar, Physic.Rev.E.2008, 78, 041703

[6] J. Christopher Love, Lara A. Estroff, Jennah K. Kriebel, Ralph G. Nuzzo, and George M. Whitesides, Chem. Rev. 2005, 105, 1103.

[7] S.V. Batty, T. Richardson, P. Pocock, L. Rahman, (1995), 96.

[8] J.Ignes -Mullol, J.Claret, R.Reigada, F.Sagues, Phys.Rep.2007, 448, 163.

[9] E.Kretchmann, Z.Physics.1971, 241, 2759.

[10] A Ulman, An Introduction to Ultra thin organic:From Langmuir Blodgett to Self Assembly, Academic Press, New york, 1991.

[11] M.C.Petty, Langmuir-Blodgett film, an introduction, Cambridge University Press. New york, 1996.

[12] M.Poonia, V. Manjula Devi, R.K Gupta, S.K.Gupta, J.Singh, P.B.Agarwal, J.Akhthar, Sci, Adv, Matters.2015, 7, 455.

[13] J.C. Love, L.A. Estroff, J.K. Kriebel, R.G. Nuzzo, G.M. Whitesides, Chem. Rev. 2005, 105, 1103.

[14] D.L. Allara, R.G. Nuzzo, Lang- muir.1985, 1, 52.

[15] M.K. Massey, C. Pearson, D.A. Zeze, B.G. Mendis, M.C. Petty, Carbon.2011, 49, 2424.

[16] Devanarayanan VP, Manjuladevi V., Monika Poonia, RK Gupta, SK Gupta, and J. Akhtar Journal of Molecular Structure (Elsevier).2016, 281, 1103.

[17] J. Umemura, T. Kamata, T. Kawai, T. Takenaka, J. Phys. Chem.1990, 94, 62.

Chapter 5

Study on adsorption of graphene on self assembled monolayer

5.1 Introduction

The SPR phenomenon is observed by generating the surface plasmon wave in the thin metallic layer (50 nm gold film) and observing its perturbation due change in the medium on the metal surface. The surface of the gold film should be functionalized chemically to establish a molecular specific interaction. This is the underlying principle of a sensor. The immobilization of ligands is very essential for the development of a biosensor. The mechanical, thermal and other physical stability are important for better performance of the sensor. The sensitivity of SPR based sensors can be improved by utilizing some reported methods which employs metal nanoparticles and nanoholes [1, 2], metallic nanoslits [3], and colloidal gold nanoparticles in buffered solution [5]. A single layer of graphite with one atom thickness and having two dimensional plane of sp^2 bonded carbon atoms arranged in honeycomb lattice is called graphene [4]. It has good conducting properties, and it can be considered as a zero bandgap semiconductor [6, 7, 8]. The extraordinary physical properties of the graphene layer can be harnessed for the development of sensors, photovoltaics, non-linear optical devices and nano-electronics [9, 10]. The π-π interaction between the hexagonal cells of graphene and the carbon based ring structures of a biomolecule results in the efficient adsorption [11, 12]. The graphene layer over gold surface can improve the sensitivity of SPR biosensor [13]. The graphene layer weakly adsorbs over the gold surface due to the absence of chemical bonds. This type of interaction of graphene with gold surface leads to the instability of the graphene

layer over gold surface. In this chapter, we discuss our studies on interaction of the graphene layer on chemically tailored gold surface through the deposition of an organic intermediate layer between graphene layer and the gold film [14].

Organosulfur-based species of molecules can chemically bind on noble metal surface to yield a single layer of molecules known as self-assembled monolayer (SAM). The mechanism of binding of organosulfur molecules with noble metal is known to be an oxidative addition of the -SH bond followed by reductive elimination of the hydrogen, thus resulting in the formation of a thiolate species. The alkanethiol adsorption on gold surface has two phases: an initial fast phase during which the sulfur containing compound is assembled onto the metal substrate, and a second slower phase during which the alkyl chains rearrange undergoing inter-chain, Van der Waals interactions to produce an extended close packed, all trans conformation [17]. Oligophenylthiols can exhibit capability of strong $\pi - \pi$ interaction with analytes. Such molecules can form stable SAM over the gold surface [15, 16]. The SAM of aromatic thiols possesses delocalized π-electrons which is useful in various applications including molecular electronics [18]. It has been reported that self assembled monolayer of octadecanethiol(ODT) was employed on gold surface for the assembling graphene oxide for improvement of sensitivity of SPR based DNA sensor [14]. However, the interaction of ODT with graphene is believed to be weak which can lead to underperforming sensor.

Here, we formed the SAM of biphenyl dithiol (BPD), octadecanethiol (ODT) and mercapto-undecanoic acid (MUA) on the gold substrate and studied the adsorption and interaction of graphene with such chemically modified surfaces. The performance of the devices using graphene can be improved by altering the adsorption sites and the orientational states of the graphene onto the solid substrates. In the present work, the interaction between the graphene and SAM surfaces with different properties is studied. The nature of the substrates is altered by depositing SAMs of organic molecules exhibiting different functional groups. The interaction of such functional surfaces with the graphene is studied using atomic force microscopy and surface plasmon resonance (SPR) phenomenon. We found the adsorption of graphene is favored onto the hydrophobic surface as compared to that of hydrophilic surface. In addition, due to $\pi - \pi$ stacking between the SAM of BPD and graphene, an uniform and homogeneous texture of planar

oriented graphene layer is observed.

5.2 Experimental Section

5.2.1 Materials

The chemicals ODT, MUA and BPD were obtained from Sigma-Aldrich and graphene was procured commercially from Redex Nano Lab. The chemical structure of the molecules are shown in Figure 5.4. The high performance liquid chromatography (HPLC) grade chloroform was obtained from Merck. The absolute alcohol of ACS reagent grade was utilized in the experiments. The water used in the experiments was ultrapure ion-free having the resistivity greater than 18MΩ-cm (Millipore MilliQ, DQ5).

5.2.2 Fabrication of SAM

The layers of 3 nm of chromium followed by 50 nm of gold was deposited onto optically flat BK7 substrates (refractive index = 1.51) by thermal evaporation technique. The vacuum pressure was maintained at 10^{-6} Torr during the deposition process. In order to deposit SAM on gold, the gold deposited substrates were ultrasonicated in chloroform and later cleaned with a solution of mixture of ammonium hydroxide, hydrogen peroxide and water in proportion of 1:1:3. Such cleaned substrates were immersed in the 1mM absolute ethanol solutions of (a) biphenyl dithiol (BPD), (b) octadecanethiol (ODT) and (c) mercapto undecanoic acid (MUA) in separate containers for 24 hrs. The substrates were taken out of the solutions, rinsed with the alcohol and ultrasonicated with chloroform to remove the unbounded adsorbed material from the substrates. The chemically adsorbed molecules on the gold surface yield a single layer of SAM. The wettability of the SAMs were checked qualitatively by putting a sessile drop of water on the SAM and monitoring the meniscus at the line of contact. The SAMs of ODT and BPD yield a hydrophobic surface whereas the SAM of MUA yields a hydrophilic surface.

5.2.3 Deposition of Graphene

The SAMs of ODT, MUA and BPD were immersed in 0.33 mg/ml ethanol solutions of graphene for 24 hrs. The surfaces were gently rinsed with deionised water for the removal of loosely adsorbed graphene before characterizations with different techniques.

5.2.4 Atomic Force Microscopy

The morphology of the films was obtained using the atomic force microscope (AFM) in the contact mode. The silicon (Si) tips of spring constants 0.2 to 1 N/m were employed to scan the surfaces. The scanning was done in the ambient and at room temperature. The average roughness (R_a) and, were estimated from the AFM images. The average roughness of a thin film is defined as

$$R_a = \frac{1}{MN}\sum_{i=1}^{MN} h_i \tag{5.1}$$

where MN are the total number of pixels in the image. h_i is the height at i^{th} pixel location.

The root mean square (RMS) roughness of the surface of a thin film can be evaluated using

$$R_q = \sqrt{\frac{1}{MN}\sum_{i=1}^{MN}(h_i - \overline{h})^2} \tag{5.2}$$

where $\overline{h}$ is the mean height. The R_a and R_q are appropriate parameters to understand the roughness of the surface of thin films [28].

5.2.5 Surface Plasmon Resonance Measurement

The home built SPR instrument operating in the Kretschmann configuration was employed for studying. The details of the SPR instrument is discussed in chapter 2.

5.3 Results and Discussion

The AFM images of the surface of gold, SAMs of BPD, ODT and MUA and graphene adsorbed on such SAMs are shown in Figure 5.1. The AFM image of the gold surface (Figure 5.1a) shows the granular texture representing the gold domains formed during the thermal evaporation process. The average size of the gold domains is around 100 nm. The surface morphology changes due to the adsorption of organic layers. It can be noted that the surface morphology of each of the SAMs (Figure 5.1) are different from each other. The difference in the surface morphology of SAMs is due to the different state of organization of molecules in the SAMs. It is commonly observed that the SAM of different molecules yields different morphology on the metal surface [19]. The SAM of ODT yields highly organized layer [20] whereas that of thiocholesterol yields defect

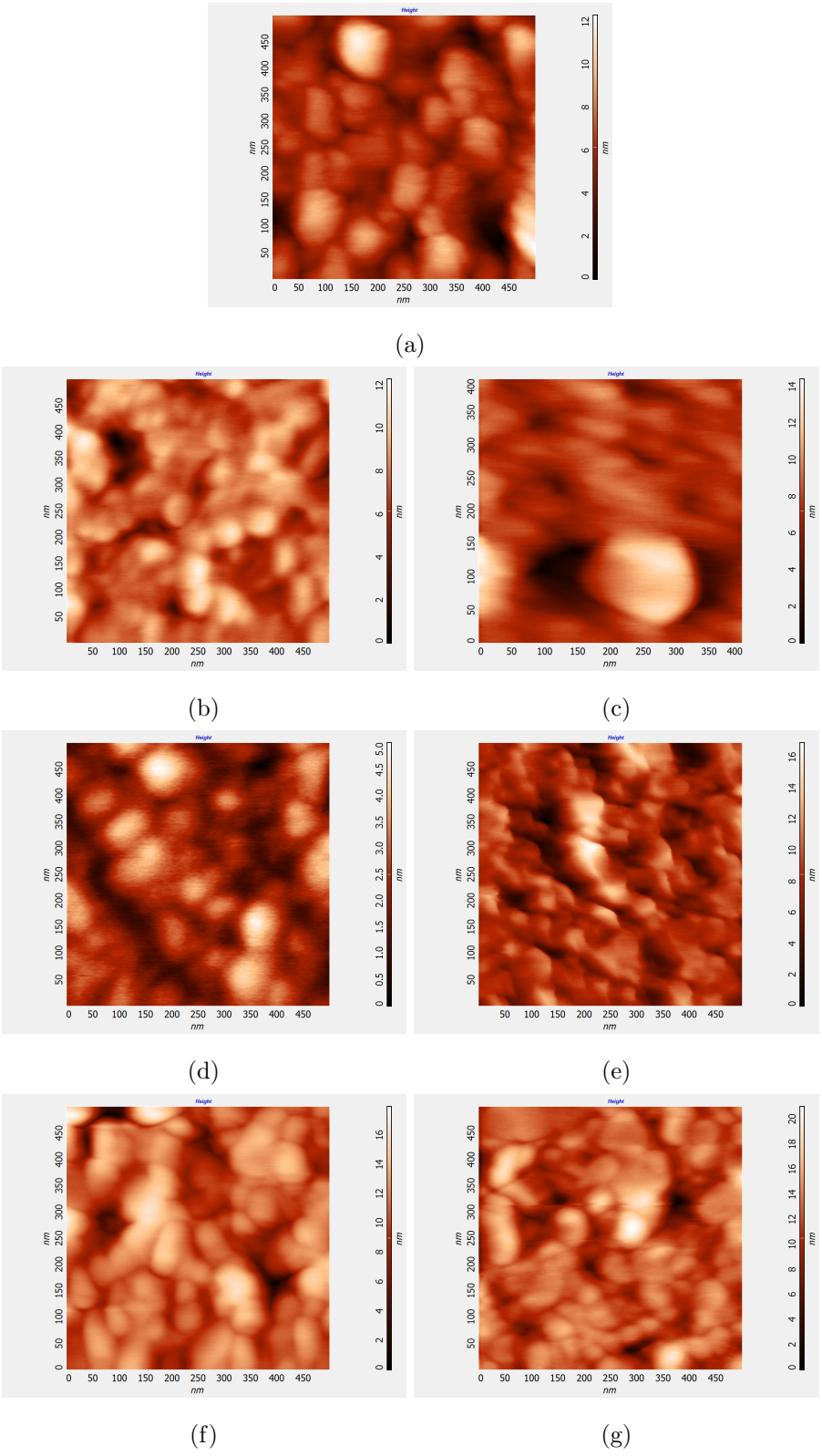

(a) (b) (c) (d) (e) (f) (g)

Figure 5.1: The atomic force microscope images of the surfaces of (a) Bare gold, (b)SAM of BPD, (c) BPD with graphene, (d) ODT, (e) ODT with graphene, (f) MUA and (g) MUA with graphene. The dimension of each image is 500 nm × 500 nm.

Table 5.1: Roughness data obtained from AFM images. The error in the data is $\backsim 0.06nm$.

Sample	Average roughness(nm)	Root Mean square(RMS)Roughness(nm)
Gold Surface	1.3	1.7
SAM of BPD	1.2	1.5
SAM of ODT	0.6	0.8
SAM of MUA	1.8	2.5
Graphene on BPD	1.1	1.1
Graphene on ODT	1.7	2.2
Graphene on MUA	1.8	2.5

rich unorganized layer [21]. Due to adsorption of graphene on the SAM of BPD, the texture appears more uniform (Figure 5.1c). This indicates a homogeneous adsorption of graphene over the SAM of BPD. The texture of the graphene adsorbed layer on the SAM of ODT reveals more corrugated structure (Figure 5.1e) as compared to the texture of SAM of ODT. This indicates that the adsorption of graphene on the ODT surface is inhomogeneous, and thus the surface appears more rough. The texture of the graphene adsorbed layer on the SAM of MUA (Figure 5.1g) shows no change as compared to that of SAM of MUA (Figure 5.1f) which indicates no adsorption of graphene onto the SAM of MUA. The average roughness (R_a) and RMS roughness (R_q) of the different surfaces were calculated from the AFM images using the equations 5.1 and 5.2 and the roughness analysis data are shown in Table 5.1. A bar diagram showing the roughnesses of different layers on gold surfaces is shown in Figure 5.2. It can be observed that the trend of the variation of R_a and R_q with respect to the nature of the film is similar. The roughnesses of the SAM of ODT decrease significantly whereas that of MUA increases largely as compared to that of gold surface. The roughnesses of SAM of BPD decreases as compared to that of gold surface. The roughnesses further decreases due to the adsorption of graphene on the SAM of BPD. The reduction in roughnesses is due to the homogeneous adsorption of graphene onto the SAM of BPD. In contrast, the roughnesses of the graphene layer onto SAM of ODT increases significantly as compared to that of SAM of ODT. Such increase in values of roughnesses is due to random and non-uniform adsorption of graphene onto the ODT surface. The roughnesses of SAM of MUA and graphene onto SAM of MUA are similar indicating poor adsorption of graphene onto

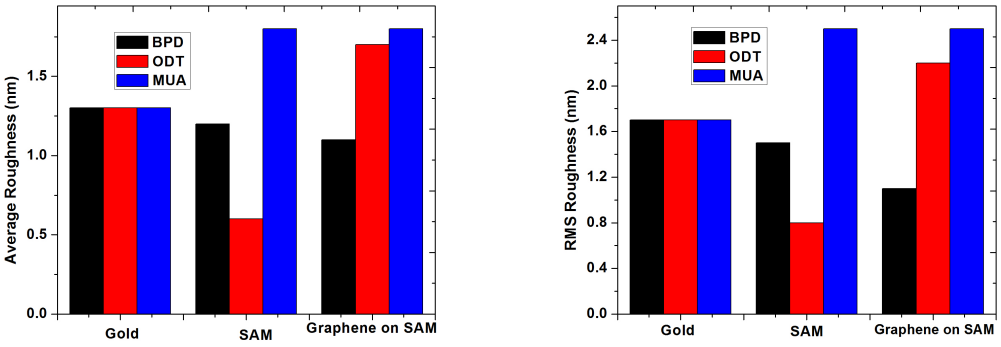

(a) (b)

Figure 5.2: Bar diagrams showing the (a) average roughness and (b) root mean square (RMS) roughness calculated from the AFM images of the surfaces of gold, SAMs of BPD, ODT and MUA, and graphene adsorbed layer on such SAMs.

the MUA surface. The atomic force microscopy on the system thus indicates that the graphene adsorbs poorly onto the SAM of MUA whereas it binds largely to the SAMs of BPD and ODT. The adsorption onto the SAM of BPD was found to be uniform as compared to that of the SAM of ODT. The properties and structure of SAMs of various organothiols have been discussed extensively in references [19, 20]. The organothiols with different terminal functional groups yield different nature of surfaces; and thereby provide possibility of altering adsorption capability of a specific analyte to the surface. In the present work, we found that by altering the terminal functional group of the SAMs, the adsorption of graphene to the surfaces can be altered significantly. The adsorption of graphene of the chemically tailored gold surface due to deposition of SAMs of different chemical species is studied using the SPR phenomenon. The graphene can adsorb to the SAMs of different material. A minute change in the dielectrics at an interface due to the adsorption of graphene can be detected from the change in the SPR spectra as compared to a reference. The SPR spectra of the SAMs and graphene onto such SAMs are recorded and shown in Figure 5.3.

The spectra of pure gold, SAM of the organic layer and the graphene adsorption layer on such SAM are shown in each figure for comparison. The resonance angle for gold is found to be 44.0^o. The resonance angle shifts due to change in the dielectric medium at the gold-air interface because of the adsorption of the organic molecules as SAM

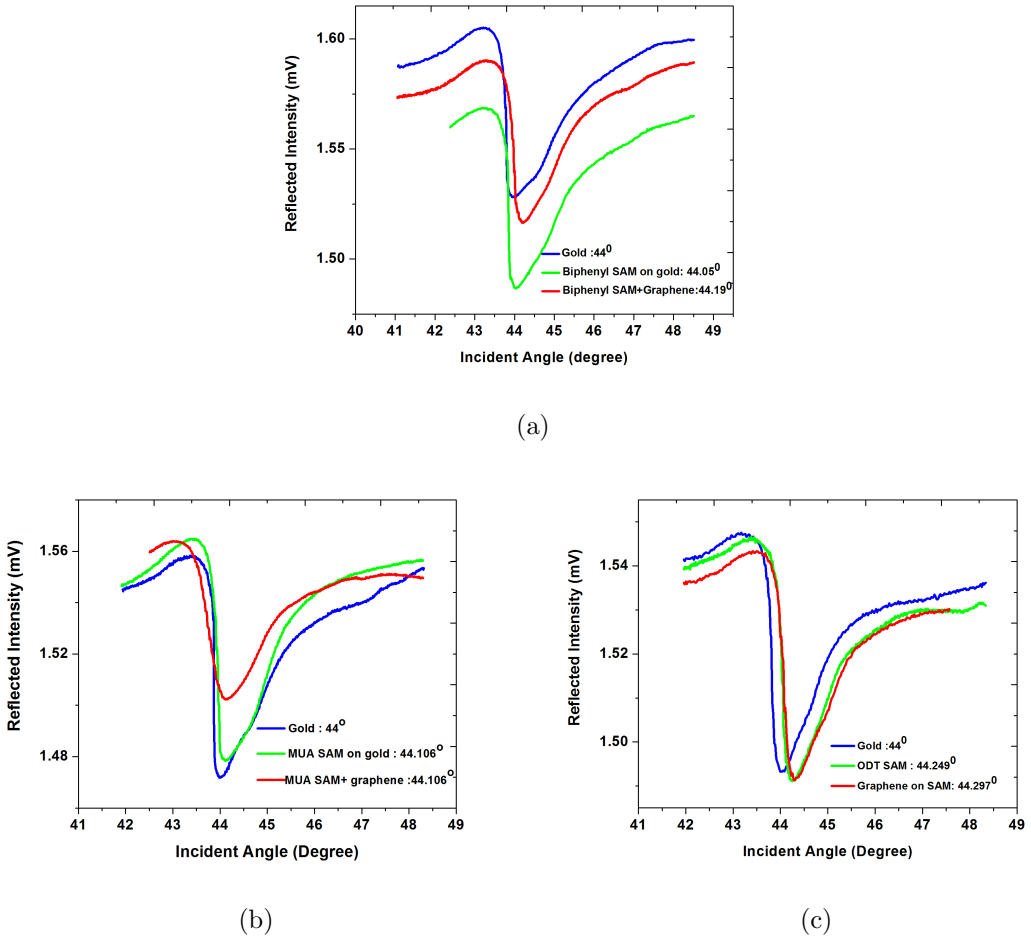

Figure 5.3: The SPR spectra of graphene deposited onto SAM of (a) BPD on gold (b) ODT on gold (c) MUA on gold.

[22]. The shifts in the resonance angle (ΔR) with respect to the gold-air and SAM-air interfaces are tabulated in Table 5.2.

The spectra of pure gold, SAM of the organic layer and the graphene adsorption layer on such SAM are shown in each figure for comparison. The resonance angle for gold is found to be 44.0^o. The resonance angle shifts due to change in the dielectric medium at the gold-air interface because of the adsorption of the organic molecules as SAM [22]. The shifts in the resonance angle (ΔR) with respect to the gold-air and SAM-air interfaces are tabulated in Table 5.2. The values in the shift of RA due to adsorption of SAM on gold surface measured with respect to gold-air interface (ΔR_1) and that of graphene adsorption on the SAM measured with respect to SAM-air interface (ΔR_2) are shown in Table 5.2. The non-zero ΔR_1 values obtained for the SAMs of BPD, ODT and

Table 5.2: The shift in resonance angle for SAMs deposited on gold surface measured with respect to the resonance angle for the gold-air interface (ΔR_1) and shift in resonance angle for graphene adsorption on the SAM measured with respect to the resonance angle for the SAM-air interface (ΔR_2). The error in the data is $\sim \pm 0.002^o$

SAM deposited on gold	ΔR_1	ΔR_2
BPD	0.05^o	0.14^o
ODT	0.25^o	0.05^o
MUA	0.11^o	0.0^o

MUA indicate the adsorption of the organic layer during the fabrication of SAM. The difference in ΔR values for such SAMs is due to different dielectric nature of the film which may result from different state of ordering and organization of the corresponding molecules on the gold surface. The ΔR_2 values for the graphene layer on the SAMs of BPD and ODT are non-zero positive values. However, it is zero for the layer on the SAM of MUA. The zero ΔR_2 value indicates no change in the dielectric property of the SAM of MUA and hence no adsorption of graphene even after being treated with graphene solution for 24 hrs. The nature of the surfaces yielded by the SAM of BPD and ODT are hydrophobic whereas that of SAM of MUA is hydrophilic. The adsorption of graphene from solution is found to be favourable onto the SAMs of BPD and ODT. However, the SAM of MUA does not support the adsorption of graphene. Like many other carbon based pristine nanomaterials, graphene is also hydrophobic in nature [23, 24, 25]. Such hydrophobic material cannot form any physical/chemical bonding with a hydrophilic surface, and therefore the SAM of MUA does not support the adsorption of graphene. The physical interaction between the hydrophobic materials can be enhanced by altering the entropically driven hydrophobic attraction [26] or by improving the delocalized $\pi - \pi$ attraction between the molecules [27]. The graphene adsorbs to the hydrophobic SAM of ODT due to attractive hydrophobic interaction. Such hydrophobic interaction is non-preferential as far as the molecular shape and structure is concerned. Thus, it is expected to have the random adsorption sites with the random orientational states of the graphene. Consequently, the AFM images indicate the random and non-uniform adsorption of graphene on the SAM of ODT. Both the thiol groups of a BPD molecule can chemically bind to the gold surface leading to a planar orientation of the molecule in the SAM. The SAM of BPD yields the surface with delocalized π-electrons. The 2D

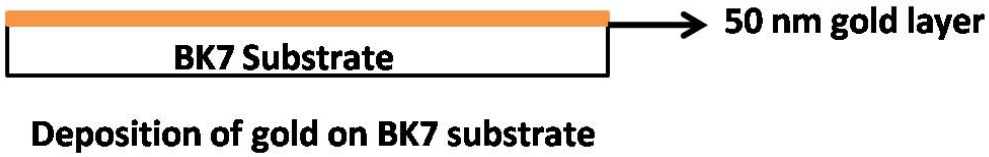

Deposition of gold on BK7 substrate

(a)

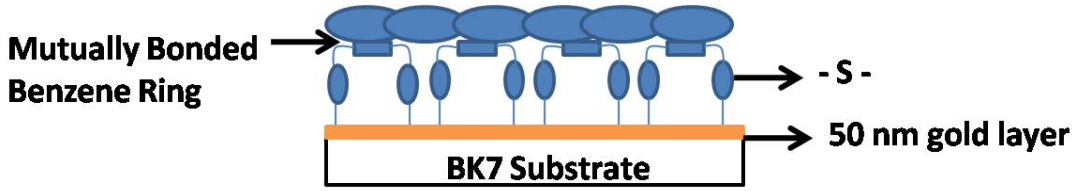

Graphene adsorption on BPD SAM

(b)

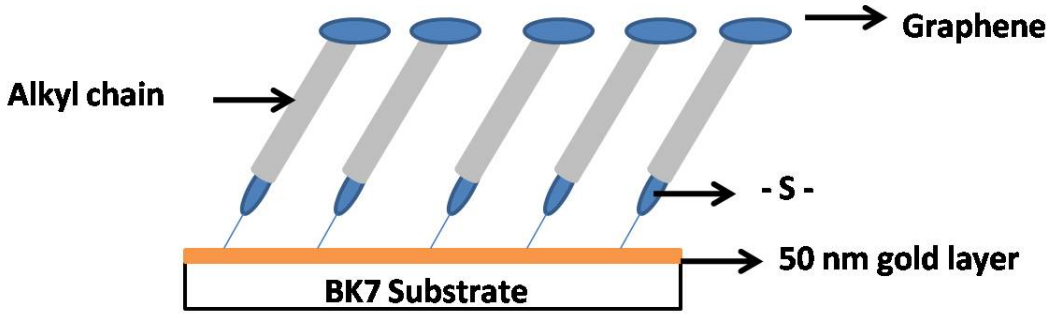

Graphene adsorption on ODT SAM

(c)

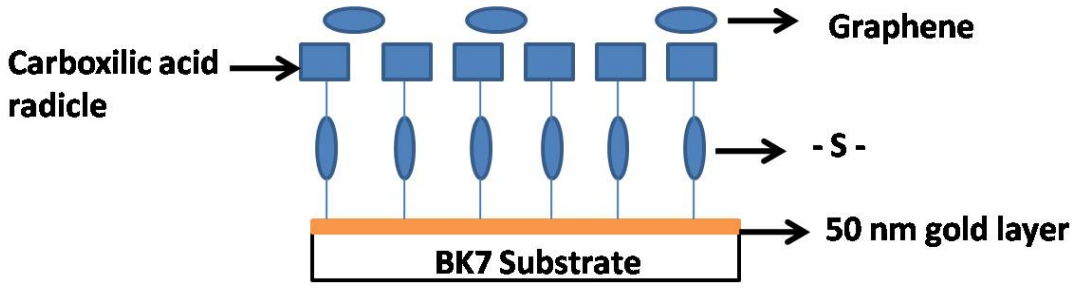

Graphene adsorption on MUA SAM

(d)

Figure 5.4: The schematic representation of adsorption of gold layer on a BK7 surface and adsorption of graphene on various self assembled monolayers(SAM).

planar graphene exhibits delocalized π-electrons. Such delocalized π-electrons favour the

attractive interaction between the graphene and the SAM of BPD leading to a planar orientation of the graphene onto the surface. Due to such preferential orientation of the graphene during adsorption to the SAM of BPD, the morphology of graphene on the SAM of BPD is found to be planar and homogeneous. Our studies indicate that in order to enhance the adsorption of graphene for sensing application, the SAM of BPD yields better landscape for its strong and uniform adsorption. The adsorption of graphene on different SAM are shown schematically in Figure 5.4.

5.4 Conclusion

The interactions of graphene with the SAMs of different chemical species are investigated. Due to hydrophobic nature of the graphene, its adsorption is favourable onto the hydrophobic surfaces like SAMs of ODT and BPD. Interestingly, the morphology of graphene onto the SAMs of BPD and ODT are remarkably different. Graphene may prefer planar orientation onto the SAM of BPD which may be due to $\pi - \pi$ interaction between the BPD molecule and the graphene. The hydrophobic interaction between the ODT and graphene leads to random and non-uniform orientation of the graphene onto ODT surface. Our study suggests that the adsorption of graphene can be altered by altering the nature of the substrates. Our further studies involve the investigation on the interaction of graphene onto the surfaces with different degree of hydrophobicity.

Bibliography

[1] J. Zhao, X. Y. Zhang, C. R. Yonzon, A. J. Haes, and R. P. Van Duy, Nanomedicine (Lond).2006, 219.

[2] M. E. Stewart, C. R. Anderton, L. B. Thompson, J. Maria, S. K. Gray, J. A. Rogers, and R. G. Nuzzo, Chem. Rev.2008, 108, 594.

[3] K. L. Lee, C. W. Lee, W. S. Wang, and P. K. Wei, J. Biomed. Opt. 2007, 12, 44023.

[4] A.K. Geim, K.S. Novoselov, The rise of graphene, Nature Materials 6 (2007) 183–191.

[5] P. Englebienne, A. V. Hoonacker, and M. Verhas, Spectroscopy.2003, 17, 255.

[6] A. Martin, A. Escarpa, Trends Anal. Chem. 2014, 56, 13.

[7] G. Eda, G. Fanchini, M. Chhowalla, Nature Nanotech. 2008, 3, 270.

[8] A. K. Geim, K. S. Novoselov, Nat. Mater. 2007, 6, 183.

[9] P. Avouris, Nano Lett. 2010, 10, 4285.

[10] F. Bonaccorso, Z. Sun, T. Hasan, A. C. Ferrari, Nature Photonics 2010, 4, 611.

[11] R. Verma, B. D. Gupta, R. Jha, Sens. Act. B 2011, 160, 623.

[12] M.Pumera, Mater. Today 2011, 14, 308.

[13] L. Wu, H. S. Chu, W. S. Koh, and E. P. Li, Optics Express.2010, 18, 14395.

[14] Nan-Fu Chiu , Teng-Yi Huang, Sens. Actuators B.2014, 197, 35.

[15] N. Tillman, A. Ulman, T. L. Penner, Langmuir 1989, 5, 101.

[16] S. D. Evans, R. Sharma, A. Ulman, Langmuir 1991, 7, 156.

[17] Silvia Ferretti, Sally Paynter, David A. Russell, Kim E. Sapsford, trends in analytical chemistry.2000, 19, 530.

[18] U. Weckenmann, S. Mittler, K. Naumann, R. A. Fischer, Langmuir 2002, 18, 5479.

[19] A. Ulman, Chem. Rev. 1996, 96, 1533.

[20] J. C. Love, L. A. Estroff, J. K. Kriebel, R. G. Nuzzo, G. M. Whitesides, Chem. Rev. 2005, 105, 1103.

[21] Z. P. Yang, I. Engquist, J. M. Kauffmann, B. Liedberg, Langmuir 1996, 12, 1704.

[22] J. Hamola, Chem. Rev. 2008, 108, 462.

[23] J. Dong, Z. Yao, T. Yang, L. Jiang, C. Shen, Scientific Rep. 2013, 3, 1733.

[24] Z. Lin, Y. Liu, C-P Wong, Langmuir 2010, 26, 16110.

[25] S. Wang, Y. Zhang, N. Abidi, N. Cabrales, Langmuir 2009, 25, 11078.

[26] J. N. Israelachivile, Intermolecular and Surface Forces, Academic Press, Amsterdam 2011.

[27] S. Kumar, Chemistry of Discotic Liquid Crystals, CRC Press, Boca Raton 2011

[28] M. Ramzan, E. Ahmed, N.A. Niaz, A.M. Rana, A.S. Bhatti, N.R. Khalid, M.Y. Nadeem, Superlattices and Microstructures.2015, 82, 399.

Chapter 6

Conclusion and Future scope

Surface plasmon resonance based sensors are gaining a major attention in the field of biomedical and pharmaceutical industries. SPR sensors are having label free sensing mechanism. The bio-chemistry research field utilizes several chemical species as labels to study the molecular interactions. In some cases, the labelling chemcals itself suppresses such molecular interaction reactions. Thus, SPR sensors are widely used in such research fields for qualitative and quantitative studies of such interactions. The SPR sensors with the proper gas chambers and respective adsorption layers makes excellent gas sensors with high sensitivity. The simple, hand held commercially available SPR sensors made the field studies convenient. The optic-fiber based SPR sensors can be used for sensing applications remotely. The fiber-optic SPR sensor though are portable but poor in sensitivity. The monochromator/spectrophotometer having high resolution in fiber-optic SPR sensor increases the price of the instrument. The SPR sensors in angular mode has economically cheap design and provides high resolution and sensitivity.

There are a wide range of angular interrogation mechanisms available for the angular mode SPR sensors. The angular interrogation mechanism which interrogates a fixed region on the prism-gold interface improves the reliability of the SPR instrument. This thesis, put forward such an angular interrogation mechanism that interrogates a fixed region on prism-gold interface with compact and simple optical alignment. The adopted new opto-mechanical scanning has stationary laser and the detector. As the angle of incidence changes due to rotation of the scanning mirror, the reference spot position on the gold surface shifts and as a consequence the spot of reflected beam on the quadrant photodiode (QPD) shifts. In order to retain the spot position fixed onto the gold surface,

the prism-assembly is translated vertically till original reference spot position is regained. The scanning mechanism is controlled using a in-house developed computer program in LabView.

The instrument is calibrated with sucrose solution having concentrations ranging from milli molar to femto Molar. The lowest detectable concentration of sucrose in aqueous medium is found out to be 1×10^{-13} M (100fM). The resolution of the instrument is found out to be $1.92\mu RIU$. The sensitivity of the instrument is estimated from the calibration curve obtained by recording the RA for different concentrations of sucrose solution with known refractive indices. The variation in data is best fitted with a linear curve and the slope is estimated. The sensitivity of the instrument thus obtained from the slope as 52.6^o/RIU. The flow cell with a very small flow chamber (10μ l) is developed for the SPR instrument. The design of the flow cell is simple, cost effective and universal to sensing elements of various shapes. The flow cell is tested with sugar solution as sample. The adsorption and desorption curves of sugar on gold surface are recorded. The respective curves have the total intensity change against the time. This yields the adsorption and desorption curves.

The shape attributes of SPR curve varies with the nature of metal and its interface. The Fresnel's reflection was employed in a three layer model for the metal-air as well as metal-water interface and the SPR spectra are simulated numerically using Matlab. Three noble metals (gold, silver, copper) are considered for this study. The metallic layer thickness ranges between 30 nm to 100 nm. The numerical study revealed that gold layer with a thickness 50 nm provides the consistent SPR attribute in both interfaces compared to other metals.

The SPR instrument is used to study the optical anisotropy in ultra-thin films. The ultra-thin film samples are deposited on gold surface through LB technique, as SAM, and spin coating. The single walled carbon nanotubes (SWCNTs) and cadmium stearate (CdSA) are deposited as LB films. The octadecanethiol (ODT) is deposited as self assembled monolayer. The stearic acid (SA) is deposited as a thin film with isotropic orientation of molecules using spin coating method with a rotating speed of 7000 rpm. The SPR spectra for these sample are recorded in the orthogonal directions of the sample with respect to the plane of incidence. The SPR data of these thin films revealed that

SWCNT LB film shows maximum optical anisotropy than other thin films. The optical anisotropy in the spin coated SA layer on gold surface is found to be negligible. This study shows the capability of the developed instrument in resolving the minor changes in refractive index at the interface.

A thin film of graphene layer improves the sensitivity of SPR instrument as a biosensor. The stable deposition of graphene layer on the gold surface is a non-trivial problem. We have demonstrated a method to stabilize the graphene layer on gold surface. The self assembled monolayer of alkanethiol molecules on gold surface enhances the adsorption of graphene layer on it. The $\pi - \pi$ interaction between SAM and graphene stabilizes the graphene layer on gold surface. The self assembled monolayers of octadecanethiol (ODT), biphenyldithiol (BPD), mercapto undecanoic acid (MUA) are deposited on gold surfaces. These three substrates are dipped in graphene solution for 24 hrs. The SPR spectra of samples are recorded. The SPR data of SAM and SAM with graphene layer revealed that the SAM of BPD supports the graphene deposition better than other SAMs. The SPR data is validated with the topographic AFM images of the respective samples.

6.1 Future Scope

The developed SPR instrument can be used for the analysis of reaction kinetics. The kinetic studies are important in biomedical and pharmaceutical industries. This angle based SPR instrument can be converted to wavelength based SPR instrument through the replacement of laser source with a polychromatic light source. In such a case, the spectrophotometer can replace the quadrant photodiode as detector. The wavelength based SPR instrument can operate without feedback mechanism as the angle of interrogation remains constant. Such SPR instrument does not require any translation stage. The fiber-optic based spectrophotometer for the detector reduces the size of instrument and improves the portability of the instrument.

SPR instrument is utilized for various studies other than the simple analyte-ligand interactions. Some of the possible applications using the developed SPR instrument is described in the following section.

6.2 Electro-chemical SPR

The electrochemistry combined with the SPR setup improves the sensitivity of the SPR instrument for the analysis of complex liquids. This method introduces suitable electrodes into the flow cell. The fluid in the flow cell act as the electrolyte. The application of voltage to the electrodes at resonance angle provides the information in change of refractive index of the electrolytes during the electrochemical process.

6.3 SPR Imaging

This SPR instrument can be modified in the imaging mode for the biomolecular interaction anlaysis. This type of imaging is an ideal surface-sensitive optical technique to detect multianalyte interactions. Multianalytes can be addressed simultaneously and therefore the selectivity and reliability of such sensor enhances remarkably .

Here, an array of sensing area is created on the gold surface by immobilizing suitable ligands at different specified location. Such specified locations (spots) are imaged using the reflected light from the sensing area.

Appendices

Appendix A

List of publication and Conferences attended

A.1 List of publication

1. **Patent:**

Title: A novel opto-mechanical system for measuring surface plasmon resonance

Reference no: E-101/99275/2014-DEL.

Application no: 2644/DEL/2014. Status: Application filed to Indian Patent Office.

2. **Measurement of optical anisotropy in ultrathin films using surface plasmon resonance**

Devanarayanan VP, Manjuladevi V., Monika Poonia, RK Gupta, SK Gupta, and J. Akhtar, Journal of Molecular Structure (Elsevier). 2016, 281, 1103.

DOI: 10.1016/j.molstruc.2015.09.018.

3. **Surface plasmon resonance sensor based on a new opto-mechanical scanning mechanism**

Devanarayanan V. P., V. Manjuladevi, R. K. Gupta, Sensors Actuators B: Chemical (Elsevier). 2016, 227, 643.

DOI: 10.1016/j.snb.2016.01.027.

4. **Interaction of graphene with self assembled monolayers**

Devanarayanan VP, V. Manjuladevi and RK Gupta, Macromolecular Symposia (Wiley). 2015, 357, 23.

DOI: 10.1002/masy.201400180.

A.2 List of Conference attended

1. Poster presentation in the International Conference on Soft Materials, MNIT Jaipur, 6-10 October, 2014. **Received BEST POSTER AWARD**.

2. Poster presentation in 8^{th} Asian Photochemistry Conference (APC-2014), IISER Trivandrum, 10-13 November, 2014.

3. Poster presentation in the National Conference on Condensed Matter Physics, BITS Pilani, Pilani Campus, 24-25 February, 2012.

Appendix B

Biography of Candidate

Mr. Devanarayanan.V.P is a full time research scholar in Department of physics BITS Pilani, Pilani Campus. He had completed his post graduation in photonics from Department of Atomic and Molecular Physics Manipal University in 2011.

His research interest is in the field of photonics. He had successfully completed the development of sensor based on surface plasmon resonance phenomenon during his PhD career in BITS Pilani. He had applied for patent in Indian patent office for his developed sensor. He had published three articles in international journals. He had participated in national and international conferences related to his field of research interest.

Appendix C

Biography of Supervisor

Prof. Raj Kumar Gupta is an experimental soft condensed matter physicist. He obtained his Ph.D. from Raman Research Institute, Bengaluru in soft condensed matter physics (experimental) in the year of 2005. He works on thin films of mesogenic molecules, nanomaterials and the composites. Currently, his research interests are focused on understanding the change in properties of materials in the ultrathin film regime and its application for device fabrication. He and his team comprising Prof. Manjuladevi V. and Mr. Devanarayanan in BITS Pilani have developed a low cost portable surface plasmon resonance instrument with the financial support from DST, India. The instrument is ready for any sensing application. His current research interests are :-

1. Optics : Surface Plasmon Resonance Instrumentation and related software development.
2. Scanning probe microscopy of thin films of nanoparticles.
3. Controlling parameters for defect formation in thin films.
4. Scanning tunneling microscopy/spectroscopy.
5. Application of ultrathin films for device development.

He has published several research articles in reputed international journals. He has authored few book chapters in the field of his research interest. At present, he is associate professor in the department of physics at BITS, Pilani.